Idaho National Engineering Laboratory

INEL-95/0561

November 1995

INEL BNCT Research Program Annual Report 1994

Edited by
J. R. Venhuizen

Lockheed
Idaho Technologies Company

INEL-95/0561

INEL BNCT Research Program Annual Report 1994

Edited by
J. R. Venhuizen

Published November 1995

Idaho National Engineering Laboratory
Lockheed Idaho Technologies Company
Idaho Falls, Idaho 83415

Prepared for the
U.S. Department of Energy
Office of Energy Research
Under DOE Idaho Operations Office
Contract DE-AC07-94ID13223

ABSTRACT

This report is a summary of the progress and research produced for the Idaho National Engineering Laboratory (INEL) Boron Neutron Capture Therapy (BNCT) Research Program for calendar year 1994. Contributions from the principal investigators about their individual projects are included, specifically, chemistry (pituitary tumor studies, boron drug development including liposomes, lipoproteins, and carboranylalanine derivatives), pharmacology (murine screenings, toxicity testing, ICP-AES analysis of biological samples), physics (treatment planning software, neutron beam and filter design, neutron beam measurement dosimetry), and radiation biology (small and large animal models tissue studies and efficacy studies). Information on the potential toxicity of BSH and BPA is presented and results of 21 spontaneous tumor bearing dogs that have been treated with BNCT at Brookhaven National Laboratory (BNL) are discussed. Several boron carrying drugs exhibiting good tumor uptake are described. Significant progress in the potential of treating pituitary tumors is presented. Highlights from the First International Workshop on Accelerator-Based Neutron Sources for BNCT are included.

CONTENTS

FIGURES

TABLES

ACRONYMS AND ABBREVIATIONS

AAF	anaplastic astrocytomas
ALT	alanine aminotransferase
ARL	Army Research Laboratory
AST	aspartate aminotransferase
BBB	blood-brain barrier
BMRR	Brookhaven Medical Research Reactor
BNCT	Boron Neutron Capture Therapy
BNL	Brookhaven National Laboratory
BPA	boronophenylalanine
BSH	borocaptate sodium
BSSB	dimer of BSH
BSSO	oxidized dimer of BSH
BUN	blood urea nitrogen
CAD	computer aided design
CN-V	cranial nerve V
CP	conscious proprioception
cpm	counts per minute
CRH	corticotropin releasing hormone
CT	computed tomography
CVM	College of Veterinary Medicine
DOE	Department of Energy
DORT	Discrete Ordinate Radiation Transport
ECC	elaidyl carborane carboxylate
EE	ethinyl estradiol
FDA	Food and Drug Administration
FTIR	Fourier transform infrared spectrometry
GBM	glioblastoma multiforme
GHRH	growth hormone releasing hormone
GSH	glutathione
HC	n-hexyl carborane
HFR	High-Flux Reactor
HP	Hewlett-Packard
IBM	International Business Machines
ICP-AES	inductively coupled plasma-atomic emission spectrometry
ICP-MS	inductively coupled plasma-mass spectroscopy
INEL	Idaho National Engineering Laboratory
ISU	Idaho State University
i.p.	intraperineal
i.v.	intravenous
JRC	Japanese Research Center
LDH	lactate dehydrogenase
LDL	low density lipoprotein
LITCO	Lockheed Idaho Technologies Company
LMIT	Lockheed Martin Idaho Technologies
MC	Monte Carlo

MIT	Massachusetts Institute of Technology
MITR	Massachusetts Institute of Technology Reactor
MR	magnetic resonance
MRI	magnetic resonance imaging
MSU	Montana State University
MW	megawatt
NCAR	National Center of Atmospheric Research
NDA	New Drug Application
NDE	New Device Exemption
NURBS	Non Rational B-splines
oCRH	ovine corticotropin releasing hormone
OHSU	Oregon Health Sciences University
OSTR	Oregon State TRIGA Reactor
pBPA	p-boronophenyalanine
PBS	phosphate buffered saline
PC	personal computer
PI	Principal Investigator
PLR	pupillary light reflex
ppb	parts per billion
ppm	parts per million
RBC	red blood cell
RBE	relative biological effectiveness
Rpte	Radiation treatment planning environment
rpm	revolutions per minute
rtt	radiation transport in tissue
SD	standard deviation
SGI	Silicon Graphics Incorporated
TIDBIT	INEL Database of BNCT Information and Treatment
TLD	thermoluminescent dosimeter
UCLA	University of California at Los Angeles
UCSF	University of California, San Francisco
U of U	University of Utah
WBC	white blood cell
WSU	Washington State University

INEL BNCT RESEARCH PROGRAM ANNUAL REPORT 1994

INTRODUCTION

The Idaho National Engineering Laboratory (INEL) Boron Neutron Capture Therapy (BNCT) Research Program completed its 8th year as a Department of Energy (DOE) funded program with a continuing increase in interest from the medical community. The goal of the program remains: to provide the scientific and technological basis for using BNCT in the treatment of human malignant brain tumors and to bring the therapy to human clinical trials. This publication summarizes the research accomplished this past calendar year. Analytical chemistry, calculational and measurement physics, and treatment planning remain the strong parts of the INEL contribution, while the university programs continue to contribute developments in new boron-containing drugs, drug evaluation, and radiation biology used for treatment protocol development. This annual report reviews the current status of 13 components of the INEL BNCT Research Program and the experimental results and developments of the past year.

Drug Development

Although significant progress toward the application of boronated low density lipoproteins (LDLs) for site selective boron drug delivery has been made during the past year, the loss of the animal and cell culture testing site at Washington State University (WSU) has seriously hampered progress on this project. The results of one in vivo biodistribution study in B16BL6-bearing mice and a series of in vitro studies that demonstrate very substantial uptake of boronated LDL in certain cell lines are reported. The influence of 17α-ethinyl estradiol on cellular uptake has also been probed. Most significantly it was demonstrated that LDL loaded with n-hexyl carborane (HC) is taken up with exceptional aridity in several lines. Significant progress has also been made in the development of a rapid infrared analysis of boron in boronated LDL solution.

The boronated liposome development and evaluation effort consists of two separate tasks. The first is the development of new boron compounds and the synthesis of known boron species with BNCT potential. These compounds are then encapsulated within liposomes for the second task: biodistribution testing in tumor-bearing animals, which examines the potential for the liposomes and their contents to concentrate boron in cancerous tissues. Recent developments in boronated liposome research have been centered upon the following topics: (a) continued development and scale-up of the most successful candidate boron species, (b) synthesis of new boron-containing compounds expected to exhibit the most favorable features of efficacious boron species, (c) the biological testing of these compounds, incorporated in liposomes, in expedient preliminary screening experiments using mice and rats to determine tumor delivery and retention of boron, and (d) intracellular distribution and mechanistic studies with liposomes labeled with fluorescent markers. Research into water-soluble species during the past year was concentrated upon the production of boron-rich species derived from the $[B_{20}H_{18}]^{2-}$ ion, which was first synthesized 30 years ago. This ion was chosen for its high boron content, ease of preparation, stability, and rich derivative chemistry related to its propensity to react with nucleophiles and to undergo redox reactions.

BNCT has also shown promise in the treatment of pituitary tumors and other endocrine associated malignancies via endocrine cell receptor specificity and internalization after hormone binding. Results are consistent with BNCT cell destruction being mediated through the AtT-20 cell corticotropin releasing hormone receptor. Experiments conducted through calendar year 1994 continue to support the hypothesis that: (a) releasing hormone ligands can be synthesized and conjugated to a $^{10}B_{10}$-cage in a manner that preserves the biological activity (receptor binding and signal

transduction) of the polypeptide hormone used for targeted pituitary tumor cells in vitro, and (b) the incubation of receptor positive cells with the appropriate $^{10}B_{10}$ conjugated ligand makes them susceptible to BNCT. Moreover, it appears that this effect is mediated through the receptor, providing evidence that other cells can be targeted via specific membrane receptors and killed with hormone $^{10}B_{10}$ conjugates.

Pharmacology

Preclinical toxicity testing of borocaptate sodium (BSH) has been conducted to aid in assessing if proposed human studies of BSH (absent neutron radiation) are likely to be acceptably safe. BSH has been administered clinically in both Japan and Europe (typically at BSH doses less than 100 mg/kg). European and Japanese experience suggests that single dose administration of BSH in amounts less than 100 mg/kg is not typically associated with serious adverse effects, at least in the clinical populations evaluated to date. Available data suggest that: (a) single doses of BSH up to 100 mg/kg are reasonably safe for healthy volunteers, (b) before studying the action of BSH in tumor patients, animal studies are needed to determine how concomitant administration of commonly used drugs might influence BSH toxicity and how reduced renal function affects BSH toxicity, and (c) that before BSH fractionation or dose escalation studies (i.e., BSH doses above 100 mg/kg) can be undertaken, more animal toxicity information is needed. Several experiments were carried out in 1994 to determine additional toxicity data associated with BSH, and are reported herein.

Radiation Biology

For the past 8 years, researchers have used the canine as the large animal model to study the effects of BNCT on normal and neoplastic brain tissue. These studies have been performed using BSH and epithermal neutrons and have had two major foci: (a) biodistribution of BSH in animals with spontaneously occurring brain tumors and (b) effects of BNCT in normal and neoplastic brain tissue. Canine subjects were chosen as a model for the human glioblastoma multiforme (GBM) because of similarities between the two species in frequency and dynamics of spontaneously occurring brain tumors, and because the dog's size permits selective irradiation of the head without a significant whole body dose. Although intended as a model for a glial tumor, dogs with several different brain tumor types have been studied since the studies were designed to evaluate tissue tolerance and not treatment efficacy.

To date, 24 dogs with spontaneously occurring brain tumors have been treated with BNCT, 22 with BNCT alone, and two with a combination of surgery and BNCT. BSH was the boron delivery agent in all but one case, which was treated following p-boronophenyalanine (p-BPA)-fructose infusion. As of January 1995, three dogs remain alive and well following treatment.

Nontumor bearing dogs were also used in dose escalating tolerance studies designed to establish the tolerance of normal brain tissue to BNCT. Tolerance of normal brain to epithermal neutrons alone, and to single and split dose BNCT has been established in the dog. Another consideration is the possible alteration in boron uptake by previously irradiated tissue. Of particular interest is modification of the blood-brain barrier (BBB). Research on normal tissue tolerance has included BNCT administered in 2 or 4 daily fractions. For the fractionation studies, the heads of canine subjects were irradiated with epithermal neutrons in two or four fractions spaced 24 hr apart.

Initial assessment of these studies indicates that fractionation of BNCT does not result in significant repair of damage to normal brain as has been postulated. A third fractionation study was recently performed by WSU researchers to determine the effect of fractionation on uptake of boron by the skin. Four dogs were treated with four equal fractions. Although, from these pilot studies, fractionation of BNCT does not seem to be beneficial, further dosimetric and radiobiological studies may be necessary to fully evaluate the procedure. Considerable debate has ensued over the aspect of fractionated BNCT. This topic is discussed in some detail in the report.

Other studies performed by researchers during the past year include initial evaluation of BSH uptake by lung tumors. Results of these studies were not encouraging.

Computational Dosimetry

Development of the radiation transport in tissue (rtt) by Monte Carlo software module continued. A new version is being readied for beta testing by interested collaborators. This version contains several new features, has the proprietary code replaced, and is integrated with the planning environment software. The radiation-transport software has been tested by comparison with analytic solutions, results from other radiation transport software, and with measurements made in the Brookhaven Medical Research Reactor (BMRR) epithermal-neutron beam. The first human treatment was planned (and executed) for the Brookhaven National Laboratory (BNL) reactor in August 1994.

Neutron Source Design

BNCT research in the U.S. and Europe has been focused on the use of an epithermal-neutron beam to generate the necessary thermal neutron field in deep-seated treatment volumes. Therapeutically-useful epithermal-neutron beams for BNCT are currently generated by nuclear reactors. Various accelerator-based neutron sources for BNCT have been proposed and some low-intensity prototypes of such sources, generally featuring the use of proton beams and beryllium or lithium targets have been constructed. Scaling of most of these proton devices for therapeutic applications will require the resolution of some rather difficult issues associated with target cooling. Description of an alternate approach to the realization of a clinically-useful accelerator-based source of epithermal neutrons for BNCT that reconciles the often-conflicting objectives of target cooling, neutron beam intensity, and neutron beam spectral purity via a two-stage photoneutron production process is described in this report.

The First International Workshop for Accelerators for BNCT was hosted by the INEL. Meeting minutes can be obtained by contacting the editor.

Chemistry

Methods to determine the purity and quality of drugs to be used in BNCT, and a variety of analytical chemical analysis techniques for boron detection in biological samples have been discussed in previous years' annual reports. No additional results are presented this year. Several thousand biological samples were analyzed this year by the INEL Analytical Chemistry Group.

Measurement Dosimetry

During 1994, twelve dogs, labrador-cross and beagles, were irradiated at BMRR as part of a 4 fraction dose tolerance study. The animals were infused with BSH and irradiated daily, for 4 consecutive days. BNL researchers irradiated two beagles as part of their dose tolerance study using BPA fructose. Dose tolerance irradiations were performed on the right hemisphere at 3 megawatt (MW) using a 5 X 10-cm aperture contained in a 5-cm thick LiOH-polyethylene mask in the beam port.

In addition to the dose tolerance dogs, a tumor dog was irradiated at BMRR after an infusion of BPA fructose. The dog was irradiated with a conical aperture that was tapered from 16 cm, which faced the beam port, to 8-cm exit port, and was 12.7 cm thick. The animal was irradiated at 2 MW for 60 min for a desired dose of 10.5 Gy with an average boron concentration of 7.6 parts per million (ppm). The client dog irradiation was performed to simulate the dose received by a human patient of BNL.

Phantom Measurements

During August 1994, the flux and gamma dose profiles were measured in two phantoms exposed to the epithermal neutron beam at BMRR. These measurements were performed as a preparatory step to the commencement of human clinical trials now in progress at the BMRR. The measurements

were needed to benchmark the INEL Patient Treatment Planning software for the case where the new conical beam aperture developed by BNL is used. The measurement plan called for:

- Remeasurement of the flux and gamma profiles inside the cylindrical phantom with a 7.6-cm diameter cylindrical aperture. The cylindrical phantom and aperture were used earlier in the BMRR epithermal neutron beam to benchmark the planning software and this test was repeated to ensure that nothing has changed.

- Measurement of the new flux and gamma profiles in the same cylinder when the new conical aperture is used.

- Measurement of the flux and gamma profiles in a full head plus torso humanoid phantom using the BNL conical beam aperture.

Measurement of neutron beams remains an area of great interest, both for real-time as well as integrated measurements. Real-time measurements using fission chambers are discussed as are initial plans for human patient monitoring during treatment.

Database of Patient Information

Two separate efforts are underway to provide information storage and retrieval about BNCT patients. The first effort is to establish and maintain a database for patients from the U.S. who have had BNCT in Japan for malignant gliomas of the brain. This database will serve as a resource for the DOE to aid in decisions relating to BNCT research in the United States, as well as assisting the design and implementation of clinical trials of BNCT for brain cancer patients in this country. The database will also serve as an information resource for patients with brain tumors and their families who are considering this form of therapy. In order to better analyze the actual efficacy of BNCT as carried out by the Japanese investigators, an attempt has been made to determine the identity of all patients from the U.S. who have traveled to Japan for BNCT. Data will be independently verified for each patient; tumor pathology, various prognostic factors relating to treatment outcome, and a comparison made between the outcome (i.e., survival) of this patient group compared to a set of patients with similar tumor pathologies and prognostic variables who received conventional treatment in the United States. Initial results are presented herein.

A separate database of INEL BNCT information, the INEL Database of BNCT Information and Treatment (TIDBIT), has been under development for several years. Late in 1993 an assessment of the current implementation status determined that the user interface was unsatisfactory for the expected users and the data structures were out of step with the current state of reality. The team evaluated several tools that would improve the user interface to make the system easier to use, and implemented the product of choice. During 1994, TIDBIT got its name, underwent a complete change of appearance, had a major overhaul to the data structures that support the application, and system documentation was begun. A prototype of the system was demonstrated in September 1994, and is discussed in this report.

LOW DENSITY LIPOPROTEIN DEVELOPMENT AND EVALUATION

Dr. Stephen B. Kahl, Principal Investigator (PI) Department of Pharmaceutical Chemistry University of California, San Francisco (UCSF)

Although significant progress toward the application of boronated LDL for site selective boron drug delivery has been made during the past year, the loss of our animal and cell culture testing site at WSU has seriously hampered progress on this project. Results are reported of one in vivo biodistribution study in B16BL6-bearing mice and a series of in vitro studies that demonstrate very substantial uptake of boronated LDL in certain cell lines. The influence of 17α-ethinyl estradiol (EE) on cellular uptake has also been probed. Most significantly LDL loaded with HC was demonstrated to be taken up with exceptional aridity in several lines. Significant progress has also been made in the development of a rapid infrared analysis of boron in boronated LDL solution, which may be useful for clinical BNCT studies in Finland.

LDL Development—Background

The 1993 INEL BNCT Research Program Annual Report contained the essential details on the biochemical basis for using LDLs to deliver boron to cancer cells; the interested reader is referred to that publication for details.

LDL Development—In Vivo Studies

The results of one in vivo study were received in 1994. Mice bearing the B16BL6 murinic melanoma on the dorsal hip were given human LDL boronated with elaidyl carborane carboxylate (ECC). Single tail vein bolus injections of ECC-LDL in phosphate buffered saline (PBS) were used for administration of the drug complex. Five mice were sacrificed at each of five time points, and samples of blood, tumor, liver, and spleen were obtained. Boron analysis were carried out using inductively coupled plasma-atomic emission spectrometry (ICP-AES) at INEL.

Results of this study appear in Table 1 and confirm earlier observations that no selectivity of uptake for tumor over blood is observed in mice bearing this tumor. Administered boron dose in this study was 4,600 μg B/kg body weight, which is a dose similar to that which was reported in the 1993 annual report. The organ data for the present study are generally quite similar to those obtained in the earlier work. Boron clears the blood relatively rapidly, probably through uptake and metabolism by the liver. The lack of selective tumor uptake is most likely due to the animal model used. The B16Bl6 tumor cell line apparently retains its capacity to over-express the LDL receptor (vide infra) in cell culture, but when these cells are placed in mice, the solid tumor does not take up LDL boron in a selective fashion. It is postulated that this phenomenon arises from the use of normal mice as the

Table 1. In vivo LDL exposure in mice ECC-LDL = 4,600 μg B/kg.

	Tissue boron concentration (μg/g)				
	12hr	18hr	24hr	48hr	72hr
Tumor	2.9±0.8	1.7±0.9	2.5±1.0	0.9±0.2	0.7±0.1
Blood	2.8±0.8	1.8±0.3	1.3±0.8	0.9±0.1	0.8±0.1
Liver	6.9±0.9	3.8±0.6	3.5±1.0	0.9±0.3	0.5±0.1
Spleen	4.8±0.5	2.7±0.5	3.0±0.5	1.0±0.3	0.7±0.1

model animal. Although the murine LDL receptor recognizes the human Apo B-100 protein found on the surface of ECC-LDL, the mouse does not use LDL as its primary cholesterol transport system. Thus it might be expected that tumor boron delivered by LDL would not be especially high. It is suggested that nude mice bearing a human tumor would be a better model system.

LDL Development—In Vitro Studies

In order to confirm that the B16BL6 cell line continues to over-express the LDL receptor and to compare it to other cell lines, a series of in vitro incubations was carried out. In each series, cells were incubated with boronated LDL containing ECC for 6, 12, or 24 hr. Cells were spun down to separate the cell pellet from the supernatant incubation medium. Both cell pellet and supernatant were analyzed for boron by ICP-AES at INEL. Six replicate incubations were used for each time point with each of the cell lines.

Table 2 presents the cell pellet boron concentrations for an incubation in which the boron concentration in the medium was 1.40 μg B/mL. (Supernatant boron levels are not shown for sake of clarity; all values were close to the incubation concentration value of 1.40 μg/g). The values obtained are quite substantial for the three cancer cell lines, especially so considering the very low exposure concentrations. The B16BL6 and RG-2 boron levels at 24 hr represent a 20-fold concentration of boron relative to medium while the Lewis lung line exhibits a 9-fold increase. The low levels for murine fibroblasts are as expected since this line represents a "basal" or normal LDL receptor active line.

It was also of interest to evaluate the influence of 17a-EE on ECC-LDL uptake. This drug has been reported to increase LDL receptor activity in women with type II hyperlipoproteinemia. For this study, cells were pretreated with EE for 12 hr followed by incubation with ECC-LDL for the times indicated. The incubation boron concentration was the same as that used in Table 2, 1.40μg B/mL and these data are shown in Table 3.

In every case, the cells pretreated with EE showed the same degree of boron uptake as those not treated (see Table 1). From these data, it is clear that treatment of these cells in culture with 17α-EE does not result in increased boron uptake.

It has also been of interest to determine whether LDL loaded with other boron compounds would behave similarly to ECC-LDL. ECC is a carborane ester of an unnatural fatty alcohol, which must be synthesized for this purpose. Although the synthesis is straightforward and gives high yields, the use of a commercially available polyhedral carborane possessing high lipophilicity might be a desirable characteristic. Previous work at UCSF had shown that certain polyhedral carboranes bearing alkyl or

Table 2. In vitro LDL exposure ECC-LDL = 1.40 μg B/mL.

	Cell pellet boron concentration (μg/g)		
	6 hr	12 hr	24 hr
Murine melanoma (B16BL6)	5.9 ± 0.2	13.5 ± 0.1	27.8 ± 1.9
Murine carcinoma (Lewis lung)	4.2 ± 0.6	8.2 ± 0.6	12.7 ± 1.0
Rat glioma (RG-2)	5.9 ± 0.9	14.5 ± 1.5	29.5 ± 4.1
Murine fibroblast	1.1 ± 0.3	2.0 ± 0.1	3.6 ± 0.7

Table 3. In vitro LDL exposure ECC-LDL = 1.40 μg B/mL.

	Cell pellet boron concentration (μg/g)		
	6 hr	12 hr	24 hr
Murine melanoma	6.5 ± 0.3	14.1 ± 0.8	27.7 ± 1.8
Murine carcinoma	5.7 ± 0.8	8.1 ± 0.7	11.9 ± 0.4
Rat glioma	5.6 ± 1.8	15.6 ± 5.8	27.1 ± 3.8
Murine fibroblast	1.0 ± 0.2	1.9 ± 0.4	2.9 ± 0.5

alkene functional groups could be reconstituted into LDL with high efficiency. Of these, HC was chosen for a series of in vitro experiments. This molecule incorporates into LDL to give much higher boron/protein ratios than ECC. In general, HC gives a ratio of about 0.8 while ECC gives a ratio of about 0.2. However, the absolute protein values from HC reconstitutions are generally only ~50% of those from ECC reconstitutions. This suggests that HC interferes in some manner with the Apo B-100 protein and, perhaps, gives reconstituted particles, which are fundamentally different from those containing ECC.

The results of one such study are presented in Table 4. The boron content of the incubation medium was measured to be 4.70 μg B/mL.

These results are quite unexpected and show truly enormous levels of intracellular boron. The 24-hr boron constant of B16BL6 cells is almost 30% greater than previously observed in V-79 cells exposed to almost five times as much boron in the form of ECC-LDL. The results with Lewis lung carcinoma cells and rat glioma cells are not as spectacular but are still very substantial, and suggest that hexyl carborane-loaded LDL may well prove useful. However, the results obtained with murine fibroblasts cast some doubt on these experiments. These cells have been observed previously to take up only minimal amounts of ECC-LDL (see Tables 2 and 3, for example), and the very high uptake seen here suggests that both receptor and nonreceptor mediated uptake contribute substantially. These results may reflect changes in the morphology of the HC-LDL particles relative to ECC-LDL. Further experiments are underway to compare the two types of LDL particles.

Table 5 presents the results of another incubation with HC-LDL, this time in the presence of EE (vide supra). On this case comparison of the results from Table 5 with Table 4 suggests that EE has a negative effect on HC-LDL uptake in B16BL6 cells and no effect in the others.

Table 4. In vitro LDL exposure HC-LDL = 4.70 μg B/mL.

	Cell pellet boron concentration (μg/g)		
	6 hr	12 hr	24 hr
Murine melanoma	143.6 ± 7.9	152.9 ± 8.2	308.5 ± 37.9
Murine carcinoma	19.9 ± 11.3	30.9 ± 12.4	34.5 ± 17.7
Rat glioma	51.9 ± 14.7	82.6 ± 24.8	67.5 ± 9.8
Murine fibroblast	46.5 ± 5.4	60.6 ± 17.8	41.1 ± 11.5

Table 5. In vitro LDL exposure HC-LDL = 4.70 μg B/mL.

	Cell pellet boron concentration (μg/g)		
	6 hr	12 hr	24 hr
Murine melanoma	71.7 ± 5.3	78.5 ± 34.9	218.0 ± 80.5
Murine carcinoma	22.5 ± 5.0	29.6 ± 7.1	22.5 ± 8.2
Rat glioma	58.5 ± 9.8	130.7 ± 24.0	70.1 ± 8.2
Murine fibroblast	40.0 ± 7.5	47.8 ± 8.4	37.0 ± 6.9

LDL Development—FTIR boron analysis

Moore et al.[1] have recently published the results of a study in which they demonstrated that Fourier transform infrared spectrometry (FTIR) could be used to quantify boron in solution or in liposomes. The technique is based on the very strong infrared absorption of the BH group at ~2,600 cm^{-1}. This region of the infrared is generally free of other common absorptions that might interfere. Extension of this technique to quantify boron in LDL solutions would provide workers with a rapid and accurate alternative to prompt gamma and ICP-AES techniques. Infrared instruments capable of this analysis are much more common than ICP-AES and cost only ~25% as much.

The protocol developed was as follows. Stock solutions of HC were made by appropriate dilutions of a 50 mg standard solution of HC in 10 mL of carbon tetrachloride. The BH absorbance of each solution was measured on a Nicolet 400 FTIR equipped with QUANT-IR software. A resolution of 8 cm^{-1} was used and 128 scans were collected for each sample. A variable pathlength cell with calcium fluoride windows was used to record all spectra. In this experiment, a pathlength of 0.5 mm was found to be ideal. A spectrum of pure CCl4 was used for background subtraction.

The standard curve obtained is shown in Figure 1. The linearity of this curve is exceptional especially considering the range of HC concentrations used.

Following construction of the standard curve, a sample HC-LDL was examined. A 0.1-mL sample

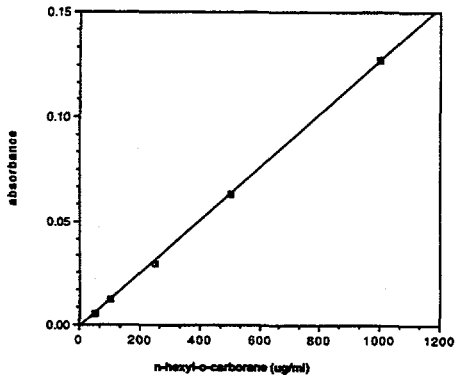

Figure 1. Standard curve for HC infrared absorbance.

of HC-LDL solution in PBS was diluted with 0.9 mL PBS (pH 7.4, 5 mM phosphate, 0.9% sodium chloride). To this was added 2 mL of a 1:1 mixture of chloroform: methanol. The resulting emulsion was centrifuged for 1 min @ 3,500 revolutions per minute (rpm), the lower (organic) layer was collected, and the upper (aqueous) layer was subjected to two further extractions with chloroform. The combined organic extracts were evaporated to dryness at 35°C on a rotary evaporator and the residue was dissolved in 1 mL of carbon tetrachloride. This sample was then used to record the FTIR absorption. Comparison with the standard curve gave a boron content of 419 μg B/mL. An independent ICP-AES value for this sample is not available for comparison, but this value is approximately what would be expected for an HC-LDL sample having the associated protein content. Efforts are currently underway to obviate the extraction step and introduce the LDL sample directly as an aqueous solution.

BORONATED LIPOSOME DEVELOPMENT AND EVALUATION

Dr. M. Frederick Hawthorne, PI, Department of Chemistry and Biochemistry, University of California at Los Angeles (UCLA)

The boronated liposome development and evaluation effort consists of two separate tasks. The first is the development of new boron compounds and the synthesis of known boron species with BNCT potential. These compounds are then encapsulated within liposomes for the second task, biodistribution testing in tumor-bearing mice, which examines the potential for the liposomes and their contents to concentrate boron in cancerous tissues.

The team at UCLA (Dr. Kenneth Shelly and Dr. Debra Feakes, with graduate students Rachel Watson-Clark and John Morales) under the direction of Dr. Hawthorne continues to develop new boron chemistry to produce a variety of boron agents with BNCT potential. These researchers also produce the boron-containing liposomes for biological screening experiments that demonstrate the efficacy of boron localization in tumor-bearing mice. Initial liposome biodistribution experiments were performed under the direction of Dr. Gary Fujii at Vestar, Inc. (a private firm specializing in the pharmaceutical applications of liposomes), San Dimas, CA, with the assistance of Teresa Krisch, A.H.T. Further murine experiments with liposomes were performed at WSU by Dr. Patrick Gavin (RG2 intracranial glioma in rats).[2] Additional liposome characterization and fluorescence studies are performed at the State University of New York at Buffalo by Dr. Robert Straubinger.

Background

One of the more pressing problems in BNCT has been the development of effective strategies for the selective localization of boron within tumor tissue. The primary difficulties to be overcome are specific delivery of therapeutic quantities of boron to tumor, while avoiding normal tissues, and the potential toxicity of the boron agent delivered. Liposomes have been studied extensively as drug delivery systems, and as such they present a novel approach for the solution to these problems as well as presenting a new and innovative method for the delivery of boron for BNCT.

Liposomes (small unilamellar vesicles) are microscopic spheroidal structures composed of a phospholipid bilayer membrane enclosing an aqueous core (Figure 2). The utility of liposomes as drug delivery systems arises from their ability to encapsulate aqueous solutions of water-soluble compounds in the aqueous core or to accommodate hydrophobic compounds within the lipid membrane. The liposomal delivery of drugs, when successful, has several attractive consequences. Sequestering the effector species in vesicles can provide it with an extended circulation lifetime, thereby increasing its opportunity to be taken up by tissue. The liposome also offers protection for the occluded species from attack by normal physiological agents in vivo and reduces potential toxicity effects (the liposome constituents themselves are nontoxic). Liposomes have been demonstrated to deliver their contents directly to the interior of cells, where their therapeutic utility is maximized. Since both tumor cell-selective delivery and cell entry is provided by the liposome, the encapsulated species need not have a natural affinity for the targeted tumor cells, thus making this method amenable to a wide variety of effector molecules.

Previous research at UCLA has demonstrated that liposomes are a viable boron delivery system for BNCT. Liposomes were shown to be capable of encapsulating polyhedral borane anions, as their soluble sodium salts, in the high concentration required to deliver a sufficient quantity of boron in a reasonable dose volume. These high concentrations, while much greater than those normally employed in liposomes, were encapsulated in stable liposomes, which demonstrated only negligible leakage over a period of months. The extended circulation lifetime and tumor selectivity provided by the liposomes permitted the use of relatively small injected doses of boron to produce significant boron concentrations in tumor. The

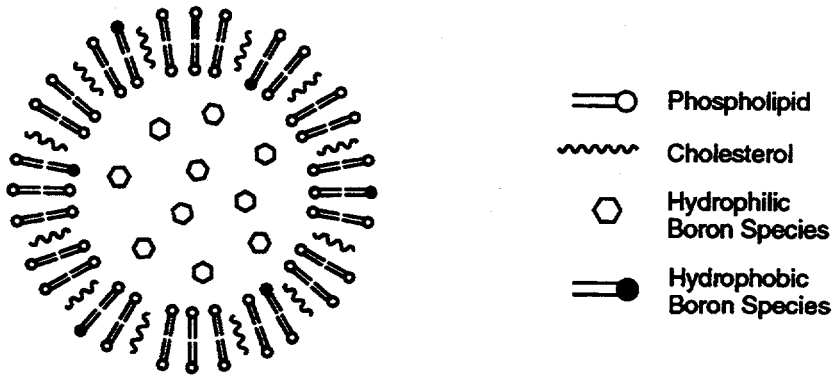

Figure 2. Diagram of a unilamellar vesicle.

relatively simple polyhedral borane anions that were initially studied normally exhibit brief circulation lifetimes and virtually no tumor selectivity as free species. These same agents were selectively delivered to tumors in mice after encapsulation in liposome carriers. Perhaps the most significant finding of this early work was the importance of intracellular chemical reactivity of the delivered boron species. Although simple, inert, nonspecific boron species were selectively delivered by the liposome to tumor cells, they were rapidly excreted since they presented no innate chemical reactions that could be used to bind them to the tumor cell interior. Excellent results have now been achieved with boron compounds equipped with the ability to chemically react with intracellular components, thereby anchoring the boron within tumor cells.

Recent developments in boronated liposome research have been centered upon the following topics: (a) continued development and scale-up of the most successful candidate boron species, (b) synthesis of new boron-containing compounds expected to exhibit the most favorable features of efficacious boron species, (c) the biological testing of these compounds, incorporated in liposomes, in expedient preliminary screening experiments using mice and rats to determine tumor delivery and retention of boron, and (d) intracellular distribution and mechanistic studies with liposomes labeled with fluorescent markers.

Compound Development

Research into water-soluble species during the past year was concentrated upon the production of boron-rich species derived from the $[B_{20}H_{18}]^{2-}$ ion, which was first synthesized in Hawthorne's laboratory 30 years ago.[3] This ion was chosen for its high boron content, ease of preparation, stability, and rich derivative chemistry related to its propensity to react with nucleophiles and to undergo redox reactions.

Nucleophilic attack of $[B_{20}H_{18}]^{2-}$ by the amide anion, $[NH_2]^-$, produces an apical-equatorial species, $[ae\text{-}B_{20}H_{17}NH_3]^{3-}$, which has demonstrated one of the most promising murine biodistributions thus far observed. These strikingly favorable biodistribution results have been attributed to a facile intracellular oxidation of $[ae\text{-}B_{20}H_{17}NH_3]^{3-}$ to the reactive $[B_{20}H_{17}NH_3]^-$. The oxidized product is, in turn, capable of reaction with nucleophilic intracellular moieties, thus providing a means of retaining the compound within the tumor cell.

Continued investigations into the chemistry of $[ae\text{-}B_{20}H_{17}NH_3]^{3-}$ have produced several related amine derivatives which exhibit the same potential for liposomal delivery as the parent compound. Other ammonio derivatives that have been synthesized include the apical-apical isomer of the parent amine, $[a^2\text{-}B_{20}H_{17}NH_3]^{3-}$, as well as analogs that

contain $-NH_2CH_3$, $-NH(CH_3)_2$, $-NH_2(CH_2)_2CH_3$, $-NH_2NH_2$, and $-NH_2(CH_2)_2NH_2$ substituents. The propylammonio derivative $Na_3[ae\text{-}B_{20}H_{17}NH_2(CH_2)_2CH_3]$ has been encapsulated within liposomes and its biodistribution in mice has been determined.

Another avenue of chemistry under investigation involved the synthesis and reactions of various isomers of $[B_{20}H_{17}NCO]^{4-}$, which is made from $[B_{20}H_{18}]^{4-}$. During the course of these studies, the molecular structure of one isomer of $[B_{20}H_{19}]^{3-}$ was determined by x-ray crystallography.[4] The structure of this anion, shown in Figure 3, is of great interest for two reasons. First, the nature of $[B_{20}H_{19}]^{3-}$ has been a matter of speculation since it was first isolated over 30 years ago, despite numerous attempts to determine its crystalline structure. Second, most substituted $[B_{20}H_{18}]^{4-}$ ions can be protonated in the same manner, and the structure of the parent $[B_{20}H_{19}]^{3-}$ ion should offer valuable insight into the reactions and mechanisms of its derivatives. In the structure of $[B_{20}H_{19}]^{3-}$ shown in Figure 3, the boron-boron distance between the two boron cages is 1.94 Å, which is significantly longer than the 1.70 Å distance seen for the B-B bond in $[B_{20}H_{18}]^{4-}$. The bridging hydrogen is displaced from the B-B vector, forming a B-H-B angle of 91 degrees. The remainder of the bond lengths are fairly normal for decahydrodecaborate cages.[5]

A water-soluble, neutral carborane derivative, *closo*-1-$CH_2OCH[CH_2OCH(CH_2OH)_2]_2$-1,2-$C_2B_{10}H_{11}$, had been reported by Yamamoto et al. (*Journal of Organic Chemistry and* 5th International Symposium on NCT). This compound was of great interest because it is uncharged and therefore has no counterions. It is presumably lipophilic, but it was reported to have a very high water solubility. The in vivo behavior of such a species could be very interesting and might indicate a potential candidate for liposomal delivery and other applications.[6] The above polyol, *closo*-1-$CH_2OCH[CH_2OCH(CH_2OH)_2]_2$-1,2-$C_2B_{10}H_{11}$, was synthesized in the Hawthorne laboratory for investigation. This polyol was found to be much less soluble than was reported. Notification has been sent to the authors,who have agreed to submit a correction to the *Journal of Organic Chemistry.*

The initial lipophilic boron compound investigated in the Hawthorne laboratory, K[*nido*-7-$[(CH_2)_{15}CH_3]$-7,8-$C_2B_9H_{11}$], is characterized by a hydrophilic head group (the *nido*-carborane) substituted with one 16-carbon hydrophobic tail anchored to the boron cage. The resulting liposomes were studied in vivo and proved to be very promising, but they were limited by a low degree of incorporation within the liposome membrane (vide infra). Presumably, a boron compound,

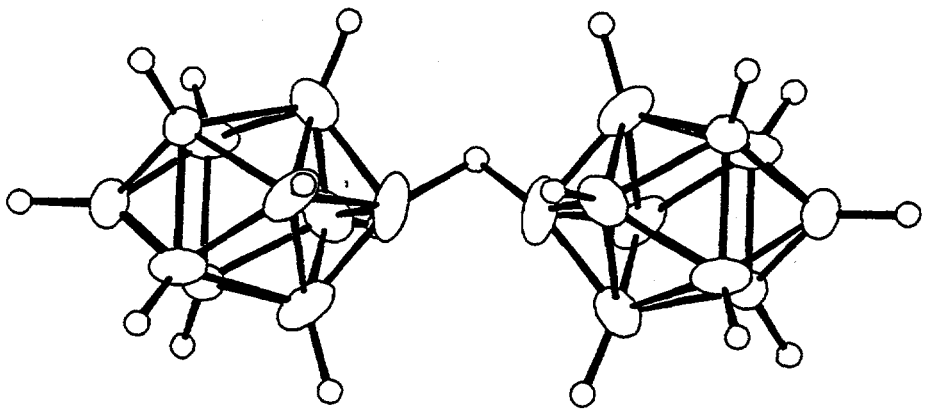

Figure 3. Molecular structure of $[B_{20}H_{19}]^{3-}$.

which more closely resembles a liposome bilayer constituent, could be incorporated within the bilayer at a higher concentration without affecting the liposome stability.

The synthesis of a boron-containing phospholipid analog is outlined in Figure 4. The target compound retains the same overall structure as a phosphtadylcholine lipid (the same lipid normally employed), but appends two carborane cages at the ends of the fatty acid tails. Figure 4 depicts the successful synthesis of a carborane-containing lipid with 14-carbon chains; other syntheses have produced a lipid with carboranes on the end of two 11-carbon chains, and a lipid analog with only one carborane cage at the end of one of the fatty acids. To date, none of these lipid analogs have been studied as components of a liposome bilayer.

Liposome Encapsulation and Biodistribution Results

Since January 1993, a total of 14 screenings have been completed using six compounds and two tumor lines. Screenings with EMT6 murine adenocarcinoma were performed at Vestar, Inc. and in the laboratory of Dr. Patrick Gavin at WSU, who also performed screenings in rats bearing intracranial RG2 glioma tumors. Mechanistic studies using liposomes labeled with fluorescent species have been performed using rats bearing intracranial 9L tumors in the laboratories of Dr. Robert Straubinger of the State University of New York at Buffalo.

The biodistribution of liposomal $Na_3[ae\text{-}B_{20}H_{17}NH_2(CH_2)_2CH_3]$ was obtained to demonstrate the viability of alkylammonio analogs of $Na_3[ae\text{-}B_{20}H_{17}NH_3]$, which is the most promising

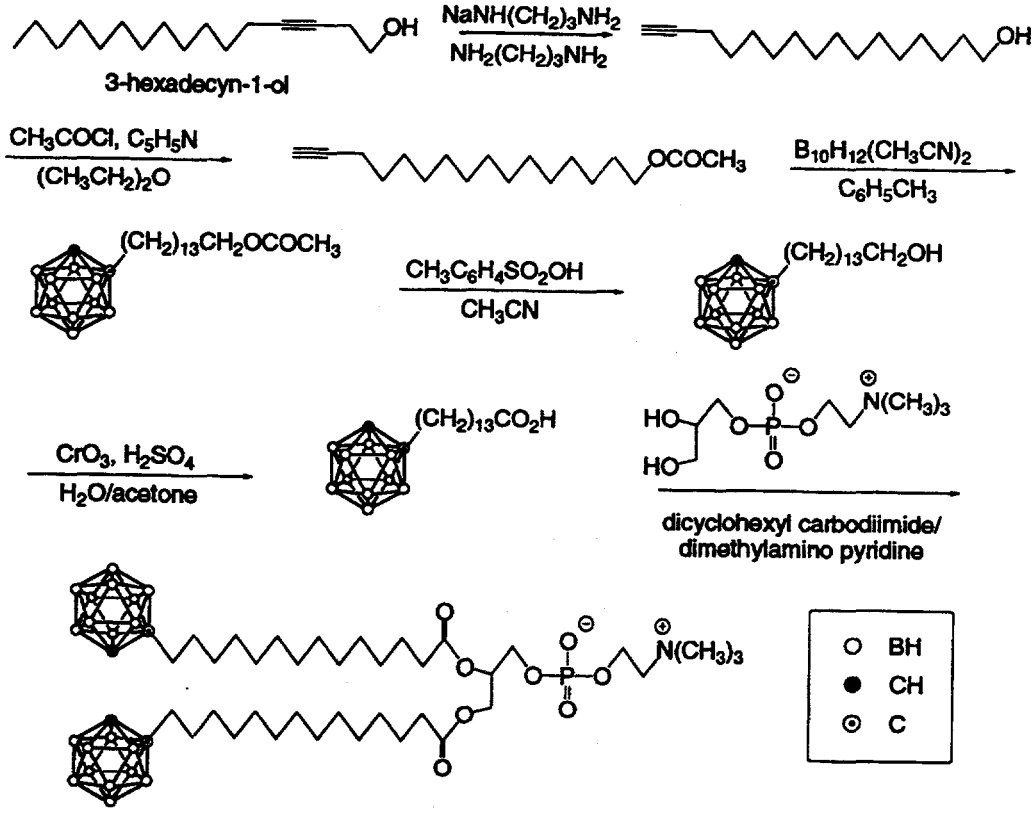

Figure 4. Synthesis of boronated phospholipid analogues containing two *closo*-carboranes at the termini of the lipophilic chains.

compound previously studied. Liposomes encapsulating the propylammonio derivative produced the biodistribution in mice is shown in Figure 5A. These liposomes (injected dose 16 mg/kg body weight) exhibited the same favorable characteristics of tumor accretion and retention observed with the parent ammonio derivative. The highest tumor-boron concentration measured was 36 μg B/g tumor at 30 hr, decreasing to 28 ppm at 48 hr at which time the tumor/blood ratio reached 3.8. These results suggest that many other substituted ammonio derivatives will exhibit the desired characteristics of the parent [*ae*-$B_{20}H_{17}NH_3$]$^{3-}$ and that the ammonio functionality may be employed to link this boron-rich anion to other organic groups without decreasing the efficacy of the system.

Several experiments were performed to investigate the effect of the composition of the lipid bilayer on the biodistribution of liposomes. For the first of these, the lipophilic compound K[*nido*-7-[$(CH_2)_{15}CH_3$]-7,8-$C_2B_9H_{11}$] was embedded within the liposome bilayer at a concentration of 30 mole%. This species had been successfully employed previously at 15 mole%, but the greater degree of incorporation could lead to higher boron delivery. The biodistribution of liposomes containing 30 mole% K[*nido*-7-[$(CH_2)_{15}CH_3$]-7,8-$C_2B_9H_{11}$] in the liposome bilayer is shown in Figure 5B (10 mg B/kg body weight). Compared to previous experiments with K[*nido*-7-[$(CH_2)_{15}CH_3$]-7,8-$C_2B_9H_{11}$], the increased boron dose provided did not translate to higher tumor delivery. As can be seen from the low blood boron values, these liposomes exhibited a circulation lifetime too short to allow for adequate boron delivery to the tumor.

Two other experiments examined the use of an altered phospholipid mixture for the bilayer. For most of the liposome preparations previously investigated, an equimiolar mixture (1:1) of phospholipid and cholesterol was employed. Another commonly used lipid ratio, 2:1 phospholipid/cholesterol, was examined to determine if it could enhance the biodistribution characteristics observed earlier. Two liposomal formulations that employed this lipid mixture were examined: one encapsulated aqueous Na_3[a^2-$B_{20}H_{17}NH_3$] (Figure 5C, 7 mg B/kg body weight), and the other encapsulated Na_3[a^2-$B_{20}H_{17}NH_3$] with K[*nido*-7-[$(CH_2)_{15}CH_3$]-7,8-$C_2B_9H_{11}$] embedded within the liposome bilayer (Figure 5D, 15 mg B/kg body weight). Both biodistributions approximate the expected liposomal behavior, considering the injected dose employed. However, neither represents a significant improvement over the results observed with the lipid formulation normally employed.

Liposomes containing boron compounds have been produced on a large scale (approximately 350 mL), demonstrating their potential use for investigations with large animals or humans. A large preparation of liposomes containing K[*nido*-7-[$(CH_2)_{15}CH_3$]-7,8-$C_2B_9H_{11}$] was investigated in a murine biodistribution experiment in order to compare the results between a small-scale and large-scale liposome preparation. The liposomes produced on a large scale presented a boron dose of 7 mg B/kg body weight for mice, and the results are presented in Figure 5E. The tumor boron values were nearly as high as those seen with small-scale vesicle preparations with the same compound, and the other tissues (blood, liver, and spleen) showed excellent clearance of boron.

The boron biodistribution results presented above were determined by the macroanalysis of bulk tissue samples and are not reliable indicators of the microdistribution of boron. However, the delivery of boron by liposomes to the tumor cell interior was strongly suggested by the sustained retention of boron in the tumor mass long after the clearance of boron from the blood. The efficiency of BNCT is amplified when the neutron capture event takes place in close proximity to the tumor cell nucleus. Therefore, an important aspect of compound evaluation is the determination of the microdistribution of boron within the tumor mass, which is characteristically afforded by the subject compound. Additional experiments have been performed to examine this microdistribution.

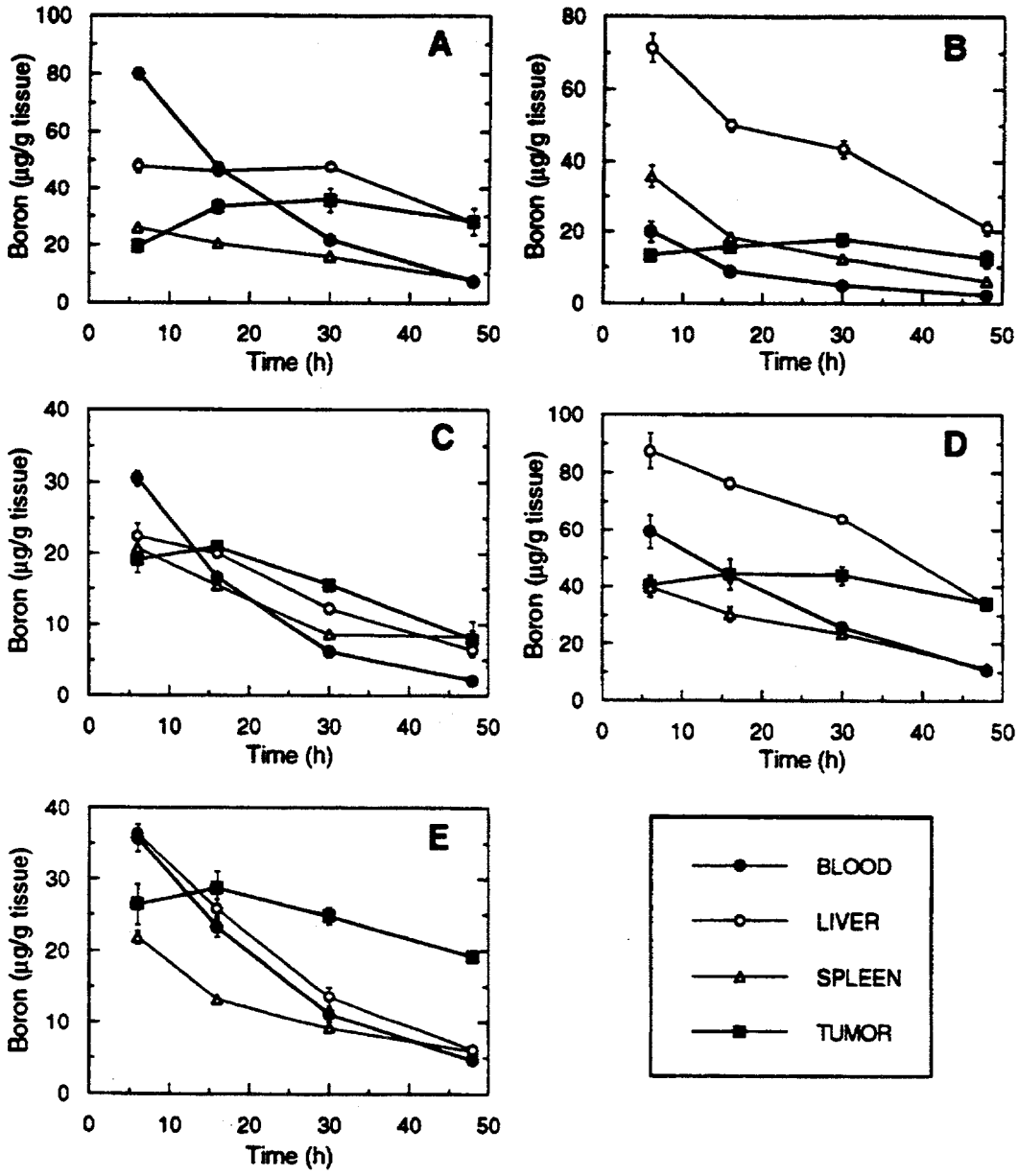

Figure 5. Time course biodistribution of boron delivered by liposomes in BALB/c mice.

In order to monitor liposome localization, two fluorophores were employed: a water-soluble species for the aqueous core (fluorescein-dextran, green fluorescence) and a phospholipid-derived compound to mark the bilayer membrane (rhodamine dihexadecylphosphatidylethanolamine, or rhodamine DHPE, red fluorescence). These two compounds fluoresce at different wavelengths, and therefore they can be followed separately and simultaneously. Two types of liposomes were examined as described below. One type of vesicles contained encapsulated $Na_3[a^2\text{-}B_{20}H_{17}NH_3]$, and the other type contained 15 mol% $K[nido\text{-}7\text{-}CH_3(CH_2)_{15}\text{-}7,8\text{-}C_2B_9H_{11}]$ embedded in

the bilayer. Each of these liposome preparations included 1 mol% rhodamine-DHPE in the lipid bilayer and 1% fluorescein-dextran dissolved in the aqueous core.

Cell cultures of 9L rat glioma were separately exposed to suspensions of the two liposome preparations described above for 24 hr and then washed free of unbound liposomes. The cells were then fixed and examined by scanning confocal microscopy. Cells exposed to the liposomes that encapsulated $Na_3[a^2\text{-}B_{20}H_{17}NH_3]$ exhibited both strong red and green fluorescence, with punctations evenly distributed throughout the cytoplasm. Cells that had been incubated with the liposomes incorporating $K[nido\text{-}7\text{-}CH_3(CH_2)_{15}\text{-}7,8\text{-}C_2B_9H_{11}]$ also exhibited strong red and green fluorescence. These cells exhibited a perinuclear accumulation of punctate fluorescence.

The same liposomal preparations were also examined in vivo. Tail vein injections of liposomes were administered to Fischer 344 rats bearing intracranial 9L tumors. Although these experiments could not be performed at the same resolution of the in vitro experiments, two important conclusions can be drawn from the images: (1) there is clear evidence of local extravasation of fluorescent liposomes into the tumor, and (2) no fluorescence could be detected in the normal brain tissue.

These studies do not provide a direct indication of the microdistribution of boron, only of the fluorescent labels, but they clearly indicate that the liposome bilayer and the encapsulated aqueous solution are both delivered to the interior of the tumor cells. This result should be observed only when intact liposomes are taken within the tumor cells by endocytosis, as has been observed for other systems. This, in turn, is a strong indication that boron compounds are delivered intracellularly by the liposomes.

Conclusion

Further investigation of the synthesis and chemistry of $Na_3[ae\text{-}B_{20}H_{17}NH_3]$ has produced several more promising candidates for liposomal delivery. Biodistribution and other data have confirmed that these amine derivatives have great potential as BNCT agents. In addition, new lipophilic bilayer addends have been developed that can provide an increased boron dose for delivery by liposomes. Furthermore, clear evidence of the intracellular uptake of hypertonic, boron-containing liposomes has been obtained both in vitro and in vivo.

BOROCAPTATE SODIUM (BSH) TOXICITY ISSUES

Dr. Tom LaHann, PI, College of Pharmacy, Idaho State University (ISU)

Since BNCT will require interstate commerce, Food and Drug Administration (FDA) approval of a new drug application (NDA), a new device exemption (NDE), or both, will be required. FDA approval is contingent upon the sponsor demonstrating that the drug, radiation, and drug-radiation combination are reasonably safe and that the drug-radiation combination is effective for its intended application. The definition of reasonable safety is influenced by the risk of available alternatives, including the risk associated with not undertaking the treatment. With GBM, the risk associated with not undergoing BNCT is roughly a 97% chance of dying from the cancer within 5 years. It seems likely that given the high probability of death in the absence of BNCT, a moderate risk associated with BNCT will be acceptable, as long as the risk is reasonably well defined.

Initial clinical evaluations are likely to employ BSH doses similar to those used in Japan and Europe, i.e., BSH doses no greater than 100 mg/kg (maximum boron dose: 56 mg/kg). Clinical efficacy studies (BSH + neutron radiation) using a BSH dose of 100 mg/kg and an epithermal neutron source are expected to demonstrate a high-quality life extension and/or a cure rate superior to that achieved by the Japanese thermal neutron treatments. Theoretical calculations indicate that the efficacy of BNCT should dramatically increase with increasing BSH dose and the related increase in tumor levels of boron. Clinical studies will be necessary to validate theoretical predictions, but before these studies can be initiated, extensive animal testing will be required to determine the maximum dose of BSH likely to be safe.

ISU's Center for Toxicology Research has been conducting preclinical toxicity testing of BSH to aid in assessing if proposed human studies of BSH (absent neutron radiation) are likely to be acceptably safe. BSH has been administered clinically in both Japan and Europe (typically at BSH doses less than 100 mg/kg). European and Japanese experience suggests that single dose administration of BSH in amounts less than 100 mg/kg is not typically associated with serious adverse effects, at least in the clinical populations evaluated to date. Available data suggest that: (a) single doses of BSH up to 100 mg/kg are reasonably safe for healthy volunteers, (b) before studying the action of BSH in tumor patients, animal studies are needed to determine how concomitant administration of commonly used drugs might influence BSH toxicity and how reduced renal function affects BSH toxicity, and (c) that before BSH fractionation or dose escalation studies (i.e., BSH doses above 100 mg/kg) can be undertaken, more animal toxicity information is needed.

BSH Interactions with Other Biological Agents

BSH binds to plasma proteins; initial reports suggested possible covalent binding between serum proteins and BSH, but the more recent work of Bauer et al.,[7] argues for noncovalent binding interactions and fast exchange between bound and unbound BSH. Current estimates suggest that at therapeutic concentrations, 50–70% of BSH may be bound to serum albumin. The binding of BSH to plasma proteins raises the concern that BSH administration may displace other protein bound drugs, increase the free (unbound) fraction of these drugs, and so produce clinically significant side effects. Cancer patients frequently receive glucocorticoids, anticonvulsants, sedative-hypnotics, and diuretics; thus the effect of BSH on the plasma protein binding of these agents is of concern. Few in vivo functional studies and no in vitro binding studies of BSH-drug interactions are available. Data from two Japanese clinical pharmacokinetic studies of BSH show an initial half-life for blood boron of 6-8 hr, but a much slower beta-phase half-life, with low blood boron levels still being detectable 14 days after administration of BSH. The fact that 90% of blood boron was cleared from human volunteers within 20 hr (BSH doses of 46–60 mg/kg) supports animal and in vitro data suggesting noncovalent binding and fast exchange between bound and free drug.

ISU's functional studies of BSH-drug interactions in rats indicated that BSH rapidly and effectively reverses respiratory paralysis induced by neuromuscular junction blocking drugs; it also reverses the ability of propranolol (beta adrenergic antagonist) to block the vascular action of dobutamine (beta adrenergic agonist). Reversal of the biological actions of these drugs probably reflects BSH binding to the exogenous drug, reducing free drug concentrations to ineffectual levels. This ability to rapidly reverse the effect of multiple drug classes is highly unusual and perhaps even unique and, in addition to the obvious drug interaction issues, leads to the question: "If BSH binds exogenous drug substances with high enough affinity to cause changes in physiological function, then might BSH not bind endogenous substances with equal affinity and with equal consequence?" It may be that truly free BSH does not exist in the blood; rather BSH may exist primarily as a complex with other low molecular weight substances present in blood. Thus, BSH toxicity and pharmacokinetics may be altered by preadministration of drugs, and treatment with other drugs or alterations in diet could result in unexpected effects on toxicity or efficacy. Formation of different complexes may explain the interspecies and intraspecies variability already observed for the pharmacokinetic and toxicity profiles of BSH, since the physicochemical nature of the BSH-chemical complexes would likely determine their distribution and thus their propensity for eliciting adverse effects. In preliminary studies to examine this issue, rats were first infused with fructose (162 mg/kg), methylene blue (60 mg/kg), n-acetylcysteine (162 mg/kg) or reduced glutathione (GSH) (554 mg/kg), and then with BSH (200 mg/kg). Tissue distribution of boron was compared to that in animals receiving only BSH. While emphasizing that available results are still preliminary, it appears that preadministration of selected compounds can markedly alter tissue distribution of BSH-boron. Prior administration of methylene blue doubled tissue distribution to some body compartments, while having little affect on boron distribution to other compartments and markedly reducing distribution to still other compartments. Prior administration of GSH seemed to dramatically reduce boron concentrations in all tissues examined. In most experiments, at least 70% of the total boron dose could be accounted for. With GSH preadministration, <25% of the total boron dose could be accounted for; fat was not sampled. Additional experimentation is required to determine if complex formation is an important determinant of BSH distribution and toxicity, but if it is, the related question of how the presence of concomitantly administered therapeutic agents influences the formation of BSH complexes will be important. In this regard, the recent report of Joel et al.,[8] is of interest. These investigators found that prior infusion of GSH markedly increased tumor uptake of BSH.

A second concern revolves around literature reports suggesting that BSH (and other boron compounds) bind to blood cells. ISU researchers found that BSH exhibits dose-dependent binding to blood cells (Figure 6). BSH binding to erythrocytes and platelets is of concern because such binding may cause cellular agglutination and/or cell lysis. Cell lysis could elevate blood potassium concentrations, precipitating cardiac arrhythmias. Cardiac arrhythmias are the primary cause of death following high

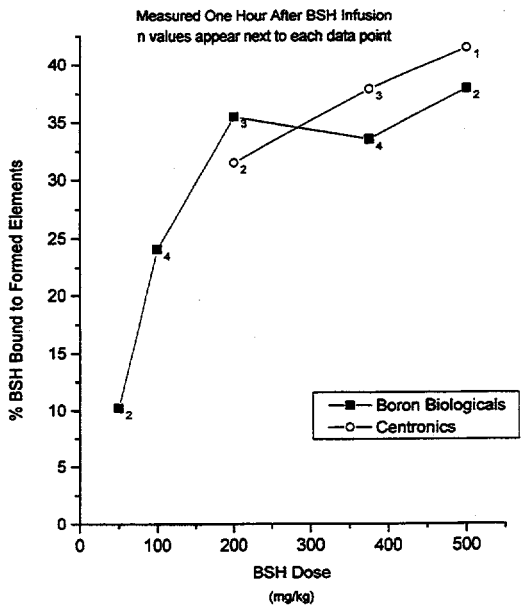

Figure 6. Boron binding to blood cells (x ± SEM).

dose infusion of BSH and seem to be temporally associated with high plasma potassium levels. BSH-mediated cell agglutination could block small capillaries, reduce blood flow to critical organs, and cause delayed tissue damage secondary to poor perfusion. Such an effect might explain observed damage to liver and kidney tissue.

Acute Toxicity Issues Associated with BSH Metabolites/ Contaminants

BSH Contaminants—BSH Lethality as a Function of Manufacturer

ISU researchers have previously reported (1993 Annual Report) that acute administration of BSH doses of 200–375 mg/kg can kill rats. Some investigators have expressed concern that the experiments may be quantifying the toxicity of BSH contaminants, rather than the toxicity of BSH. If this were the case, differences would be expected in lethality between lots of BSH with qualitative and quantitative differences in the contaminants present. The odor of BSH differs from lot to lot and even within lots (BSH of the same lot is packaged in 1 gram vials, some of which smell like rotten eggs). The odor differences contribute to the concern that there might be differences in the amount or nature of contaminants present, and that these differences might influence the observed safety profile. Specifications for BSH demand 95% purity, which is independently verified for each lot by Dr. W. Bauer at the INEL. The INEL supplies ISU with BSH, which they obtain from Boron Biologicals, Inc. However, the European BNCT Consortium purchases their BSH from the English supplier, Centronic Limited. The European BNCT Consortium provided ISU with 2 grams of Centronic's BSH. Different synthetic routes are used by Boron Biologicals and Centronic to produce their BSH, and each manufacturer's BSH have quantitative and qualitative differences in the amount of BSH contaminants present. Table 6 reports the direct comparison of Boron Biological's and Centronic's BSH in terms of their acute lethality. No gross differences in BSH lethality could be detected. Data displayed in Table 6 were collected from rats drawn from consecutive shipments from the same supplier, and both volume and dose rate of BSH solutions were kept constant. Blood samples from each animal (same number and volume) were drawn approximately hourly, and both sets of experiments were completed over a 1-month period.

Table 6. Comparison of the lethality of Centronic's BSH and Boron Biological's BSH.

Boron Biological's BSH		Centronic's BSH	
Dose	Ratio of dead/injected	Dose	Ratio of dead/injected
625	1/1	625	1/1
500	2/2	500	2/2
375	2/2	375	3/3
200	1/2	200	0/2

Centronic's BSH had a very strong odor and resulted in a clear, but slightly yellow colored infusion solution. By contrast, Boron Biological's BSH did not always have a distinguishing smell and, when prepared for injection, was a clear, colorless solution. Although comprehensive physiological monitoring was not undertaken in these experiments (to avoid any instrumentation-BSH interactions), the general impression was that similar physiological alterations resulted from administration of either batch of BSH. Although the number of animals evaluated was small, there seemed to be a tendency for the Centronic treated animals to survive longer (i.e., Centronic BSH: death in 2–24 hr; Boron Biologicals BSH: death in 2–5 hr). ISU researchers conclude that while BSH metabolites might contribute to the observed toxicity, there currently is no reason to believe that acute toxicity evaluations of BSH are primarily measuring the toxicity of contaminants present within different lots of BSH.

Pharmacokinetics

Measurement of the time course of blood boron as a function of BSH dose suggests possible dose-dependent kinetics in rats (Figures 7–11, thick lines indicate average values). At BSH doses averaging 23 and 48 mg B/kg, blood boron levels declined sharply within 1 hr of the termination of infusion. At

average BSH doses of 96 and 185 mg B/kg, a more gradual initial decline in blood boron levels was observed, while a BSH dose equivalent to 280 mg B/kg resulted in little or no initial decline. Following the rapid initial decline, a more gradual decline was evident following the 23 and 48 mg/kg doses, such that blood boron levels should be approaching assay detection limits 6–8 hr after termination of dosing. The time course of this beta phase loss of B also appeared to be dose-dependent; doses equivalent to 96 mg B/kg showed a markedly prolonged beta phase and doses above 185 mg B/kg seemed to lack a beta phase - blood levels being stable over the period of observation. ISU researchers suspect that the altered beta phase may reflect renal impairment and a consequent inability to excrete BSH or its metabolites. This tendency to retain boron in blood has also been observed in some dogs and patients, and is cause for concern.

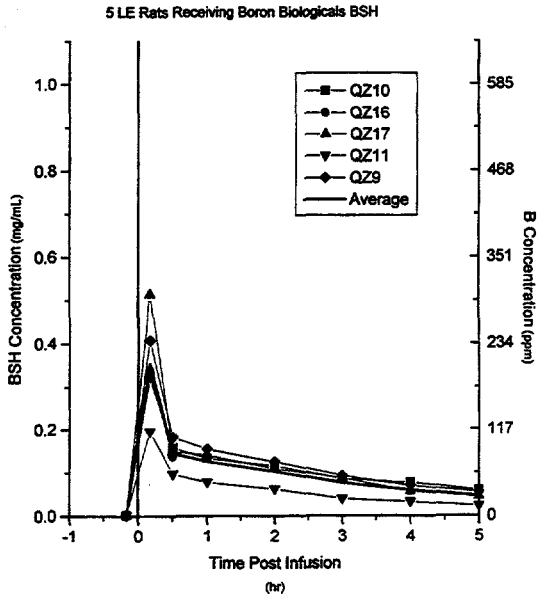

Figure 8. Boron in blood following BSH equivalent to 47.6 ± 5.8 mg B/kg.

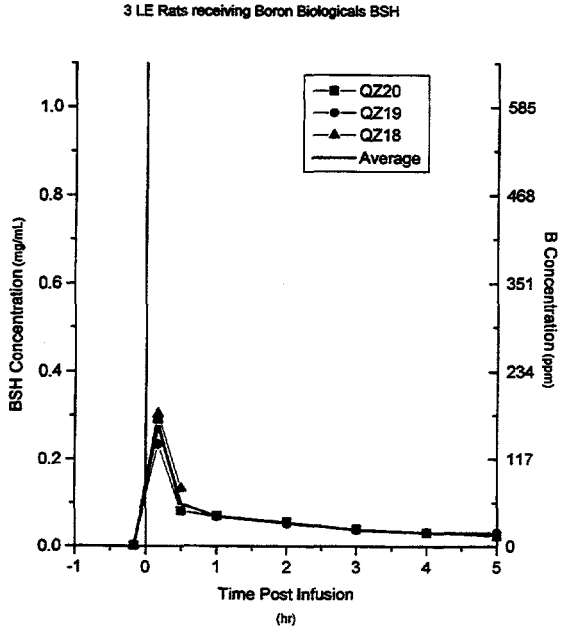

Figure 7. Boron in blood following BSH equivalent to 23.0 ± 1.8 mg B/kg.

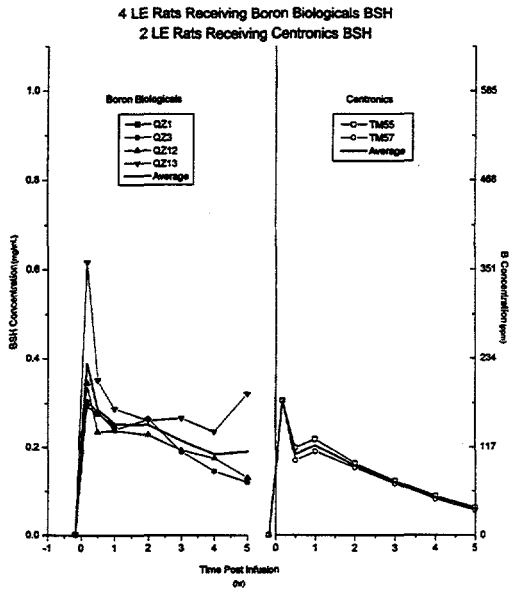

Figure 9. Boron in blood following BSH equivalent to 96.3 ± 12.9 mg B/kg.

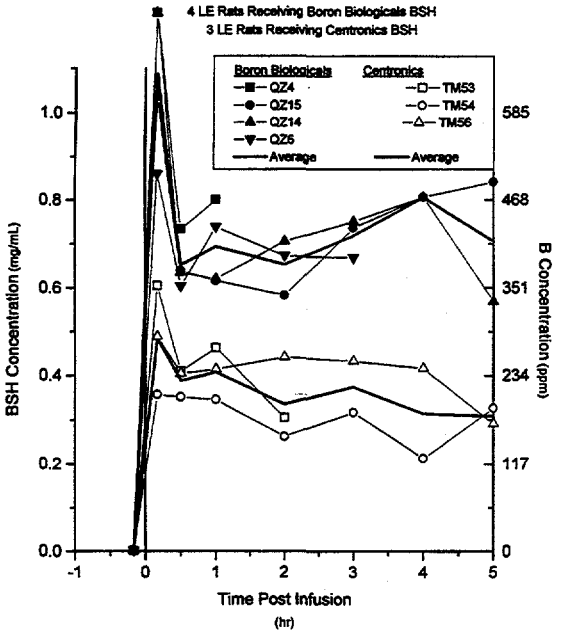

Figure 10. Boron in blood following BSH equivalent to 185.4 ± 7.3 mg B/kg.

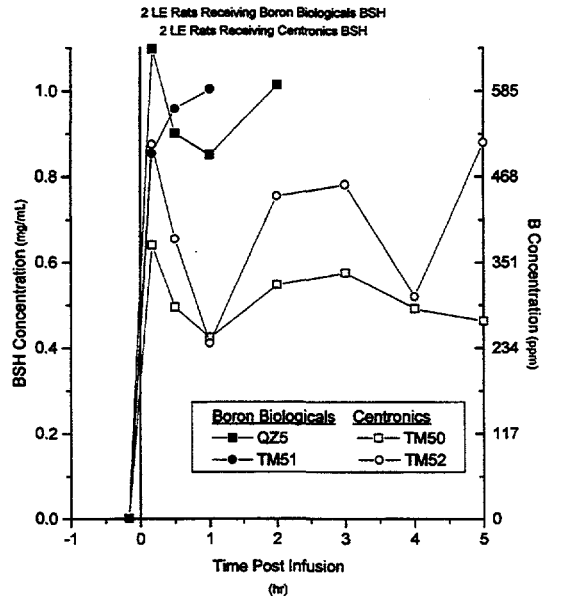

Figure 11. Boron in blood following BSH equivalent to 280 mg B/kg.

In male, Long Evans rats of 250–350 g body weight, intravenous (i.v.) infusions of Boron Biologicals BSH at average boron doses of 23, 48, 96, 185, and about 280 mg/kg resulted in average peak whole blood boron levels of about 160, 200, 230, 600, and 525 ppm respectively. Rats dosed with Centronic BSH achieved what appear to be lower blood boron levels; area under the concentration-time curve for Centronic BSH was less than that achieved with Boron Biologicals BSH (Figure 12). The dose actually administered was determined from the weight of the solution infused and the measured boron concentration (via ICP-AES) of each infusion solution. Analysis of the composition of the Centronic's BSH indicates that it met specifications, i.e., at least 95% pure (communication from W. Bauer). ISU researchers cannot explain why the formulations might differ in boron bioavailability. However, a lack of blood boron bioequivalence would indicate a need to monitor tissue distribution of boron after dosing with the different lots of BSH. It also raises questions again about the extent to which the results of toxicity testing may be influenced by issues of distribution, metabolism, or excretion.

Limited studies were undertaken to evaluate the acute toxicity associated with the BSH byproducts, BSSB and oxidized dimer of BSH (BSSO). One male, Long Evans rat, dosed i.v. with 25 mg/kg BSSB, survived until sacrificed on Day 7 for pathology. One of three rats dosed with 50 mg/kg BSSB died within 7 days, while the other two were sacrificed on Day 7 for pathology. One rat dosed i.v. with 75 mg/kg BSSB died within 24 hr of dosing. Pathology results are pending. Cardiovascular parameters were monitored in one rat dosed with 50 mg/kg BSSB; no changes in left ventricular dP/dt or end-diastolic pressure were noted and the rat was sacrificed after 6 hr of recording. Three rats were dosed with BSSO. Two rats were given i.v. infusions of 50 mg/kg; one died within 30 hr, while the other survived until sacrificed for histopathology on postinfusion Day 7. One rat administered BSSO (i.v., 75 mg/kg) died within 6 hr of infusion.

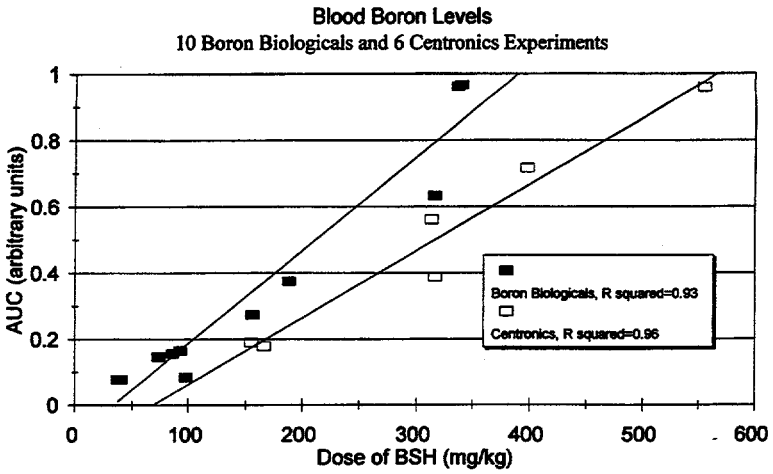

Figure 12. Area under the concentration-time curve for BSH.

Evaluation of the Effect of Repeat Dose Administration of BSH to Rats

There are relatively few studies of the effect of repeat dose administration of BSH. An early study (Soloway et al., J. Med Chem, 1967) indicated that repeated, rapid, i.v. infusion of BSH can kill rabbits. Soloway's New Zealand White rabbits (2.1–3.1 kg) received 40 mg/kg B (68 mg/kg BSH) once daily for 5 consecutive days. Some rabbits died before receiving all doses. Rabbits that died showed evidence of hemorrhagic infarction of the brain stem and scar-like foci in lungs, kidneys, and liver. Survivors were observed for 30 days, but exhibited no obvious adverse effects. The significance of the deaths in this study is difficult to judge, since the BSH formulation apparently contained considerable amounts of the more toxic BSH oxidation products (e.g., BSSB or BSSO). Rabbits that died received rapid i.v. injection of an isotonic BSH solution. Rabbits that received slow i.v. infusions of BSH at quarter-isotonic concentrations tolerated the 5 day cumulative dosing regimen (total BSH dose: 340 mg/kg) without obvious ill-effect, and no abnormal pathology at autopsy (30 days postdosing). Buchar et al., (Cancer Chemother Phcol, 1992) and Janku et al., (Toxicology, 1993) reported that repeated, low dose administrations of BSH to Chinchilla rabbits (25 or 50 mg/kg/day, 7 days) were associated with nephrotoxicity and death. Two rabbits died after receiving a cumulative BSH dose of 125 mg/kg, a third rabbit died after receiving a cumulative BSH dose of 250 mg/kg. Marshal et al., (Basic Life Sciences, 1989) reported that intraperineal (i.p.) infusion of BSH (osmotic minipump) to mice at an average rate of about 1.66 mg/kg/hr for 9 days (average total dose of about 350 mg/kg) elicited reversal hepatotoxicity but no signs of renal toxicity.

The purpose of this experiment was to better assess the probable risk associated with repeat dosing of BSH in clinical use situations. Assessment of risk was based on evaluation of the effect of repeated BSH administration on the overall health status of rats. Overall health status was evaluated by assessment of gross function and monitoring of hematology, clinical chemistry, and urine parameters. Gross examination of major organs was done at study termination and selected tissues were collected for histopathological assessment of morphological damage. The source of BSH, number of doses, spacing of doses, rate of dose administration, and concentration of BSH were selected to approximate those parameters anticipated for clinical use of BSH, in order to facilitate extrapolation of animal results to anticipated clinical studies. ISU studies indicate that repeat administration of BSH to rats is not as toxic as it reportedly is to rabbits. However, BSH-induced renal damage was observed and in conjunction with the Buchar and Janku rabbit studies, this strongly suggests that

renal damage could occur in clinical situations involving repeat dose administration of BSH.

Experimental Design

Groups of male, Long Evans rats, weighing between 183–229 g received either 5 or 6 i.v. infusions (once daily for 6 consecutive days) of BSH or vehicle control. Based on European and Japanese clinical experiences, it seems likely that the BSH dose used in U.S. clinical studies would probably equate to a boron concentration of 50 mg/kg. Because the same dose of drug, given across species, can result in different levels of exposure, ISU researchers did not dose rats with a BSH dose equivalent to boron, 50 mg/kg. Rather, comparing ISU rat pharmacokinetic data with the published clinical bioavailability data, it was concluded that a human BSH dose equivalent to 50 mg B/kg can be approximated by dosing rats with BSH, 125 mg/kg.

Blood samples were drawn from all animals before the first infusion, 24 hr after the first, third and last infusions, 4 days after the last infusion, and again just before autopsy, to monitor for drug-induced changes in hematology or clinical chemistry parameters. Urine volume and composition, fecal production, and food and water consumption were evaluated daily, as was general physical appearance and gross physiological responses. Animals were either sacrificed 24 hr after the last dose, or maintained for a period of 7 days following the last dose. At sacrifice, tissues were examined for gross evidence of morphological damage and samples were collected for histopathology. All boron analysis was performed by INEL (W. Bauer) using ICP-AES.

Methods

1. Screening of Experimental Subjects: Before entering a treatment group, each rat underwent the following: clinical chemistry, hematology, and urinalysis screening and a gross physical examination. Acceptance of animals into the experiment was based on the results of selected clinical chemistry and hematology parameters.

A. Clinical Chemistry

During the study the following items were monitored:

- Glucose
- Blood urea nitrogen (BUN)
- Creatinine
- Sodium
- Potassium
- Chloride
- Calcium
- Phosphorus
- Total protein
- Albumin
- Total bilirubin
- Direct bilirubin
- Alkaline phosphatase
- Lactate dehydrogenase (LDH)
- Gamma glutamyltransferase (GGT)
- Aspartate aminotransferase (AST or GOT)
- Alanine aminotransferase (ALT or GPT)
- Uric acid
- Triglycerides
- Cholesterol.

BUN, creatinine, total protein, sodium and potassium were used as selection criteria. Only animals whose selection criteria values differed from the group mean value by less than 1.96 standard deviation (SD) (95%) were entered into the study.

B. Hematology

White blood cells (WBC), red blood cells (RBC), hemoglobin, hematocrit, differential WBC count, and platelet count were monitored. WBC count and platelet count were used as selection criteria. Only animals whose selection criteria values differed from the group mean value by less than 1.96 SD (95%) were entered into the study.

C. Urinalysis

Specific gravity, pH, glucose, total protein, bilirubin, blood, ketones, creatinine, and sodium were monitored.

D. Gross Physical Examination

Evaluated parameters included assessment of respiratory depth and rate, ptosis, diarrhea, ataxia, nystagmus, fasiculations, tremors, convulsions, skin color, en/exopthalos, dehydration/edema, salivation, lacrimation, skin lesions, and fur condition/piloerection.

2. Group Assignments

Animals were randomly assigned to each group and the means of each screening parameter were calculated and compared to ensure that there were no statistical significance differences between groups before initiation of the experiment.

3. Borocaptate Sodium

Natural enrichment BSH (lot 0100394), obtained via INEL from Boron Biologicals, Inc. was used. Ninety-nine percent of boron was present as BSH, but the lot was contaminated with common salt (analysis courtesy of W. Bauer, National Center). Sterile solutions of BSH were prepared in distilled water. Room temperature solutions were made fresh daily, adjusted to pH 7.2–7.6, purged with nitrogen and used within 8 hr of preparation. Vehicle control was 0.9% saline adjusted to mimic BSH osmolarity by addition of 105 mg mannitol/mL. Sterile solutions of room temperature vehicle control were prepared daily, adjusted to pH 7.2–7.6, purged with nitrogen, and used within 8 hr of preparation.

4. Boron Analysis of Food, Water, Blood, Urine, and Injection Solutions

Representative samples of rat food and drinking water, whole blood and urine samples, and each BSH solution were assayed for boron content. Before drug infusions were initiated, samples of blood and urine were collected from each rat, in order to quantify the background boron levels present.

5. Infusion of Drug

Under aseptic conditions, sterile, indwelling venous catheters (microrenethane pretreated with 2% TDMAC heparin complex and filled with 40% glucose in sterile water, heparin 5,000 IU/mL) were threaded through a femoral vein and implanted so that the tip extended into the vena cava at a point just above the bifurcation of the ileac veins. Antibiotics were administered prophylactically to avoid any infection. All infusions were made through this venous cannula and blood samples were withdrawn through this cannula. If blood samples could not be withdrawn from the cannula, the blood samples were collected by free-hand withdrawal from the jugular vein, accessed via a skin incision.

BSH (target concentration: 50 mg BSH/mL, target dose: 125 mg BSH/kg) was infused in freely roaming rats housed in metabolic cages, at a target rate of 12.8 mL/kg/hr (0.0213 mL/min/100g). The target dose for vehicle control infusions was 2.5 mL/kg, which is a volume equivalent to that which would be administered if the dose were to have been 125 mg/kg dose of BSH. The infusion rate was 12.8 mL/kg/hr and following each infusion, the catheter was flushed with sterile, heparinized 0.9% saline. Once the time for an infusion was set, each rat was dosed at the same time each day (+/- 30 min).

6. Monitoring Food and Water Intake, Feces, and Urine Production

   A. Urine collection: Urine volumes and weights were determined each 24-hr period and a sample of each days urine was submitted for boron analysis. Urine collection began 48 hr before the first infusion and continued until sacrifice.

   B. Water consumption: Water consumption (expressed as g of water consumed) over each 24- hr period was determined each day of the study. Water consumption was measured daily until sacrifice.

   C. Food consumption: Food consumption (expressed as g of food consumed) over each 24- hr period was determined each day of the study. Food consumption was measured daily until sacrifice.

   D. Feces production: Feces production (expressed as g of feces produced) was determined each day of the study. After determination of the weight, the collected fecal samples were homogenized with an equal weight of distilled water and a sample of the suspension was submitted for boron analysis.

7. Evaluation of Gross Function: Once daily, each rat was subject to a gross assessment of function and a physical assessment. The following functions were scored by monitoring attitude, pain response, motor activity, and presence of stereotypic behaviors. The following functions were scored after provocation: pinna reflex, corneal reflex, righting reflex, and grip strength. Physical assessment measures included assessment of:

   - Body weight change
   - Respiratory depth and rate
   - Ptosis
   - Diarrhea
   - Ataxia
   - Nystagmus
   - Fasiculations
   - Tremors
   - Convulsions
   - Skin color
   - En/exopthalos
   - Dehydration/edema
   - Salivation
   - Lacrimation
   - Skin lesions
   - Fur condition/piloerection
   - Body posture
   - Rectal temperature.

8. Blood Sampling: The venous line is used both for infusion of BSH or vehicle and for collection of venous blood samples for boron analysis. To minimize the possibility that BSH injection solution remaining in the catheter could contaminate the venous blood sample used for boron analysis, blood from the venous line was drawn in two aliquots. The first draw collected blood for hematology and clinical chemistry. The second draw collected the blood sample for boron analysis. The ability of this method to prevent contamination of the boron blood sample was confirmed in preliminary experiments. After all blood samples were withdrawn, an equivalent volume of blood drawn from donor Long-Evans rats was reinfused into the rat. This reinfusion was not done after drawing the last blood sample (at necropsy).

9. Necropsy: Ether anesthetized rats were perfused using "whole animal" retrograde perfusion via the abdominal aorta. Perfusion of

body temperature Ringers solution was followed by fixation with 0.067 molar phosphate-buffered 4% paraformaldehyde. The following tissue/organs were excised within 10 min of organ perfusions: heart, lungs, brain, liver, kidneys, adrenals, and testes. As the tissues were excised, they were examined for evidence of gross alteration. Kidneys were cut to determine if evidence of infarctions was present; infarctions possibly indicating that microthrombi were being generated by the presence of the indwelling catheter. Tissues were embedded in JB-4 Plus embedment and sectioned 1.0–2.5 micrometers thick and stained for viewing by bright-field microscopy.

Results

Experimental Design: The results of three experiments are reported. The first experiment, designated as September, involved two groups of rats, intravenously dosed once daily with either BSH (n=8) or vehicle control (n=7), for 5 consecutive days. The second experiment, designated November, also involved two groups of rats, although both groups received vehicle control. One group received six consecutive, daily i.v. infusions of vehicle, and was then observed for a 7-day postdosing period. The other group was sentinel animals and was sacrificed at intervals over the first 10 days of the study to monitor for the presence of any confounding problems. The third experiment, designated December, used two groups of rats. One group (n=8) was dosed once daily with BSH for 6 consecutive days and then observed for a 7-day postdosing period. The second group (n=5) received vehicle control on 6 consecutive days, followed by a 7-day observation period.

Dose and Volume Rate of Drug Infusions

Actual concentrations for each day's BSH infusion solutions were determined by boron assay (ICP-AES) and were used along with the weights of infused drug solution to calculate dosing accuracy. A summary of the BSH infusion data is provided in Table 7. Weights of infused control solution were used to determine control infusion accuracy. Results of water analysis indicated there were no significant amounts of boron in the vehicle control solutions, but all control solutions were analyzed to determine the exact boron content. Table 8 contains a summary of the control infusions. Infusion dose averages from the September experiment were within 5% of the targeted dose and the December experiment averages were within 3% of the intended doses.

Overall Survival

All rats in the September experiment were sacrificed after 5 days of infusions. Several animals in this experiment exhibited signs of a systemic infection attributed to a break in sterile technique either

Table 7. BSH Infusions (x ± SD).

	Experiment	
	September	December
Target Dose (mg BSH/kg)	125	125
Actual Dose (mg BSH/kg)	130.9 ± 6.9	122.3 ± 7.4
Dose Accuracy	104.7%	97.8%
Target Rate (mL/kg/hr)	12.8	12.8
Actual Rate (mL/kg/hr)	12.7 ± 0.6	12.8 ± 0.7

Table 8. Control Infusions (x ± SD).

	Experiment	
	September	November/ December
Target Dose (mL/kg)	2.5	2.5
Actual Dose (mL/kg)	2.5 ± 0.1	2.5 ± 0.1
Dose Accuracy	99.4%	100.5%
Target Rate (mL/kg/hr)	12.8	12.8
Actual Rate (mL/kg/hr)	12.7 ± 0.6	12.8 ± 0.7

during surgery or at times of drug infusion. Two animals treated with vehicle control and three rats treated with BSH died. Necropsy of these animals revealed evidence of sepsis (microorganisms were detected in kidney and lung) and death is attributed to sepsis-related events. Animals in the November experiment received only vehicle control. Approximately half of these animals were maintained for the 6- day dosing period and the 7-day postdosing period, while the remaining rats were sacrificed at various times during the study to monitor for any problems noted in the earlier study. No such problems were observed. No treatment related deaths occurred in the third experiment (designated December) (6 doses of BSH or vehicle, 6-day dosing period, and 7-day postdosing period), although two rats died from unrelated issues (one due to technician error and another under anesthesia as blood was being collected from the jugular vein via direct puncture).

Physical Assessment: No remarkable alternations were noted in any of the experimental subjects of November or December experiments. Figure 13 illustrates the lack of effect of BSH dosing on body weight gain. Because vehicle effect elicited no observable effect, vehicle control treated animals from November and December experiments were treated as a single group. Five of 15 rats in the September experiment developed edema at one or more of the surgical incision sites. Four displayed nasal discharge and eight displayed abnormal body postures (hunched back).

Functional Assessment: No alternations of function were noted in any of the experimental subjects of November or December experiments. In the September experiment, three rats receiving BSH displayed functional abnormalities. Animals were depressed, exhibited an impaired righting reflex, and weakened grip strength. At necropsy, all animals displayed overt signs of sepsis.

Food and Water Consumption, Urine, and Feces Production: These parameters were monitored throughout the infusion period for all experiments and through the 7-day observation period in the December experiment. Compared to vehicle control, repeated daily infusions of BSH elicited no

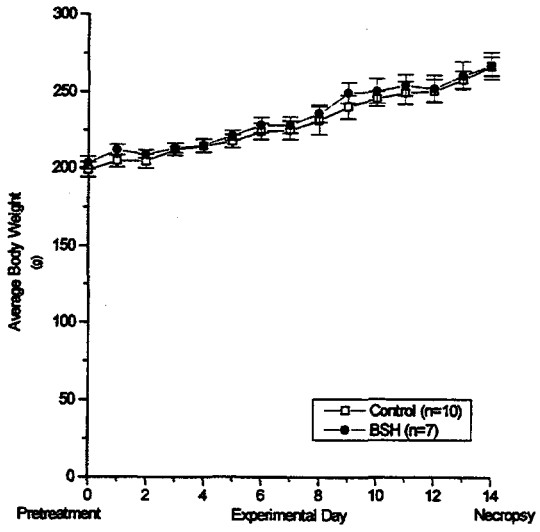

Figure 13. Effect of BSH and vehicle on body weights (mean ± SEM).

significant effects on food and water consumption or urine and feces production. The boron content of urine and feces samples were measured, but data are not yet available. The effect of infusions on food consumption is shown in Figure 14, and is indicative of the effects on water consumption, and urine and feces production.

Clinical Chemistry: Analysis of clinical chemistry parameters is still ongoing. Currently, it appears that the repeated BSH dosing had no significant effect on blood sodium, chloride, calcium, phosphate, total protein, albumin, total bilirubin, or alkaline phosphatase. During the first few days of the December experiment, two BSH treated rats exhibited elevated BUN and creatinine levels, implying kidney damage. However, both BUN and creatinine levels subsequently returned to normal, suggesting any functional impairment of renal function was transitory. Figure 15 illustrates the effects of vehicle and BSH infusions on the BUN:creatinine ratio. Clinical chemistry measurements made during the September experiment were confounded by the presence of infection.

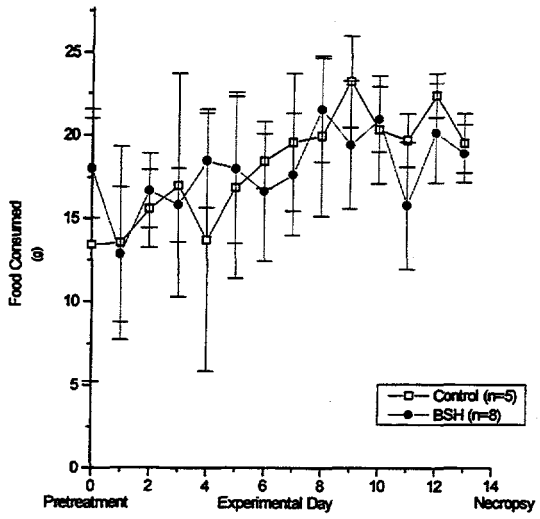

Figure 14. Summary of food consumption (mean ± SD).

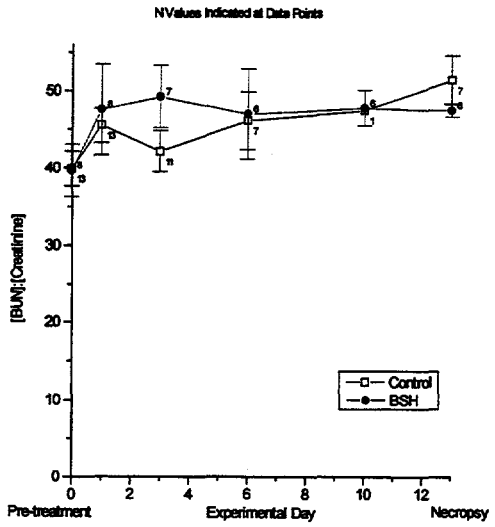

Figure 15. BUN/Creatinine ratio (mean ± SEM).

Hematology: Analysis of hematology parameters is still ongoing, but initial review indicates that hematology parameters are within normal ranges in both vehicle- and BSH-treated rats.

Urinalysis: Analysis of the effect of vehicle and BSH treatments on urine parameters is not yet complete.

Gross Pathology: Animals were examined at necropsy for evidence of surgical complications, infection, and drug-induced alteration of organ morphology. Animals from the November and December experiments showed no evidence of gross pathology, except for the presence of varying amounts of pannus (exuberant vascular endothelial growth) around the tip of the indwelling venous catheter. This pannus is likely due to tip-induced irritation of the vascular endothelium. In several animals, pannus formation was associated with blood vessel collateralization around the tip area. Neither the pannus nor the blood vessel collateralization were judged to be treatment-related. Nine of the 15 rats from the September experiment showed obvious signs of infection, including enlarged organs, and patchy nodules or cysts on kidneys and lungs.

Histopathology: Samples of heart, lung, brain, spleen, adrenal, liver, kidney, and testis were examined histologically for microscopic lesions. Of these organs, only the kidney exhibited histopathological lesions clearly attributable to borocaptate administration. Renal changes were characterized by widespread but localized cortical tubular epithelial injury (blebbing, vacuolation) and necrosis, detachment of the tubular epithelium, apparent attempts at reepithelialization of the injured tubules, and the presence of cellular and both hyaline and fine-granular casts. While these changes were seen mostly in the proximal segments of the nephrons, some distal segments were also affected. Only occasionally were these tubular lesions accompanied by (mild) inflammatory infiltrates. Glomeruli and the medullary and papillary portions of nephrons and collecting ducts apparently were spared. Subtle BSH-induced changes in other organs may also have occurred, but additional study is required to determine if this is the case

Conclusions: Repeat administration of BSH, under conditions intended to approximate clinical use in BNCT trials, did not significantly impair function in male, Long-Evans rats. Clinical chemistry and histopathology indicated that some renal damage occurred, but in general, animals tolerated the repeat dosing of BSH surprisingly well. This is in contrast to reports that chronic administration of low dose BSH can be lethal in rabbits. ISU researchers believe that repeat administration studies in rabbits, under conditions similar to those of our rat studies need to be conducted to determine if significant species differences exist with respect to the acceptability of repeat dose, intravenous administration of BSH.

TREATMENT PROTOCOL DEVELOPMENT

Dr. Carol Schwartz, Dr. Patrick Gavin, PI, WSU, College of Veterinary Medicine (CVM)

For the past 8 years, researchers at the WSU-CVM have used the large animal model developed at the WSU-CVM to study the effects of BNCT on normal and neoplastic canine brain tissue. These studies have been performed using BSH and epithermal neutrons and have had two major foci: (1) biodistribution of BSH in animals with spontaneously occurring brain tumors and (2) effects of BNCT in normal and neoplastic brain tissue. Canine subjects were chosen as a model for the human GBM because of similarities between the two species in frequency and dynamics of spontaneously occurring brain tumors and because the dog's size permits selective irradiation of the head without a significant whole body dose. Although intended as a model for a glial tumor, dogs with many different tumor types have been studied since the studies were designed to evaluate tissue tolerance and not treatment efficacy.

To date, 24 dogs with spontaneously occurring brain tumors have been treated with BNCT, 22 with BNCT alone, and two with a combination of surgery and BNCT. BSH was the boron delivery agent in all but one case, which was treated following p-BPA-fructose infusion. As of this writing, three dogs remain alive and well following treatment. One dog treated with BNCT alone in October 1989 remains clinically stable despite apparent regrowth of the tumor starting 18 months ago. The regrowth has been slow and a magnetic resonance (MR) scan performed in September showed no progression since April (Figure 16). A second dog that received a combination of surgical debulking of the tumor followed by BNCT is also clinically stable. An MR scan at 9 months posttreatment showed areas of treatment induced damage that had not progressed as of the 12 month-recheck. A third dog is stable 4 weeks following treatment.

Nontumor bearing dogs were also used in dose escalating tolerance studies designed to establish the tolerance of normal brain tissue to BNCT.

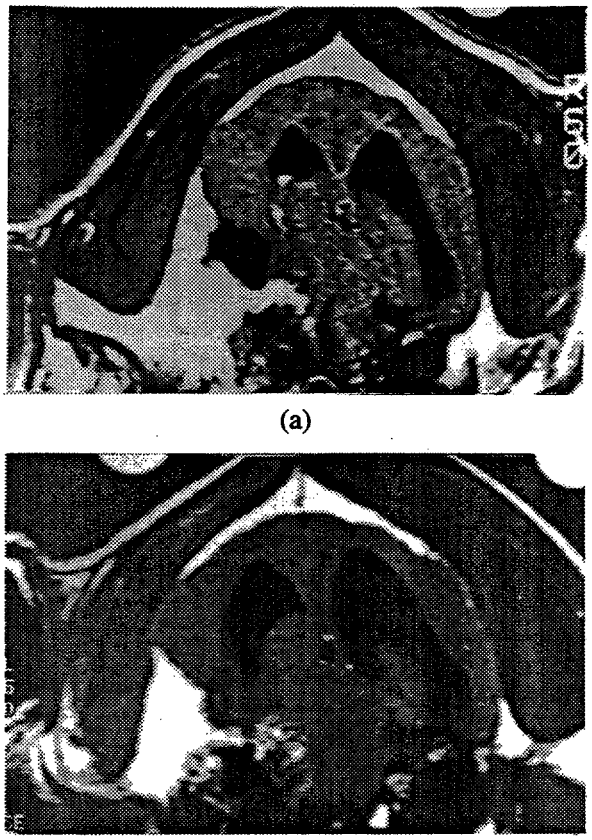

(a)

(b)

Figure 16. Magnetic resonance images of dog treated with BNCT alone at 3 years (a) and 5 years (b) posttreatment. Note new area of enhancement in left midbrain in b.

Tolerance of normal brain to epithermal neutrons alone, and to single and split dose BNCT has been established in the dog (Table 9). Considerable debate has ensued over the aspect of fractionated BNCT. Fractionated BNCT should allow repair of sublethal damage caused by the relatively low linear energy transfer (LET) dose components of BNCT, which is mainly gamma radiation, while damage caused by the high LET radiation produced by the boron capture reaction would not be repaired.[9] Hence, in the ideal situation, where high tumor:blood and tumor:normal tissue ratios are achieved and there is no contamination of the incident beam by fast neutrons, fractionation would be beneficial. Normal brain tissue would be able to repair the sublethal damage caused by low LET

Table 9. Normal brain tissue tolerance levels for BNCT.

Treatment	Peak physical dose (Gy)
Epithermal neutrons only	15
Single dose-BSH (25 ppm)	28.4
Two fraction-BSH (25 ppm)	27.6

gamma radiation, both that produced in the capture reactions (primarily by hydrogen in the normal brain) and any gamma that contaminated the incident beam. Tumor cells, where primarily boron capture reactions would occur, would not repair the damage caused by the high LET fission fragments.

With current technology in BNCT, however, this situation does not exist. All existing neutron beams contain some level of contamination by fast neutrons. According to standard convention, these fast neutrons would add to the nonrepairable high LET dose received by normal tissue.[10] Relatively recent research, on the other hand, showed that at least some tissues, most notably skin, may benefit from a fractionated schedule of fast neutron irradiation, indicating that some repair may occur.[11] Currently available boron compounds do not achieve adequately high tumor:normal tissue ratios in all exposed tissue. As a result, these tissues may receive significant doses from the boron capture reaction products. Damage caused by the high LET α and Li particles produced by the boron capture reaction are likely nonrepairable. Normal tissue with high boron content would not benefit from fractionated BNCT schedules and may be compromised due to repeated boron administration necessary for fractionation.

Another consideration is the possible alteration in boron uptake by previously irradiated tissue. Of particular interest is modification of the BBB. Some sources contend that the BBB is highly radioresistant and that relatively high acute doses are necessary to significantly alter BBB permeability.[12] Other research indicates that there is increased uptake of boron in normal brain following radiation, possibly due to changes in BBB permeability.[13] This could be both detrimental by increasing the chance for boron neutron capture in normal brain and potentially beneficial by making the boron species available to a greater percentage of tumor cells.

Research on normal tissue tolerance at WSU has included BNCT administered in 2 or 4 daily fractions. The doses chosen for these fractionation studies were based on a previous single dose study in which four dogs were irradiated at a target blood boron concentration of 25 µg/g and a target peak physical dose of 2,700 cGy. (Actual average blood boron concentrations and peak physical doses are given in Table 10.) All four dogs showed lesions on MR at 6 months following BNCT. At 12 months posttreatment, lesions were not evident on MR scans of three of the four dogs; all three remained symptom free during the entire 12-month followup. The fourth dog (which received the 3,024 cGy dose) required euthanasia at 9 months posttreatment due to sudden onset of seizures and recumbency. Using subclinical MR changes to define normal tissue tolerance to BNCT, a dose of 27 Gy at 25 µg/g average blood boron was considered the limit for single dose BNCT and was used to determine fractionation schedules for the present study.

For the fractionation studies, the heads of canine subjects were irradiated with epithermal neutrons in two or four fractions spaced 24 hr apart to total doses of 27-32 Gy. An i.v. infusion of BSH at 25 mg/kg body weight was administered before each irradiation. The desired average blood boron concentration for each irradiation was 20–30 µg/g. The dogs were monitored for occurrence of neurological abnormalities following treatment and MR scans were obtained when possible at 6 months posttreatment or as soon as neurological signs appeared. The results are presented in Table 11.

Table 10. Single dose BNCT with BSH and epithermal neutrons.

Dog number	Average blood boron concentration (µg/g)	Peak physical dose (cGy)
2320	26.3	2,792
2465	26.6	2,883
3300	33.2	2,841
2311	26.8	3,024

Table 11. Results of BNCT fractionation on canine brain.

Dog number	Peak physical dose (cGy)	Treatment dates	Neurological abnormalities (date)	MR changes (date)	Euthanasia-days post-treatment	Neurologic signs at euthanasia
2 Fraction study						
2051	2,764	5/20&21/93	11/30/93	11/20/93	249	decreased PLR[a] on rt
2112	2,742	5/17&18/93	none	none	367	none
2146	2,662	3/11&12/93	none	none	376	none
2157	2,710	5/19&20/93	none	none	364	none
373	2,675	6/14&15/93	10/10/93	10/15/93	188	anisocoria, decreased menace lt, CP[b] deficits- lt hind
1848	2,669	6/16&17/93	11/19/93	12/16/93	216	CP deficit- lt hind
2148	2,663	6/14&15/93	10/14/93	10/15/93	189	anisocoria, CP deficits- both hind
2162	2,719	6/16&17/93	10/20/93	10/23/93	209	CP deficit- rt hind
4 Fraction study						
372	2,794	4/4-7/94	8/1/94	8/1/94	118	seizures, ataxia, depression
2571	2,804	4/4-7/94	9/16/94	8/30/94	127	vision deficit- lt, CP deficits - both hind, CN-V[c] deficit-lt
2492	2,797	4/4-7/94	none	none	NA	NA
2482	2,827	4/4-7/94	8/9/94	8/10/94	126	anisocoria, vision deficit -lt, CP deficit- lt fore & hind
2570	3,204	4/18-21/94	8/9/94	8/10/94	217	seizures, recumbent
2569	3,206	4/18-21/94	8/5/94	8/5/94	109	seizures, vision deficit- lt
2568	3,220	4/18-21/94	8/4/94	8/5/94	117	vision & CP deficits-lt circling to rt
2551	3,218	4/18-21/94	8/9/94	8/10/94	109	depression, disorientation

a. PLR = pupillary light reflex.

b. CP = conscious proprioception.

c. CN-V = cranial nerve V.

All split dose dogs were treated to peak physical doses of 2,662–2,742 cGy. Dogs receiving BNCT in four fractions were treated with four equal fractions to a target of 700 or 800 cGy per fraction (2,800 or 3,200 cGy total dose). Five of eight split dose dogs had lesions on MR at 4 to 6 months following treatment. These same dogs had at least mild neurological deficits as well. Three dogs had neurological deficits requiring oral steroid treatment to control. Of eight dogs receiving BNCT in four fractions, seven developed moderate to severe neurological abnormalities and accompanying MR lesions 4 to 5 months after treatment. All seven were euthanized due to progression of neurological signs. Two of these dogs had also developed progressive dermal necrosis before euthanasia (Figure 17).

Initial assessment of these studies indicates that fractionation of BNCT does not result in significant repair of damage to normal brain as has been postulated. Seven of eight and three of four dogs receiving 2,700–2,800 cGy total dose in 2 or 4 fractions respectively, developed lesions equal to or greater in severity to those seen in the single dose group receiving a similar peak physical dose (Figure 18). The appearance of dermal necrosis in only dogs receiving four fractions would suggest a detrimental effect in some normal tissues; for example skin. A third fractionation study was recently performed by WSU researchers to determine the effect of fractionation on uptake of boron by the skin. Four dogs were treated with four equal fractions to a total target dose of 2,400 cGy. On days 2, 3, and 4, a skin biopsy was taken at sites on the edge of the radiation field immediately following irradiation. These samples are currently being analyzed for boron content. Although, from these pilot studies, fractionation of BNCT does not seem to be beneficial, further dosimetric and radiobiological studies may be necessary to fully evaluate the procedure.

Other studies performed by researchers at WSU during the past year include initial evaluation of BSH uptake by lung tumors. Results of these studies were not encouraging. Infusion of 50 mg/kg BSH according to the standard schedule in dogs with spontaneously occurring lung tumors resulted in no preferential uptake of BSH by the tumor compared with surrounding normal lung tissue.

Figure 17. Dermal necrosis in a dog treated with 4 fraction BNCT.

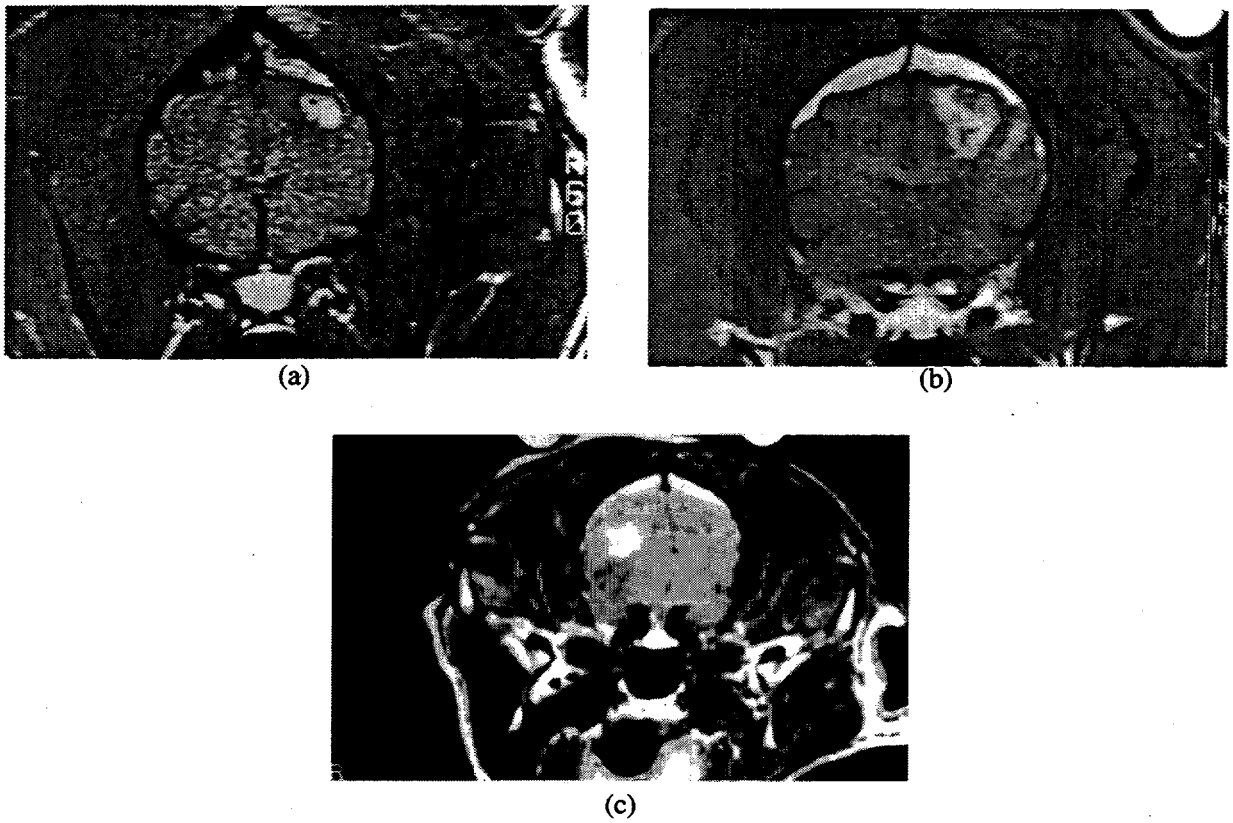

Figure 18. Magnetic resonance images showing posttreatment contrast enhancement following (a) single dose, (b) split dose, and (c) 4 fraction BNCT. All three dogs were treated to similar peak physical doses.

DEVELOPMENTS IN BORON MAGNETIC RESONANCE IMAGING (MRI)

Dr. Martin Schweizer, PI, Department of Medicinal Chemistry, University of Utah (U of U)

This report summarizes progress during the past year on maturing Boron-11 magnetic resonance imaging (MRI) methodology for noninvasive determination of BNCT agents (BSH) spatially in time. Three major areas are excerpted: (1) Boron-11 MRI of BSH distributions in a canine intracranial tumor model and the first human glioblastoma patient, (2) whole body Boron-11 MRI of BSH pharmacokinetics in a rat flank tumor model, and (3) penetration of gadolinium salts through the BBB as a function of tumor growth in the canine brain.

Detailed accounts of this work are in the following manuscripts:

1. Bradshaw et al., "BSH Distributions in the Canine Head and a Human Patient Using Boron-11 MRI," Magnetic Resonance in Medicine, in press, 1995.

2. Hendee et al., "In Vivo NMR Evaluation of the Pharmacokinetics of Boronated Compounds in the Rat Model," Proceedings, Sixth International BNCT Conference, Kobe, Japan, in press, 1995.

3. Tang et al., "T1 Measurement to Study the Penetration of BNCT Agents into Canine Tumors Caused by Blood Brain Barrier Damage," Proceedings, Sixth International BNCT Conference, Kobe, Japan, in press, 1995.

Boron-II MRI Distributions in the Canine and Human Brain Tumors

Boron-11 MRI, with the rapid 3D Projection Reconstruction algorithm (Glover et al., J. Magn. Reson. Imaging, 2, 47-52(1992), can readily noninvasively follow uptake of natural BSH into tumor and muscle tissue. No BSH in normal brain is observed. Pharmacokinetically, BSH absorption into temporalis muscle peaks about 20 min after the end of 1-hr i.v. infusions of 80 mg (as Boron-11)/kg. Peak levels in muscle are estimated at about 130 ppm. Tumor entry is somewhat slower, peaking at about 100 ppm, 35–40 min post-infusion termination. These semiquantitative results do not take into account the likely tissue specific effect upon Boron-11 signal intensity, which is the subject of current and future research. The elimination rates, after the apparent 1-hr distribution phase, from blood, temporalis and tumor are essentially equivalent. Boron content estimates at the end of 1–1.5 hr elimination of 40–50 ppm agree fairly well with ICP-AES data from necropsy samples.

A human patient was imaged about two weeks postsurgical resection and approximately 2 week before BNCT treatment in Japan. BSH was readily taken up by small amounts of residual tumor tissue, which were also penetrated by gadolinium salts. BSH infusion into the resection mass was much slower.

The results show the promise of the method as an indicator of tumor residuals and as a potential BNCT drug prescreen.

Whole Body Boron-II MRI of Rats

In the work of Hendee et al., the rat 9L gliosarcoma model was chosen in order to facilitate examination of the new, less-prevalent candidate BNCT agents. Flank inoculation of fresh tissue culture harvest of 9L cells produced large flank tumors, which were readily amenable to Boron-11 MRI visualization using the large human magnet with weak gradients, but with a very sensitive quadrature coil. (Rock Hadley, U of U Electrical Engineering Department).

As an example using the generic boronated drug, bolus injection of BSH (approximately 48 mg Boron-11/kg) into the lateral tail vein of a rat followed by whole body Boron-11 imaging, again with the 3DPR method, permitted facile evaluation of BSH content in various organs of elimination

(liver, kidney, and bladder) as well as the flank tumor. The latter displayed heterogeneous uptake of BSH, with a peripheral ring of absorption, surrounding an apparently impenetrable core(undoubtedly poorly vascularized and at high interstitial pressure due to incomplete venous return). Whereas kidney, liver, and tumor Boron-11 intensities slowly decreased over the 1-hr imaging period, bladder content rose dramatically, as anticipated. The slow decline in the other tissues may in fact reflect tissue binding effects during the distribution of BSH.

Other rats have been infused with approximately 6 mg(as Boron-11)/kg amine borane encapsulated in DPPS liposomes. Here the Boron-11 image data again reveal differential tissue pharmacokinetics, with high initial spleen/liver content, which dramatically diminishes over 24 hr. Asymmetric flank tumor absorption is apparent at the 24-hr juncture. ICP-AES data at 24 hr postinfusion showed tumor total boron at 28 ppm, with heart and liver at about 50 ppm, pulmonary blood at 132 ppm, and spleen at 186 ppm.

Further meaningful work, including investigation of intracranial lesions in the rat model awaits completion of implementation of the 3DPR method on a small magnet with much stronger gradient fields. However, it might be interesting to note that U of U researchers have successfully imaged boronophenylalanine (BPA)/fructose in the rat. Boron-11 image signal-to-noise is generally higher than BSH at equivalent boron levels, since the BPA T1 is apparently much lower and was not subject to partial saturation as in BSH. BPA imaging will be pursued further in the next year.

Penetration of the Blood Brain Barrier

Tang et al. have been pursuing the question of tumor penetrability in the intracranial canine gliosarcoma model as a means of charting parameters of BNCT agent entry related to total tumor boron content in single versus multiple dosing motifs. Consequently, gadolinium salts as ionic analogs of BSH and enhanced relaxivity of tumor water protons as evidence of permeating gadolinium have been used. This work shows that as the tumor matures, gadolinium progressively gains entry as the BBB weakens and a tumor blood supply is recruited.

These data will be used to indicate when the first of multiple BSH infusions should be initiated, followed by Boron-11 MRI as an indicator of potential BSH accumulation.

HUMAN APPLICATIONS OF THE INEL PATIENT TREATMENT PLANNING SYSTEM

F. Wheeler, D. Wessol, C. Atkinson, and D. Nigg, Reactor Physics, INEL

INTRODUCTION

During the last few years, murine and large animal research, as well as human studies have provided data to the point where human clinical trials have been initiated at the BMRR using BPA-F for gliomas and at the Massachusetts Institute of Technology Reactor (MITR) using BPA for melanomas of the extremities. It is expected that glioma trials using BSH will proceed soon at the Petten High Flux Reactor (HFR) in the Netherlands. The first human glioma epithermal BNCT application was performed at the BMRR in the fall of 1994. This was a collaborative effort by BNL, Beth Israel Manhattan hospital, and INEL. The INEL planning system was chosen to perform dose predictions for this application.

Parallel to these efforts, work has proceeded on the development of analytical tools required for treatment planning.[14] There are presently four approaches to analytical radiation transport calculations: (1) methods based on the MCNP Monte Carlo code[15] developed at Los Alamos; (2) methods based on the three-dimensional (3D) TORT discrete ordinates code[16] developed at Oak Ridge; (3) the Radiation Transport in Tissue by Monte Carlo (rtt_MC or rtt) code[17] developed at the INEL and; (4) a semi-empirical method developed by Mijnheer.[18]

BNCT requires an accurate 3D solution for epithermal- and thermal-energy neutron transport. The fast-neutron and gamma components of the beam must also be included as well as the important induced gamma field, which is primarily due to the 2.22-MeV gamma released upon neutron capture in hydrogen. For conventional photon therapy, the suggestion of the Monte Carlo approach brings to mind codes such as EGS, ETRAN, and TIGER. These codes however are not appropriate for BNCT because of the dominant epithermal- and thermal-energy neutron component.

The patient geometry also must be based on medical image for the specific patient just before therapy. This is not so much because there are not good standard models of head anatomy but because the suspect tumor volume and shape of surrounding tissue is so variable and unique to each patient. The BNCT Radiation Treatment Planning Environment software (BNCT_Rtpe or Rtpe)[19] is used at INEL in conjunction with the radiation transport method (now Monte Carlo, possibly discrete ordinates, diffusion or collision probability theory in the future). Rtpe is used to construct the imaged-based model for the transport calculation and to display the rtt results where the calculated radiation doses are correlated precisely to medical image.

Presently, the Rtpe approach is the use of Non Rational B-splines (NURBS). The NURBS representation incorporates the properties of B-splines, interpolating splines, and Bezier curves and surfaces. NURBS may be best described as a naturally smooth curve (or surface) represented as a piecewise polynomial expression. NURBS are easy to form into complex, sculptured shapes and require much less storage than the polygonal representation they have replaced. Because of the rational property of NURBS, they can also exactly represent conic sections. A summary of NURBS, as incorporated in the Rtpe planning system is available.[20]

The Rtpe approach to this user interface is the X11 Window Environment system and the Motif graphical interface. Most, and eventually all input will be through various widgets (specially designed windows on the computer monitor) that are tailored to make the setup as easy and accurate as possible. Upon receipt of the medical image [completed tomography (CT or MR)] files in a standard format, the images are loaded and a 3D model constructed using automatic surface-fit (and other tools in the Rtpe library). The rtt transport solution is then obtained for one field (requires about 3-4 hr computer time on an HP 750). Several fields are typically calculated and, using an edit widget, the user investigates the number of fields, number of fractions etc., and determines an optimum plan.

This process is still only partially automated but there is the capability to register contour data to images and generate dose/volume histograms automatically, which speeds the process.

In the rtt transport simulation, particle tracking is performed over the model geometry and, to provide the required detail, tracking is also performed through a uniform 3D mesh (voxels). Each voxel is a cube of a specified dimension and flux and dose tallies are stored into each voxel for every ray passing through the voxel. Ray tracing and scoring in voxel geometry is very fast and affects processing time by only 10-20%. Currently, a 30x30x30 (27,000 voxels) voxel mesh is imposed over the model. This voxel edit is stored and 0-, 1-, 2-, and 3D edits can be performed following the transport run to obtain results required by the oncologist. The neutron flux is calculated using the common weight-reduction Monte Carlo methods and all dose components are calculated in a single run. There is a bias option to improve the efficiency for the slowly-converging fast-neutron dose (consisting primarily of the recoil protons from collisions of neutrons with hydrogen). Following the neutron calculation, the incident and induced gamma calculation is performed. At this time, the assumption is made that electron charge balance exists; i.e., no electron transport calculation is made.

APPLICATION

Noninvasive Imaging

Either MR or CT images are used to develop the patient models for dose calculation. Typical MR images are shown in Figure 19. All prior work (mostly dog irradiations) using Rtpe was based on MR. Using CT, it was soon discovered that Rtpe could not tune in the images to resolve soft tissue structure. The images Rtpe displayed contained all information (bone window) but could not tune in the portion of the information corresponding to detail in soft tissue (brain window). The bone-window displays were completely adequate for anatomical reconstruction but were not adequate for defining malignant tissue. This limitation was circumvented by using the identification of tumor as drawn on film by the radiologist, digitizing it and transferring the information to the 3D model. Since that time, the Rtpe software has improved such that it is now possible to view the brain window. A partial rendering of a typical 3D model is shown in Figure 20.

Beam

The therapy beam delimiter at BNL consists of a lithium-containing polyethylene slab, three inches thick. The opening in this beam delimiter is a cone which has an 11-cm opening on the reactor side and an 8-cm opening on the patient side. Because of the thin section of delimeter toward the smaller opening, the effective diameter of this aperture is approximately 10 cm. This aperture was designed by Dr. Ben Liu (BNL) using the criteria of minimizing the volume of healthy brain exposed and maximizing dose at depth. The beam is consistent with the philosophy throughout the therapy to affect tumorcidal dose while very conservatively exposing the healthy brain to a binary treatment where there is limited knowledge of brain tolerance.

Fractionation

Because there has been no evidence of significant therapeutic gain in BNCT fractionation and because of the added complexity to the procedure, BNL decided to administer one drug dosage and deliver the neutron irradiation at a relatively low dose (< 27 cGy/min) in two sessions separated by a period allowing patient rest and intermediate boron quantification.

Multi-Field

Probably the greatest advantage of epithermal-neutrons (compared to thermal-neutrons) for efficacy in cancer therapy is the ability to apply two or more irradiation fields. Multi-field irradiation was considered for the first patient and several fields were calculated and combined to investigate the benefits. In the end however, it was decided to only

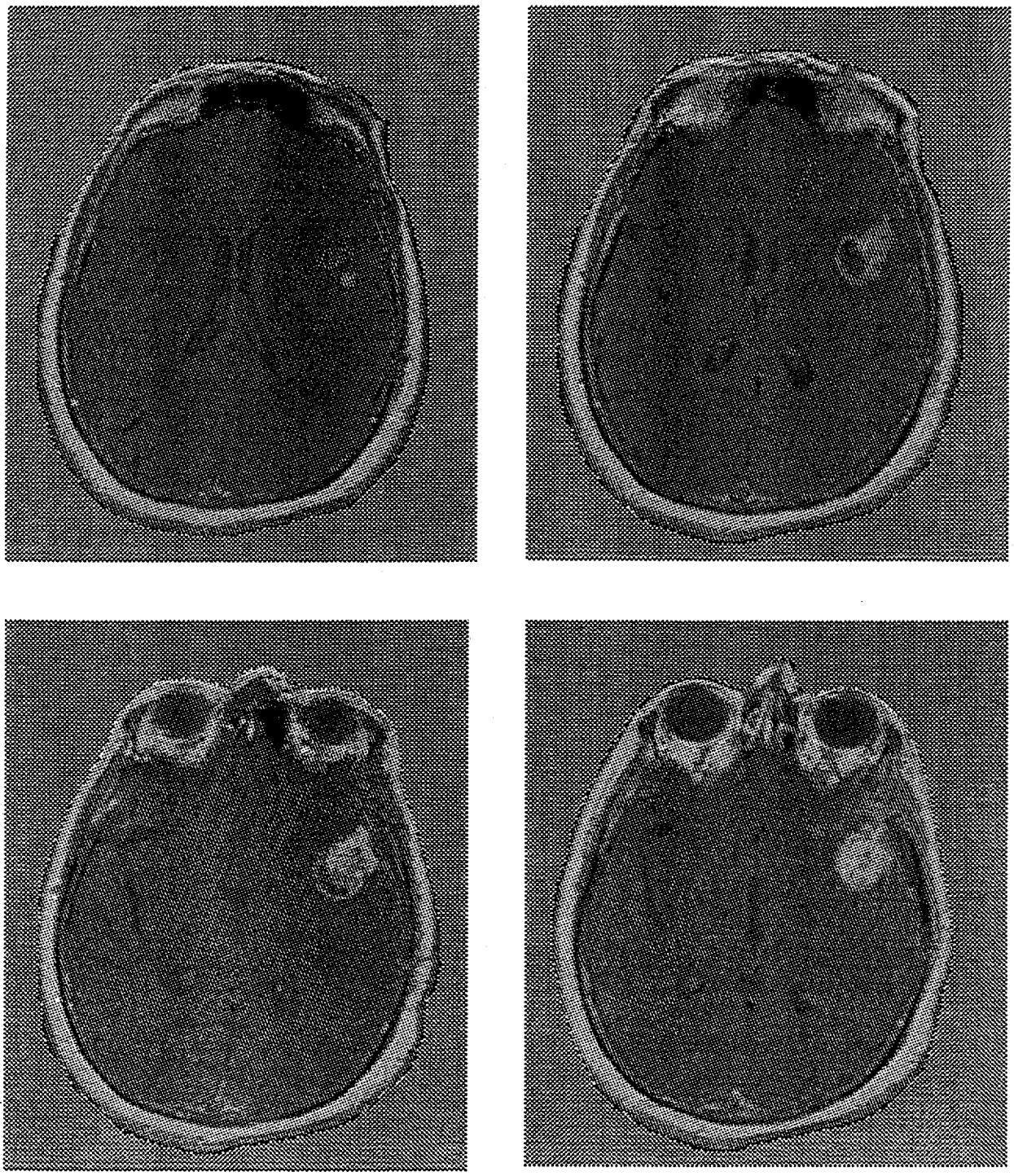

Figure 19. MR images of a glioma patient.

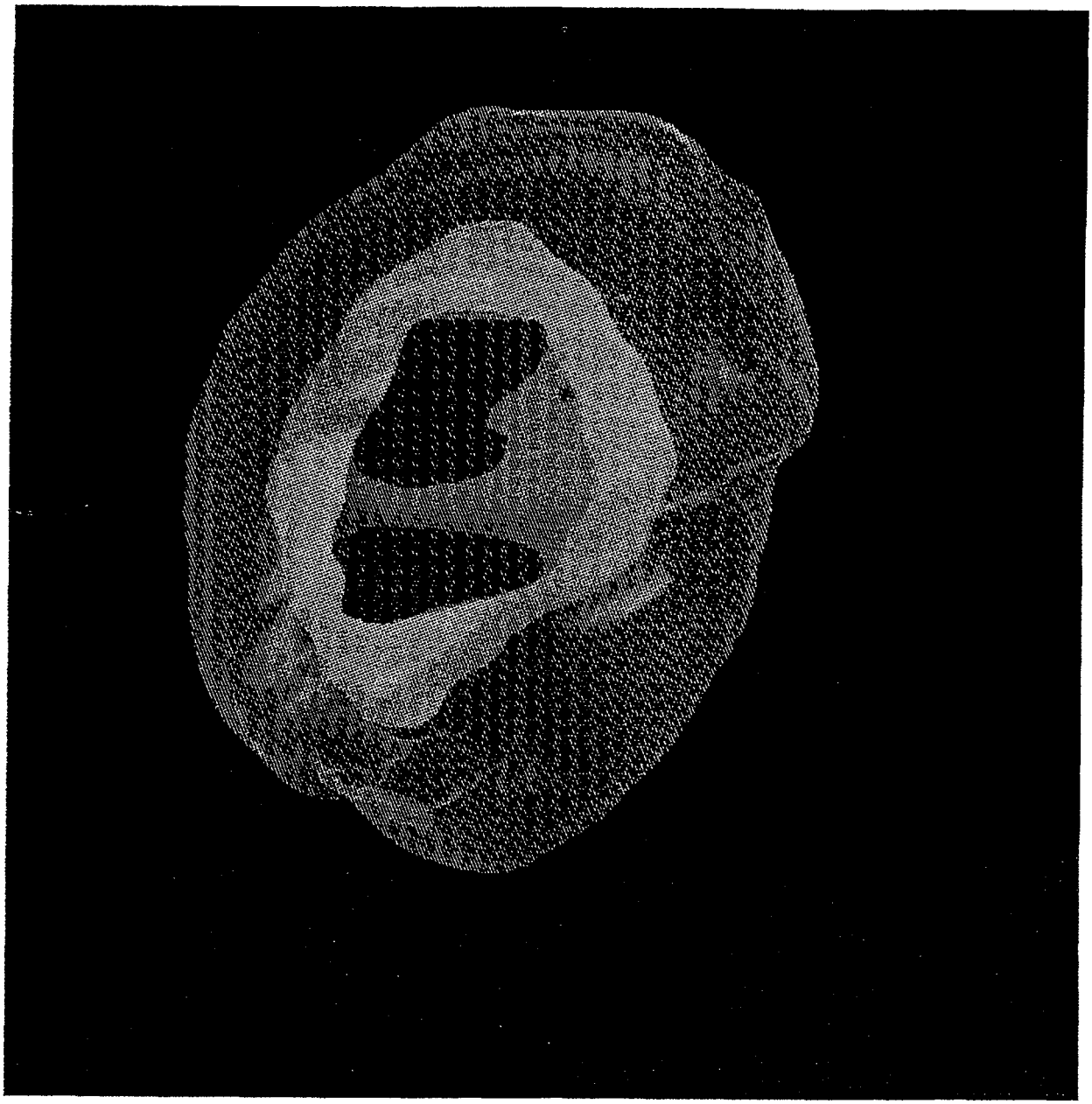

Figure 20. Beam's eye view of brain, target, and tumor from surface rendering.

use a single field. This decision was made because: (1) the defined clinically-observable gross tumor volume was quite superficial for this first patient and well covered by a single field; (2) there is no device yet developed to ensure that precise positioning can be achieved. For single field there is a generous tolerance in positioning due to spreading of the neutron field but for two or more fields closely overlapping (as they would have to be for the first patient) precise positioning is critical; (3) there is no device yet developed for maintaining position (motion control) during the irradiation when the patient is alone in the room; and (4) with multi-field irradiation, there is a very significant increase in irradiated healthy tissue and a correspondingly increased risk in using a new drug with little knowledge of healthy brain tolerance. In view of the many added safety concerns and the lack of strong benefit in multi-field irradiation for a superficial tumor, the decision was made to use a single fraction treatment for the first patient series.

Positioning

For single-field irradiations it would not (initially) seem that positioning the patient would be a difficult problem. The BMRR irradiation room has lasers for alignment as well as a special table. Positioning, however, turned out to be a significant problem to solve. It is one thing to mathematically describe a beam/patient orientation but quite another to realize it. The beam exits from the wall plane and the beam-patient entry point is placed as close as possible to the beam-wall exit; because of this some fields are impossible to obtain simply due to patient anatomy. Positioning was successfully accomplished however. During the CT acquisition, the first patient had four metal beads positioned at four locations marked indelibly on the skin. These beads were identified in the CT images using Rtpe and registered to the 3D model. The locations of the beads were then transformed to a coordinate system at the beam wall and used to position the patient. Better methods for this positioning process are still desired.

Calculations

Calculations showed that for single-field irradiation, small lateral displacements of the field are not consequential. The planning system allows the option of specifying a target point (e.g., midpoint of target, furthest part of target or some other criteria) and it finds the field such that the beam center line passes through the minimum thickness of tissue between the beam and target point. The beam position is specified by the target point, the distance to the beam source plane and two rotation angles. Variations of five degrees in rotations were found to have little consequence on isodose contours or dose volume histograms for the target. A five degree offset in the beam angle translates to an approximate five mm lateral displacement of the field center. It is felt that positioning within five mm is achievable. Specified limits for maximum biologically-equivalent healthy-tissue dose was 10.5 Gy to the volume exceeding the 90% dose. Equivalent dose was calculated using the BNL compound factor of 1.3 for BPA in healthy tissue and an relative biological effectiveness (RBE) of 3.2 for the hydrogen recoil proton and the nitrogen-capture proton. Of course, the desired goal for therapy is to deliver the maximum dose to all points in the target. In these cases it was also desired to ensure the delivery of at least 20 Gy Eq. to the tumor volume. Tumor-cell dose was calculated assuming the BNL compound factor of 3.8 for BPA. Selected isodose plots are shown in Figure 21 and dose-volume histograms for the target and healthy brain are shown in Figure 22.

ACKNOWLEDGEMENTS

A significant amount of the development of the user-interface software has been achieved by staff and students in computer science at Montana State University (MSU) in Bozeman, Montana.

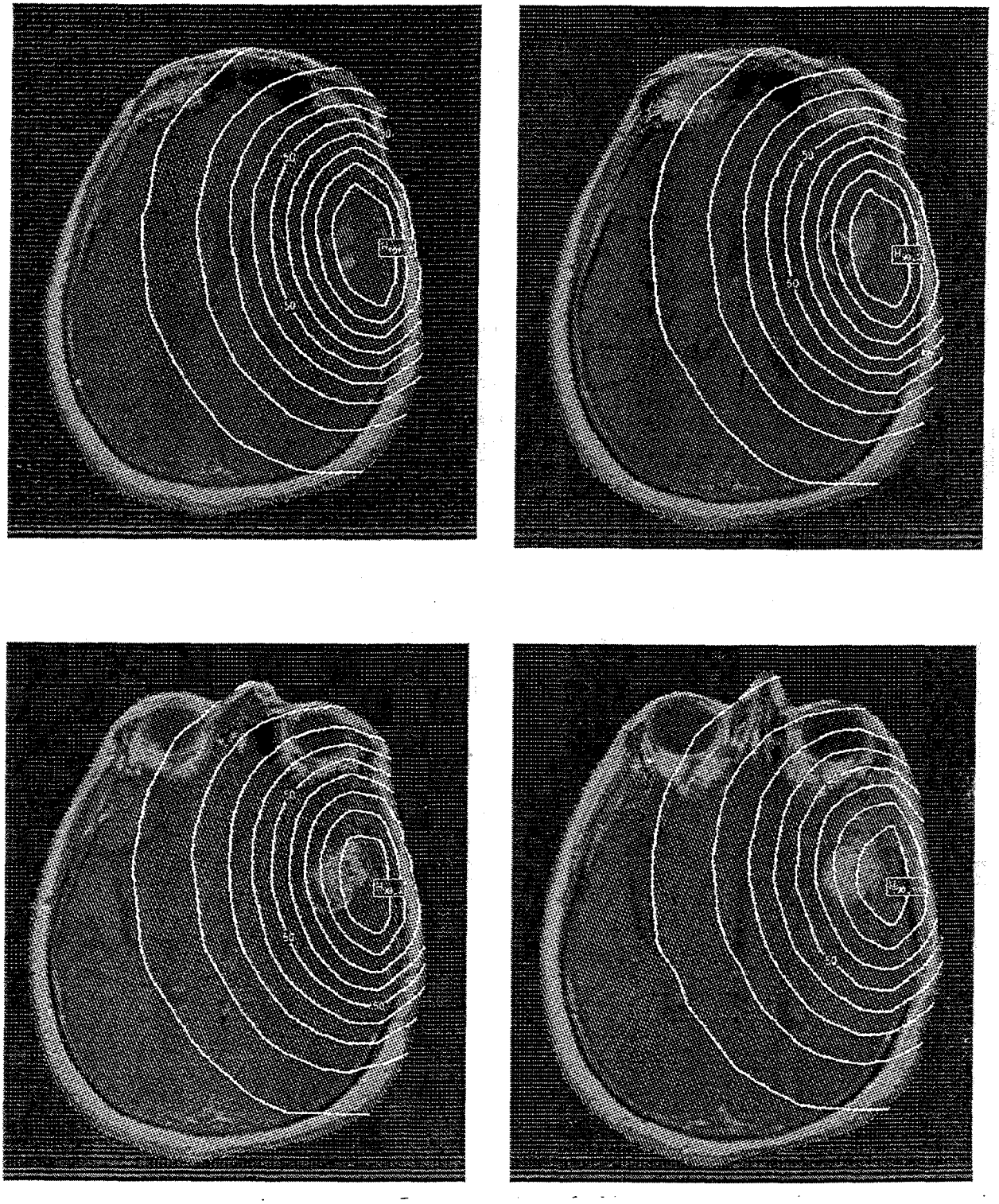

Figure 21. Typical isodose plots displayed over image.

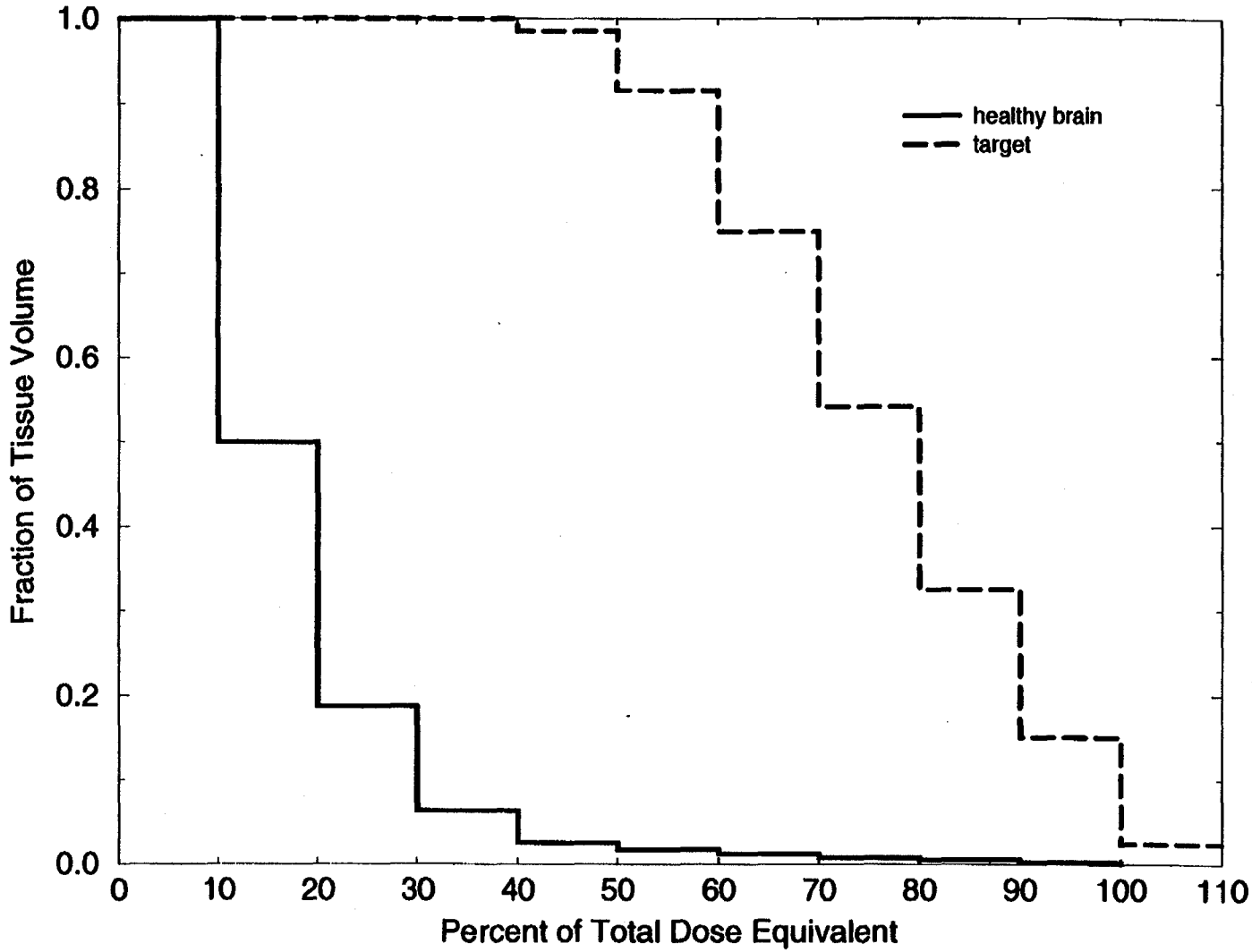

Figure 22. Equivalent dose/volume relationship.

BNCT-RTPE: BNCT RADIATION TREATMENT PLANNING ENVIRONMENT

D. E. Wessol, INEL, R. S. Babcock, Jeremy Cook, John Evans, Gary Harkin, Denbigh Starkey, Computer Science Department, Montana State University (MSU), and F. J. Wheeler, INEL

Introduction

Several improvements have been developed for the BNCT radiation treatment planning environment (BNCT_Rtpe) during 1994. These improvements have been incorporated into Version 1.0 of BNCT_Rtpe which is currently installed at the INEL, BNL, Japanese Research Center (JRC), and Finland's Technical Research Center. Platforms supported by this software include Hewlett-Packard (HP), SUN, International Business Machines (IBM), and Silicon Graphics Incorporated (SGI). A draft version of the BNCT_Rtpe user manual is available. Version 1.1 of BNCT_Rtpe is scheduled for release in March 1995. It is anticipated that Version 2.x of BNCT_Rtpe, which includes the nonproprietary NURBS library and data structures, will be released in September 1995.

Nonproprietary NURBS development

Version 2.x of BNCT_Rtpe will not contain any proprietary U of U software. Instead, all of the U of U NURBS libraries will be replaced with a nonproprietary set derived from the Army Research Laboratory-Computer Aided Design (ARL-CAD) distribution. An efficient ray-tracing method was developed that will interrogate the new NURBS surfaces, which is based on the hierarchical bounding box method developed at the U of U. This ray-tracer will be presented at the ARL-CAD symposium in May 1995. At this time the new method does not adaptively refine the NURBS surfaces but relies on oversampling the surface based on the smallest polygon, which meets the necessary refinement criteria including surface cracking. This results in large memory consumption, which will be mitigated by either an adaptive and coarser polygonal mesh or a reduced level of bounding coupled with Newton iteration to find the final intersection point.

Additionally all of the U of U data structures, display lists, and macro functions are being replaced. This has turned out to be a very significant effort since this coding is interwoven with the INEL coding.

Image Plane Dose Contours

A dose contouring function (Xcontours) has been developed, which displays the rtt_MC dose data computed for a specific plane onto the image corresponding to that plane. This function allows the researcher to quantify and spatially locate the dose delivered to the patient.

The Xcontours function uses the contouring utilities from the National Center of Atmospheric Research (NCAR) and requires a license from NCAR. Xcontours may be run either in stand-alone mode or from BNCT_Rtpe's image widget. The Xcontours function has a self-explanatory portable interface based on X11/Motif software standards.

Features include variable contour levels, smoothing, label sizes, and options to manipulate the color map and contour colors. Xcontours is dynamically dimensioned and will work with either evenly or unevenly spaced gridded data. The dose factor option, which allows the user to interactively specify RBE, was added to Xcontours in 1994. A masking feature that will remove contours lines generated outside the active image area was also developed.

Future options include a print option, simultaneous dose display, the ability to handle a variety of image formats, measuring tools, and additional image analysis tools.

Automated Control Point Selection Algorithm

The automated external and internal edge detection algorithms have been included in Version 1.0 of BNCT_Rtpe, which allows for automatic curve definitions of distinguishable bodies or regions in an image. This option has some implementation difficulties that should be resolved in Version 1.1 and later.

B-Spline Surface Interference Checking Algorithm

This option was scheduled for implementation in 1994 but this effort was preempted by several higher priority items including the new NURBS development and the patient treatments at BNL. This is also a major effort that is scheduled to start in 1995.

Miscellaneous New Features and General Cleanup

Several improvements and fixes were made for Version 1.0, which included the following:

- Developed color map stabilization among the various hardware platforms including the support of multiple hardware color maps
- Improved image normalization and the use of 128 gray-scale levels
- Changed pixel locator to report coordinates in millimeters with respect to the origin at the center of the image
- Developed image ruler that provides image distances and angular information
- Developed two utilities that provide the dose volume histograms and dose line edits
- Developed ad hoc positioning scheme for BNL patients
- Fixed render option
- Improved capping interface
- Generation of material/region correspondence file for rtt_MC
- Cleaned up of some of the QSH utility functions.

Work in Progress

A much improved interface between rtt_MC and BNCT_Rtpe is still under development and this must be completed before the software is generally useable by the clinician.

Besides the major development with the new NURBS implementation and the B-Spline surface interference checking algorithm, the following items for Version 2.x and beyond are being developed:

- Improved image processing and display tools
- Image film strip
- Beam/patient visualizer
- Simultaneous edit/measure option
- Store all surface geometric information in modeling space
- Integrate dose volume histogram and line edit code
- Prevent counterclockwise control point entry
- Develop nonrigid fiducial marker-based multimodality image registration tool
- Investigate useable three dimensional displays for BNCT
- Investigate nonmanifold geometries (voxel-based) and associated transport model for BNCT (Version 3.x).

The integration of the more widely used medical image file formats into the BNCT_Rtpe file input interface (besides just QSH) needs to be considered. There are consistency problems with the QSH header files that must be addressed before QSH can be considered an acceptable intermediate image file format for BNCT.

Finally, the current bead-based positioning scheme used for the BNL patients is tedious and error prone and a better method needs to be developed.

AN ACCELERATOR-BASED EPITHERMAL PHOTONEUTRON SOURCE FOR BNCT

David W. Nigg, Hannah E. Mitchell, Yale D. Harker, Woo Y. Yoon, James L. Jones, INEL, and J Frank Harmon, Physics Department, ISU

INTRODUCTION

Therapeutically-useful epithermal-neutron beams for BNCT are currently generated by nuclear reactors. Various accelerator-based neutron sources[21,22,23] for BNCT have been proposed and some low-intensity prototypes of such sources, generally featuring the use of proton beams and beryllium or lithium targets have been constructed. Scaling of most of these proton devices for therapeutic applications will require the resolution of some rather difficult issues associated with target cooling. This paper describes an alternate approach to the realization of a clinically-useful accelerator-based source of epithermal neutrons for BNCT that reconciles the often-conflicting objectives of target cooling, neutron beam intensity, and neutron beam spectral purity via a two-stage photoneutron production process.

CONCEPTUAL DESIGN FOR A CLINICAL FACILITY

A conceptual design for a device to produce epithermal photoneutrons having a spectral distribution appropriate for epithermal-neutron BNCT is shown in Figure 23. In this concept, electron beams impinge inward upon tungsten targets located at the outer radius of a small cylindrical tank of heavy water (D_2O) and possibly beryllium. A fraction of the energy of the electrons is converted in the tungsten targets into radially-inward-directed bremsstrahlung radiation. Photoneutrons are subsequently generated in the D_2O (and beryllium) region within the tank. The photoneutron yield per incident electron (about 10^{-4} at the incident electron beam energy of interest) from this arrangement appears to be comparable to the neutron yield attainable[21] with published accelerator-based epithermal-neutron sources for BNCT that use low-energy protons impinging on a lithium target. Photoneutrons produced in the central region enter a surrounding cylindrical moderating and filtering region composed, in this particular design, of 90% aluminum fluoride (AlF_3) and 10% lithiated aluminum, by volume, with 1% by weight of natural lithium fluoride added to suppress the thermal neutron flux. The filter/moderator region is followed by a bismuth-lead gamma shield and a lithiated-polyethylene neutron beam delimiter. The geometry of the device provides for two horizontally-opposed treatment beams, as shown.

Calculations to estimate the performance of the proposed photoneutron device were performed using the ACCEPT[24] three-dimensional electron-photon coupled transport code to compute the bremsstrahlung flux throughout the device, and the Discrete Ordinate Radiation Transport (DORT)[25] neutron-photon transport code (with the BUGLE-80[26] cross-section library) to compute the transport of photoneutrons (and neutron-capture gammas) to the irradiation position. These two codes were coupled using appropriate photoneutron production data from various sources. Confirmatory neutron and capture-gamma transport calculations were performed using the MCNP[27] Monte-Carlo neutron and photon transport code.

The DORT results for the calculated scalar neutron flux spectrum at the irradiation point for the concept illustrated in Figure 23 are presented in Figure 24 for the case of 100% D_2O in the central conversion region with an incident 6 MeV, 1 mA electron beam configuration. Similar results are obtained using MCNP. Scaling the electron beam current to 100 mA and integrating the computed

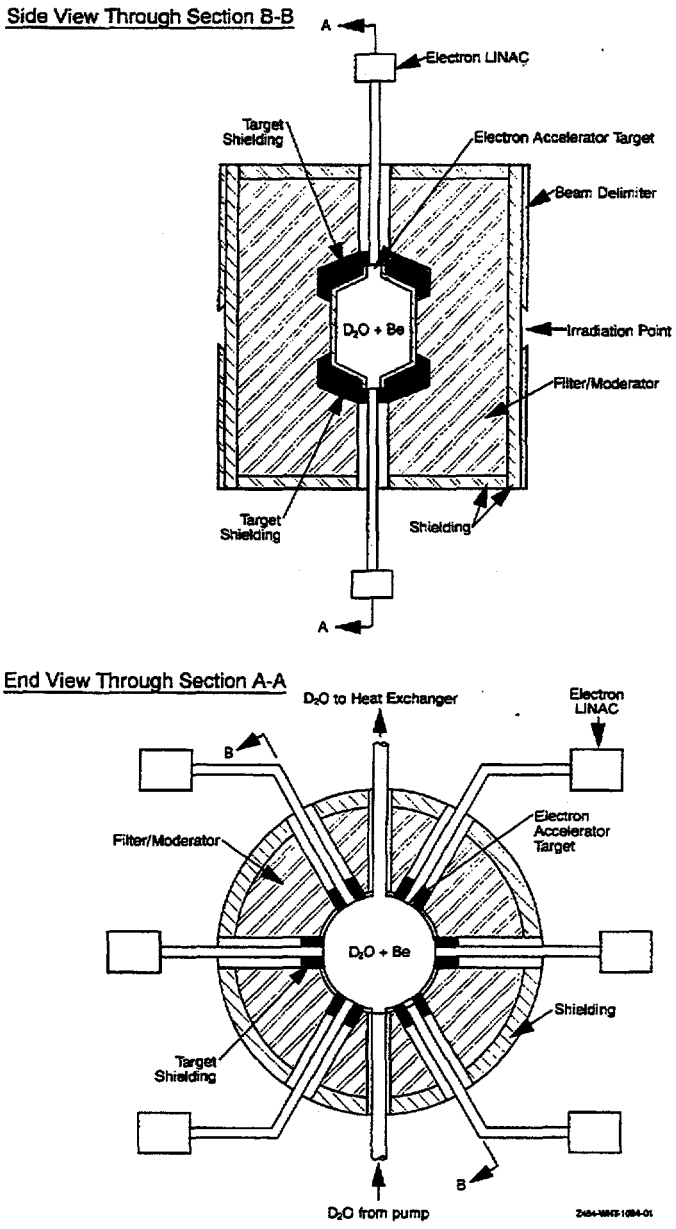

Figure 23. Epithermal photoneutron source (patent pending).

neutron spectrum shown in Figure 24 over the appropriate lethargy range yields a therapeutically-useful total epithermal flux intensity in the free-field at the irradiation point of approximately 1×10^9 n/cm^2-s. The calculated nonselective neutron-beam-induced proton recoil dose in hydrogenous tissue per unit useful epithermal neutron flux at the irradiation point for this case is 1.6×10^{-11} cGy/n-cm^2, which is below what is believed to be the radiobiologically-acceptable maximum. The incident gamma dose at the irradiation point due to neutron capture gammas originating within the device is approximately 1.5×10^{-11} in the same units. The incident gamma dose at the irradiation point due to direct source bremsstrahlung is controllable to approximately

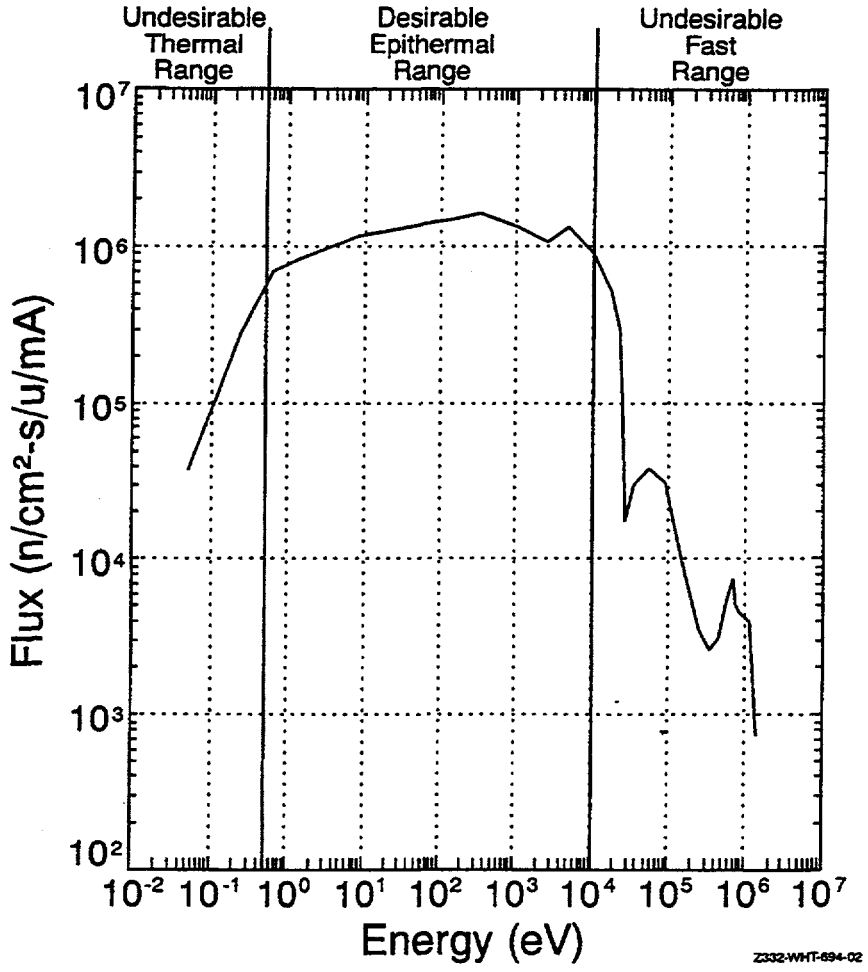

Figure 24. Free field flux spectrum for the conceptual BNCT photoneutron epithermal neutron source design (E_e = 6 MeV).

the same level (or less, as needed) by appropriate shielding placed at various strategic locations within the device as shown in Figure 23. Waste heat from the entire process may be removed using standard heat transfer techniques by flowing the D_2O through the central tank to an external heat exchanger and thence back into the central tank. Modest (10–20 liters/second) D_2O flow rates appear to be sufficient to remove the expected waste heat without exceeding reasonable temperature levels within the system.

BENCHMARK EXPERIMENTS

Experimental proof-of-principle testing for a low-current benchtop prototype of the epithermal photoneutron source concept is currently ongoing. The primary objective of these experiments is to validate the computational methods used as described previously to estimate the performance of the full-scale conceptual device.

A tunable electron linear accelerator manufactured by the Varian Corporation, shown in Figure 25, was used for the benchmark experiment described here. The main drift tube of this accelerator incorporates a water-cooled tungsten target for converting the electron beam energy into bremsstrahlung radiation. A direct measurement of the electron current impinging on the target is obtained by magnetically diverting the electron beam from the tungsten target into a second drift tube terminated by a Faraday cup. The average energy and spectral distribution of the electron beam can also be directly estimated by varying the magnetic field used to divert the electron beam into the second drift tube and correlating the measured beam current with the strength of the magnetic field as the beam is swept across the Faraday cup. A heavy cylindrical tungsten collimator was placed around the accelerator target. The bremssrtahlung radiation emerging from the collimator is directed into a sealed cylindrical lucite tank of D_2O having a radius of approximately 76 mm (3 in.) and a thickness of approximately 100 mm (4 in.). The measured activation of indium foils placed at the outer radius and on the end of the D_2O tank is used to infer a measured photoneutron production rate within the tank. This is done with the aid of a fine-mesh, 27-group, two-dimensional, DORT discrete-ordinates neutron transport calculation of the foil activation per photoneutron produced within the tank, assuming the theoretical photoneutron source spectrum. The DORT model included the lucite tank, the heavy water inside the tank, and the indium foils.

The measured photoneutron production rate within the tank for three different electron beam energies was compared with the theoretical photoneutron production rate within the tank, calculated from first principles using the computational sequence described previously. The theoretical calculation was normalized to the measured bremsstrahlung radiation field at a known location in the geometric setup (just downstream of the D_2O tank on the beam axis). With this arrangement, two independent methods for normalizing the theoretical calculation of the photoneutron source strength were thus available (the direct electron beam current measurement, and the normalization to the bremsstrahlung radiation flux at a known location).

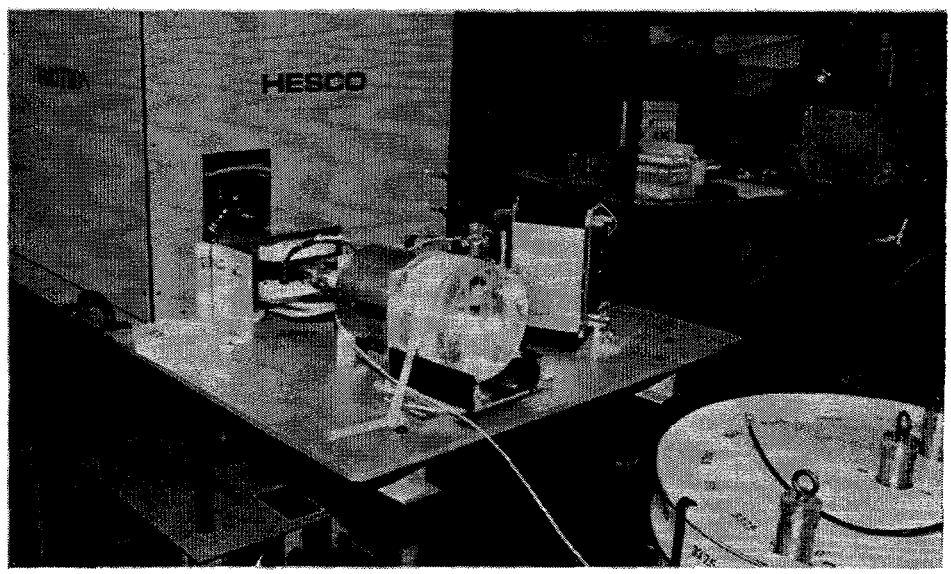

Figure 25. Experimental apparatus for the photoneutron production experiment.

The results of the photoneutron experiment are shown in Figure 26. The theoretical calculations of the photoneutron source produced within the tank, normalized to the downstream bremsstrahlung flux measurements for each electron beam energy, are also shown for comparison. (Normalization of the theoretical calculations to the directly-measured electron beam current for each beam energy produces essentially the same results). Agreement between theory and experiment is well within a factor of two over the electron energy range considered, validating (to the extent demonstrated) that the computational methods used to estimate the performance of the conceptual clinical device described earlier do indeed produce realistic results for the photoneutron source that can be generated by this concept.

CONCLUSIONS

The computational results and initial benchmark experimental data presented here indicate that the described photoneutron concept may offer a very promising alternative approach to the production of accelerator-based epithermal neutrons for BNCT. Clinically-useful neutron source intensity and spectral purity levels appear to be attainable. Future work will involve the measurement of actual filtered epithermal-neutron spectra rather than the unfiltered photoneutron source, again with a scaled-down benchtop model of the concept. If these measurements are, as expected, in agreement with theoretical predictions, then scaling and system optimization studies for a full-scale device will be conducted.

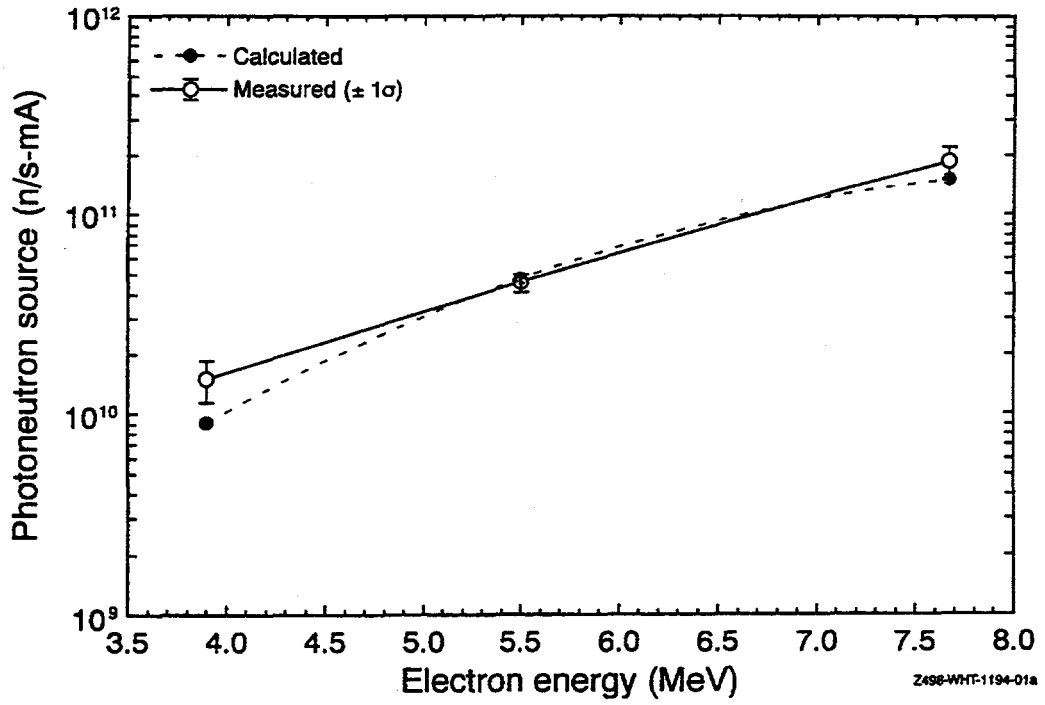

Figure 26. Calculated and measured total photoneutron sources for the Varitron photoneutron experiment.

AMERICAN BRAIN TUMOR PATIENTS TREATED WITH BNCT IN JAPAN

George E. Laramore Ph.D., M.D., Brian R. Griffin M.D., and Alexander Spence M.D., Ionix Corporation

PURPOSE

The purpose of this work is to establish and maintain a database for patients from the United States who have received BNCT in Japan for malignant gliomas of the brain. This database will serve as a resource for the DOE to aid in decisions relating to BNCT research in the United States, as well as assisting the design and implementation of clinical trials of BNCT for brain cancer patients in this country. The database will also serve as an information resource for patients with brain tumors and their families who are considering this form of therapy.

BACKGROUND

The Japanese BNCT program as carried out by Dr. Hiroshi Hatanaka constitutes the world's largest experience in treating patients with BNCT. However, the Japanese experience is hard to interpret due to a dearth of published data regarding treatment details, patient characteristics, etc. In order to better analyze the actual efficacy of BNCT as carried out by the Japanese investigators, an attempt is being made to determine the identity of all patients from the United States who have traveled to Japan for BNCT. Their tumor pathology will be independently verified, various prognostic factors determined relating to treatment outcome,[28] and then a comparison made between the outcome (i.e., survival) of this patient group compared to a set of patients with similar tumor pathologies and prognostic variables who received conventional treatment in the United States.

All patients who have been treated in Japan have received sodium-mercaptoundecahydrododecaborate (BSH) as the ^{10}B carrier. This is the same drug that will be used in Europe when patient treatment begins at the Petten, the Netherlands reactor, but is different from the drug that is currently being used for patient treatment at the BMRR (i.e., p-borono-L-phenylalanine or BPA). Hence, this work may also serve as a basis for comparing the efficacy of these two boron compounds.

The initial phase of this work has been focused on patient survival. Patients from the United States went to Japan to receive BNCT through two main channels: (1) via contacts at the INEL or (2) via contacts at the BNL/Massachusetts Institute of Technology (MIT). Knowledgeable individuals who have been involved with patient referrals have been contacted, the names, addresses, and phone numbers of these patients obtained, and then either the patient or next-of-kin contacted. Permission has been obtained to acquire certain medical records and tumor pathology for review. Standard guidelines relating to patient material have been followed in this regard. The information is incorporated into a computerized database using FOX-BASE software.

Because tumor pathology is a key determinant in outcome, a qualified neuropathologist and a neurologist has been recruited to review the pathology and grade the tumors according to the Nelson schema[29] as either anaplastic astrocytomas (AAF) or GBM. Twelve patients to date have had a complete review of their tumor pathology and had their relevant prognostic factors determined from a review of their medical records. Interestingly, one patient who had been considered to have a GBM actually had a central nervous system lymphoma based on pathology review. This latter diagnosis was confirmed using special tumor markers on the cell blocks, and two other institutions confirmed this diagnosis. This shows the importance of central pathology review in such studies. Of the 11 other patients, two have AAF, eight have GBM, and one has a gliosarcoma (treated as a GBM for purposes of analysis).

Figure 27 compares the survival of these patients compared to a pseudomatched set from the Radiation Therapy Group database[28] treated conventionally.

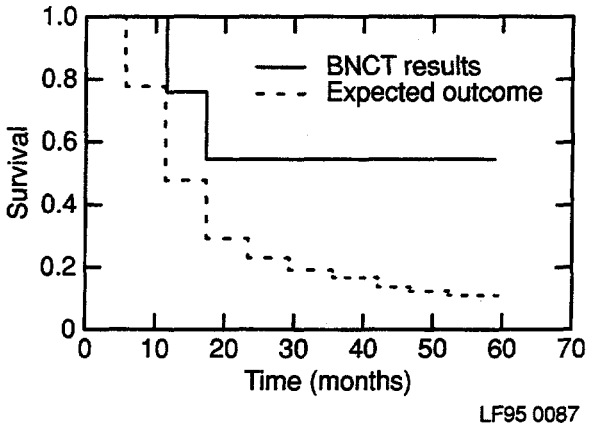

Figure 27. Survival of brain tumor patients treated in Japan.

Based upon a one-sided log rank test, there is no significant difference in survival between the two patient groups. Moreover, the two longest survivors had AAF histology (one dead at 79.5 months and one alive at 26 months) with the longest survival time of a patient having a GBM histology being 16.5 months at last followup.

This database is being continually updated via telephone calls to the surviving patients and/or their families. In addition, three other patients have been identified who may be suitable for inclusion into the database. Two of these are deceased with approximate survival times of approximately 6 and 8 months, respectively. The status of the third is unknown. Work is progressing in evaluating these patients.

FUTURE WORK

Work will continue on updating and augmenting this database. Results of the analysis will be submitted for presentation at the 1995 meeting of the American Society for Therapeutic Radiation and Oncology and a publication will follow in the conference proceedings issue of the International Journal of Radiation Oncology Biology and Physics.

The scope of the effort will be extended to analyzing the pattern of failure, evolution of radiographic changes of tumor and normal brain on MRI and CT scans, complications of BNCT, and functional outcomes of the treated patients. Information will be obtained regarding the radiation doses received by the patients and isodose distributions calculated for the various radiation components using Monte Carlo codes with geometries determined from pretreatment CT and/or MRI scans. Boron distributions will be estimated from measurements of ^{10}B blood levels at the time of therapy. Damage to normal brain tissues and areas of tumor recurrence will be correlated with these isodose distributions and clinical outcome in these patients. The information will be stored in a graphical database to facilitate retrieval and analysis, as well as to aid correlation with similar information from canine studies. This information may serve as a basis for refinements in radiation treatment planning technique to maximize tumor control and minimize neurologic complications of BNCT treatment in future clinical trials.

TIDBIT—THE INEL DATABASE OF BNCT INFORMATION AND TREATMENT

C. A. Mancuso, M-L Computer Technologies

INTRODUCTION

The INEL Database of BNCT Information and Treatment (TIDBIT) has been under development for several years. Late in 1993, a new software development team took over the project and did an assessment of the current implementation status, and determined that the user interface was unsatisfactory for the expected users and that the data structures were out of step with the current state of reality. The team evaluated several tools that would improve the user interface to make the system easier to use. Uniface turned out to be the product of choice. During 1994, TIDBIT got its name, underwent a complete change of appearance, had a major overhaul to the data structures that support the application, and system documentation was begun. A prototype of the system was demonstrated in September 1994.

THE USER INTERFACE

The initial implementation of the database was started using native Informix database tools that were character-based and function key intensive. This meant that users either had to keep a template taped to their keyboard or memorize a plethora of function keys. For a user who has frequent contact with a system, the function key approach is not a problem. For TIDBIT, however, researchers at the INEL anticipate that, except for a few "power" users, any one person's exposure to the system will be infrequent. In cases like this it is unreasonable to expect users to memorize sets of function keys because the usual result is that users won't use the system.

If the user interface can be made intuitive, infrequent users of a system are more likely to attempt to use it. Windows and its tremendous popularity are a good example. The goal was to find a way to bring "point-and-click" ease of use to TIDBIT. It was not, however, as simple as creating a Windows application that could talk to the Informix database. Potential users have as many as four different platforms with which to access the system:

- Microsoft Windows ™ users on personal computers (PCs)
- Macintosh users
- Motif users on Unix workstations
- Character based terminals.

Another mandatory requirement was that users be able to connect to the database across a wide area network. Figure 28 shows the current set of network connections.

After looking at several products, Uniface was selected. It is designed to handle all the user interfaces listed above without any redevelopment. The applications are built once and will work on all four platforms. The choice about which user interface to display is made at run time. In addition, Uniface is built around a client/server model that supports network connectivity. A product called "Polyserver" connects the database to the Internet using industry standard protocols, with the particular implementation using the TCP/IP protocol. The client side also runs TCP/IP and users can connect to the database from anywhere in the world if they can get on the Internet.

Figure 29 shows the front screen that comes up when the user runs the application. To run TIDBIT on Windows systems, the user clicks on a TIDBIT icon. On Motif and character based systems, the user types "TIDBIT" on the command line. The options on the front screen are:

Names and Places — This module is used to specify the names and addresses of all project participants including researchers, veterinarians, physicians, patients, and research facilities. It also provides a method for relating these named entities. (Figure 30).

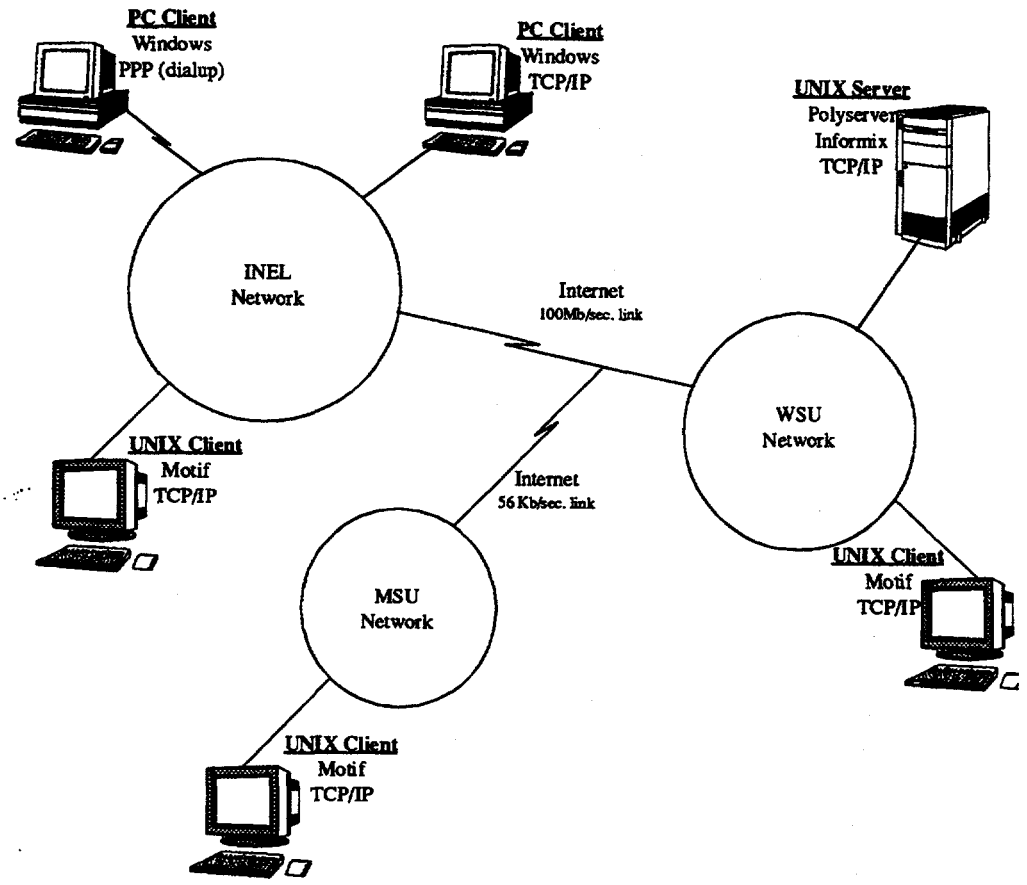

Figure 28. Current network configuration.

Patient Info — This module is used for keeping track of data related to a patient. It includes forms for planned procedures, actual results, admitting data, and clinical records. (Figures 31 through 36).

Reports — Presently this module only contains test reports. The current selection of reports is something anticipated to spark requests for additional information. (Figure 37).

Sys Admin — This module is used by system administrators to maintain the reference table data. A primary objective in the data model was to provide validity checking on as many data fields as was practical. This option is used to keep the "valid choices" up to date. (Figure 38). This module is only available to the system administrator.

The thread that runs through the operation of all of these forms is "point and click." From the main screen, the user selects the Patient Info module by pointing at the button with that label and clicking the mouse. The system then brings up the Patient Info screen (Figure 31). From there, there are other options that are "button" activated. The menu at the top of each form provides functions such as "Retrieve" and "Store." The user doesn't have to memorize anything.

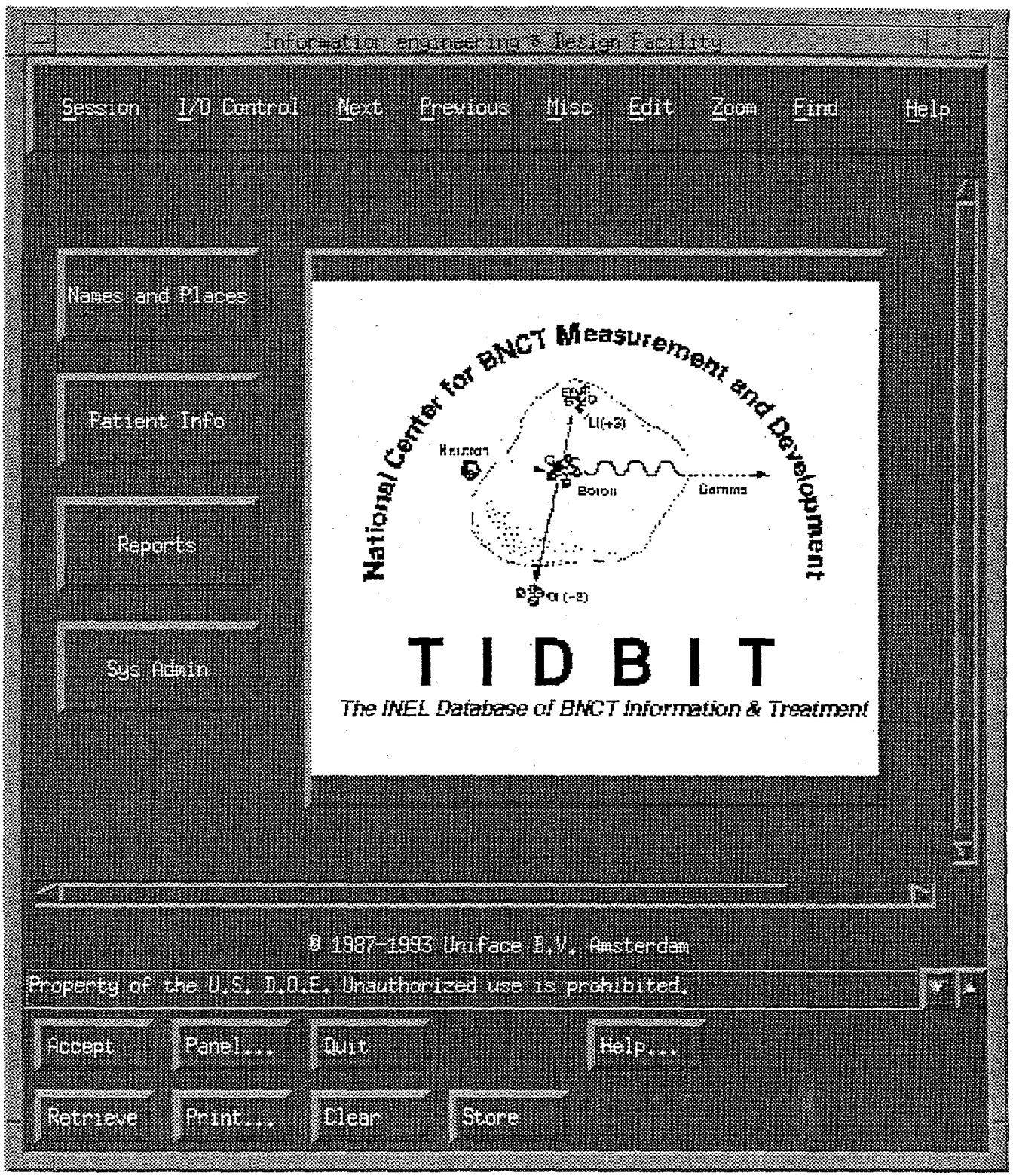

Figure 29. TIDBIT front screen.

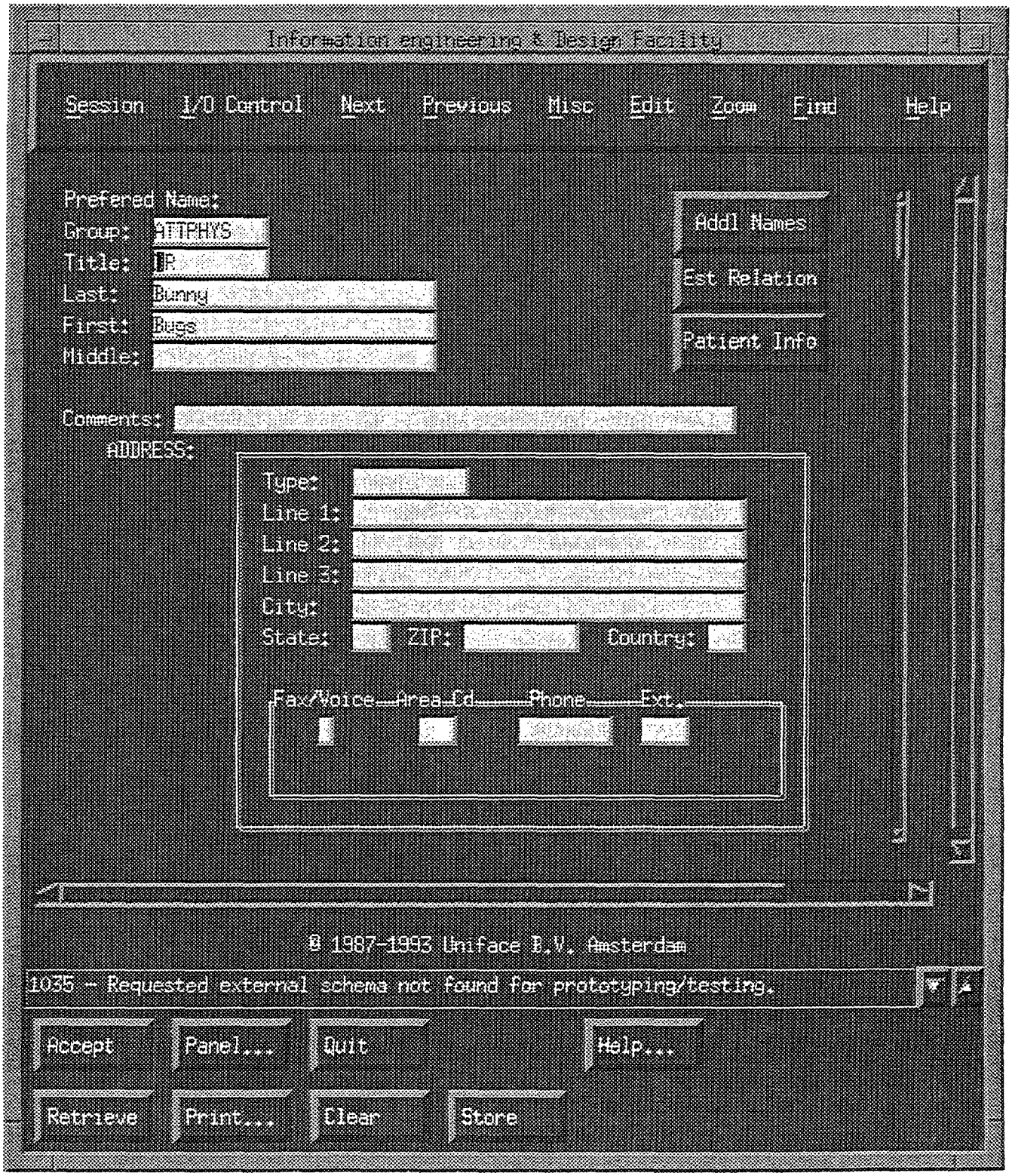

Figure 30. Names and place screen.

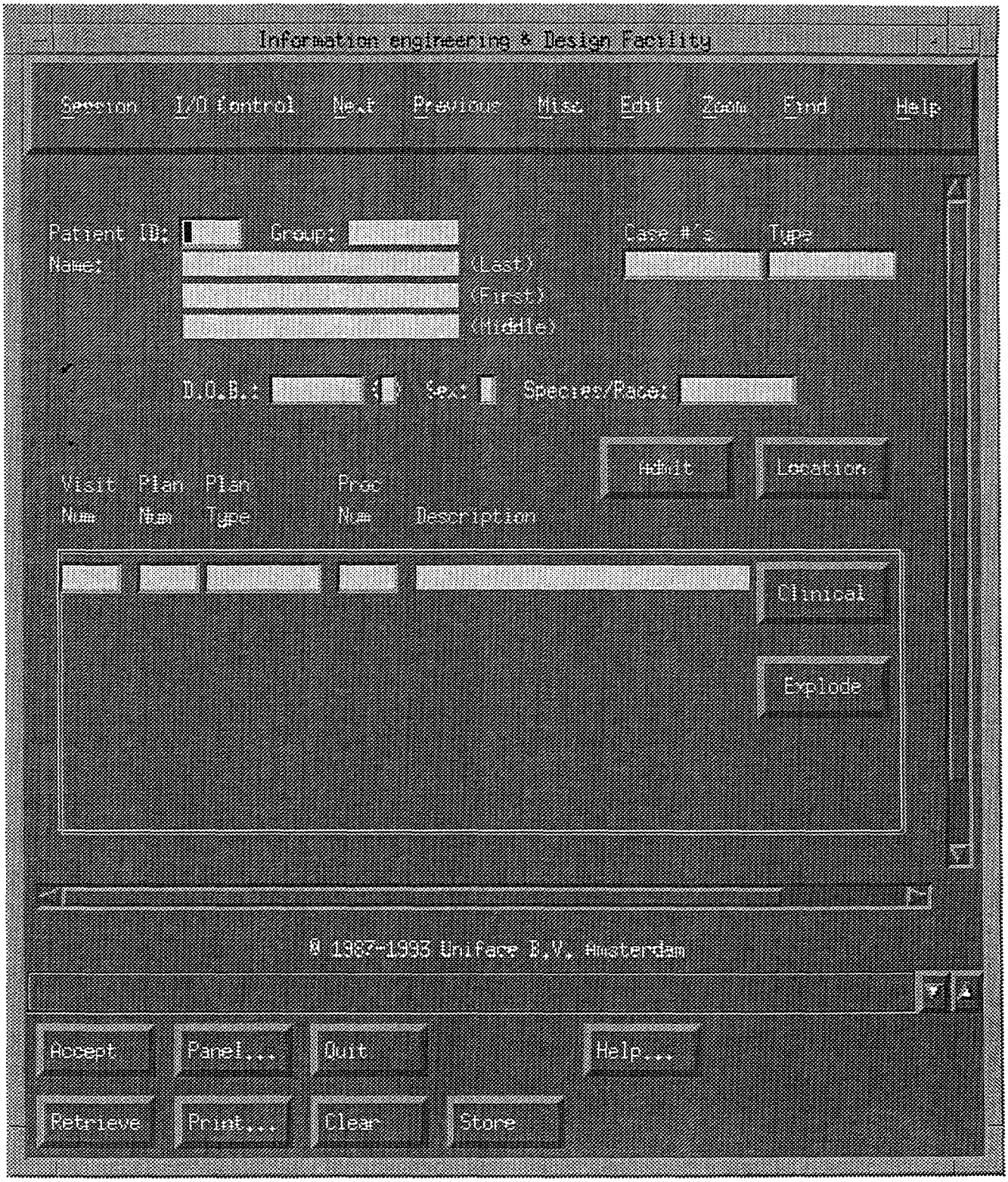

Figure 31. Patient information screen.

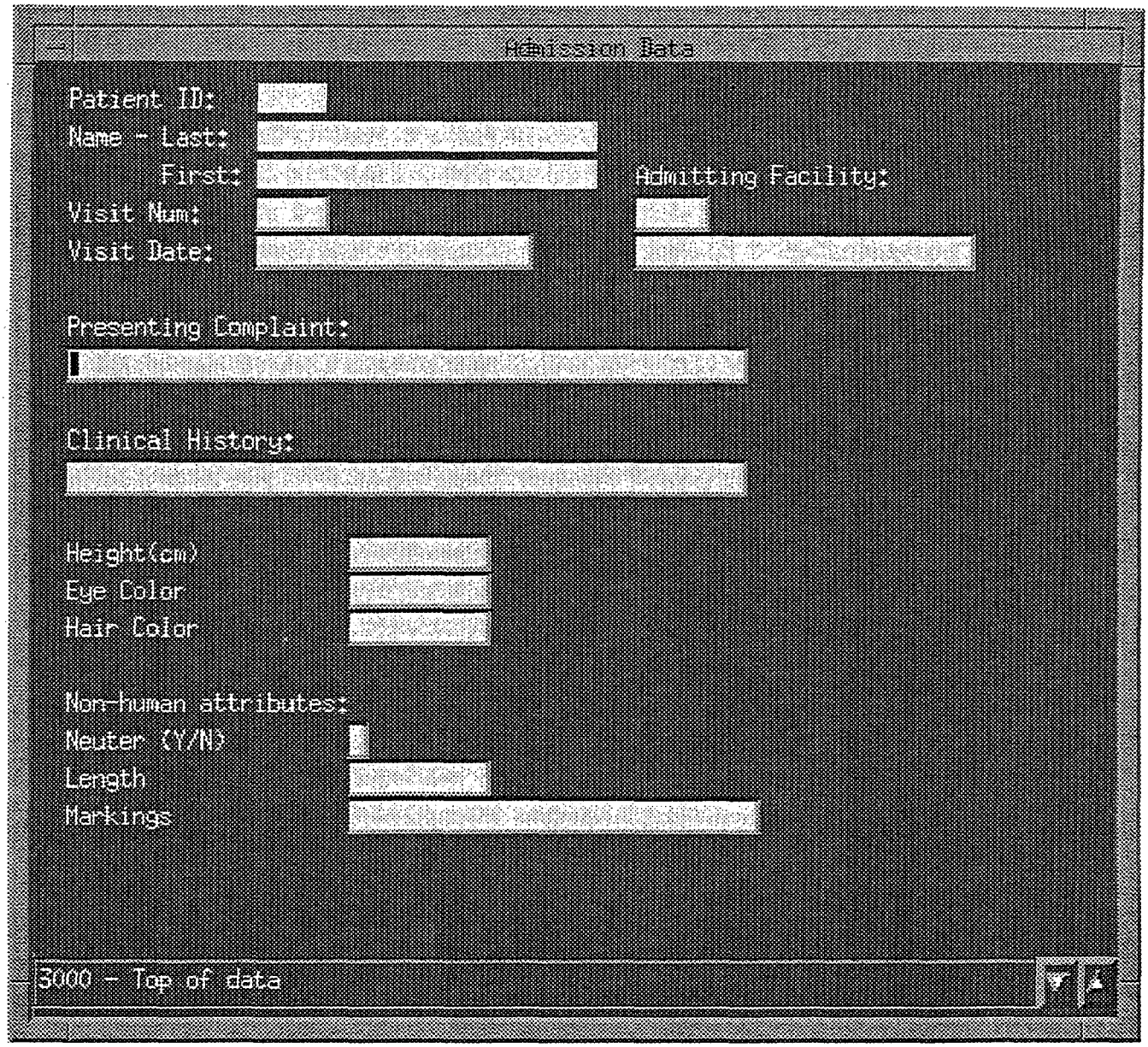

Figure 32. Admission data screen.

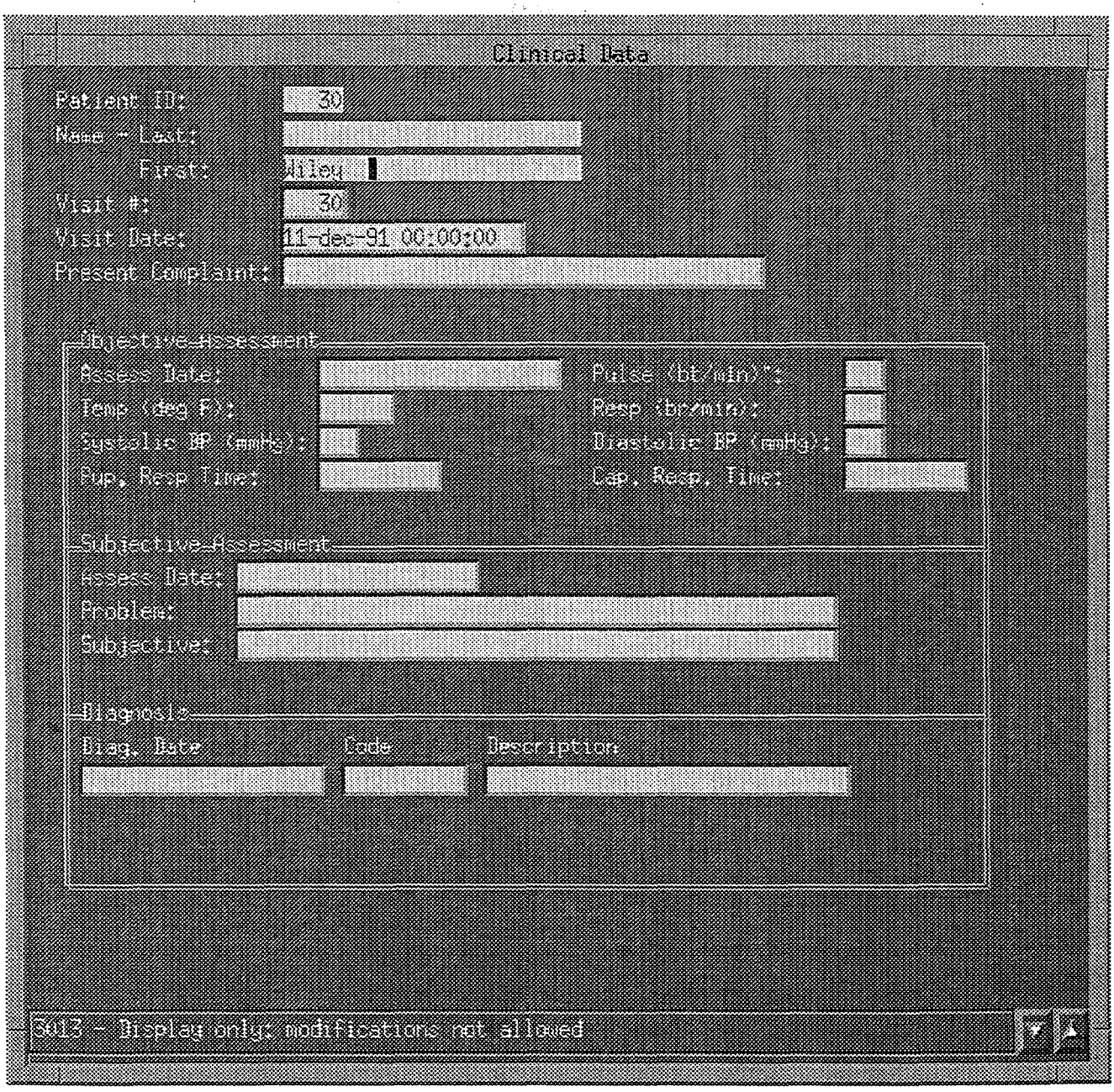

Figure 33. Clinical data screen.

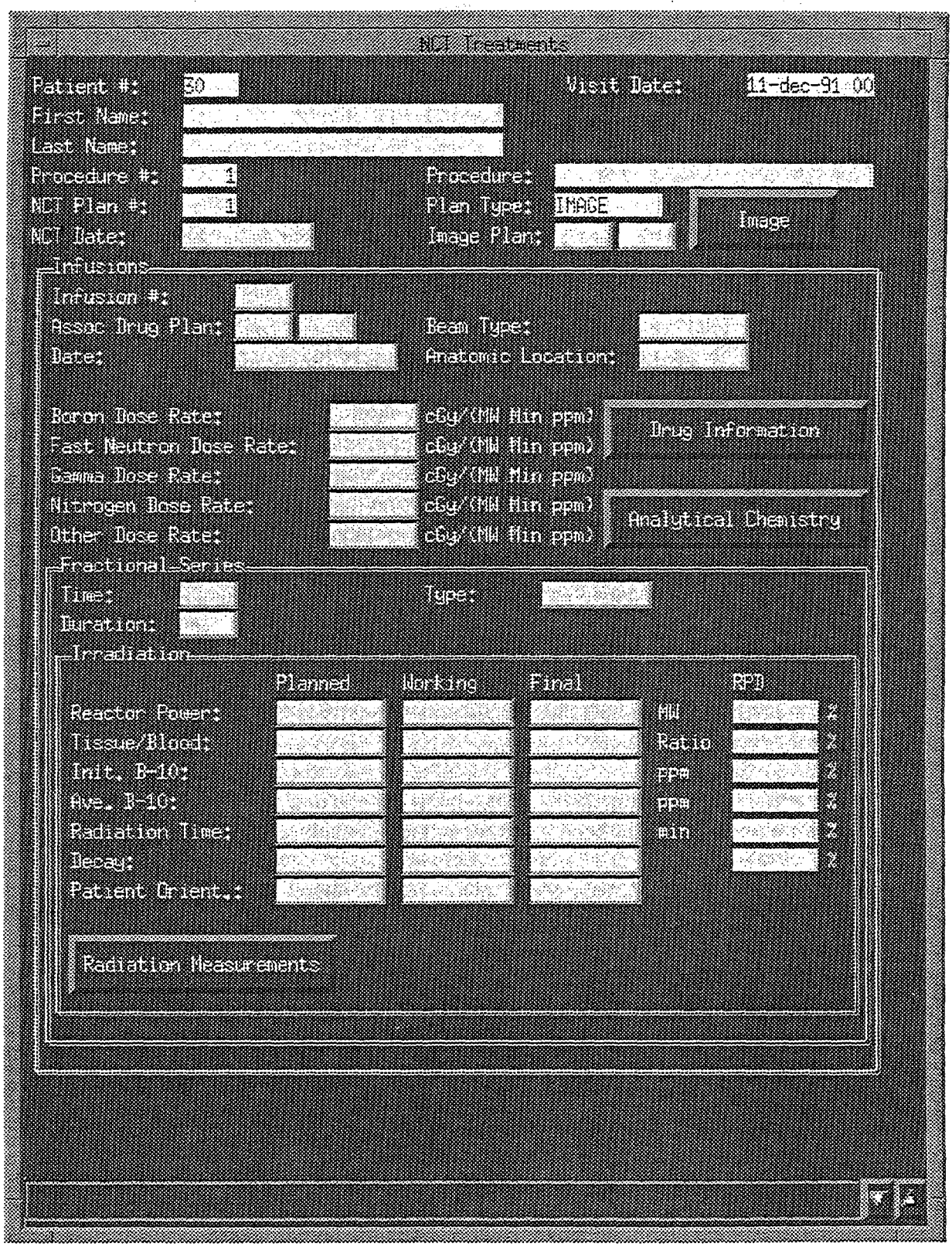

Figure 34. NCT treatment screen.

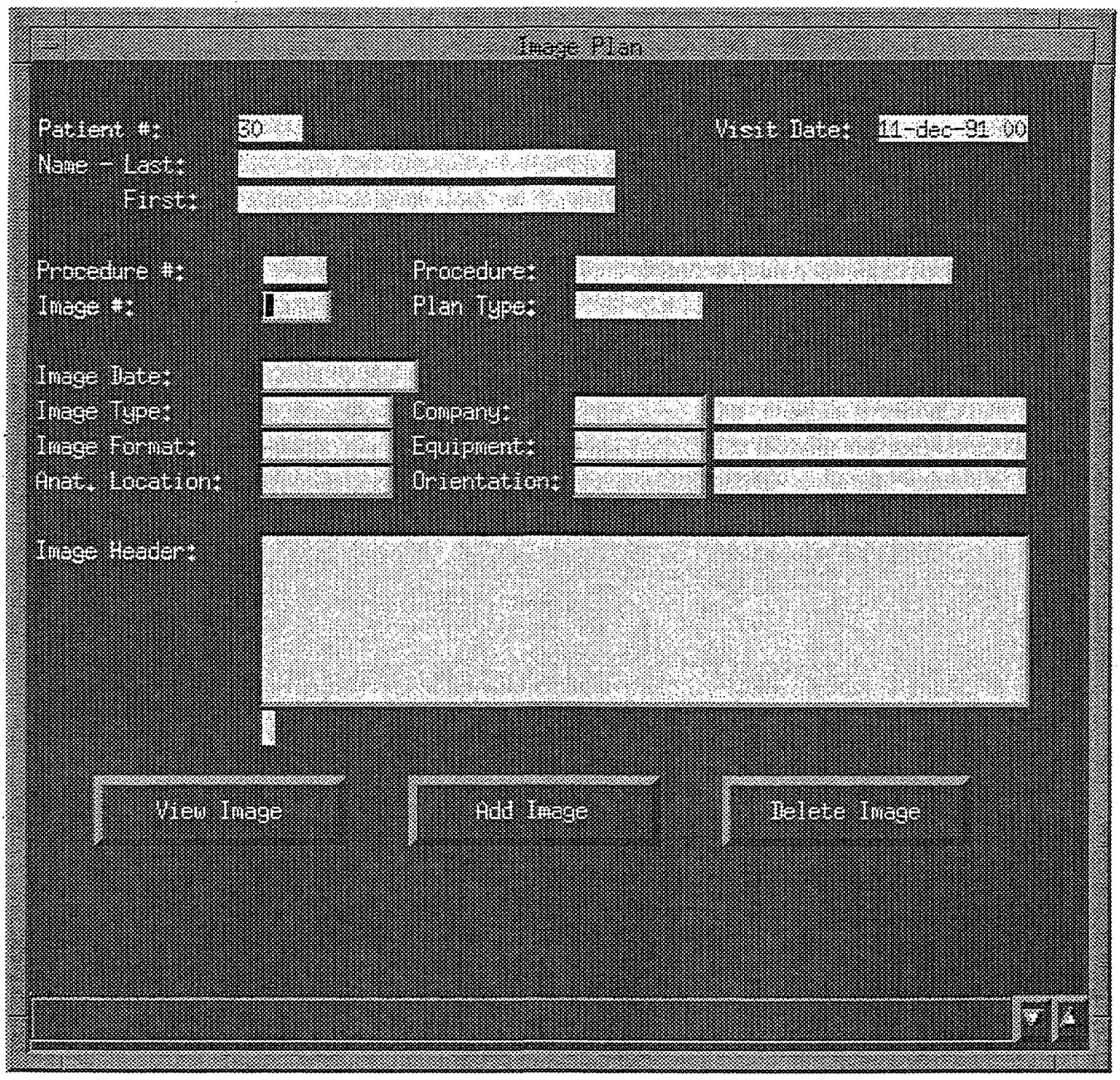

Figure 35. Image plan screen.

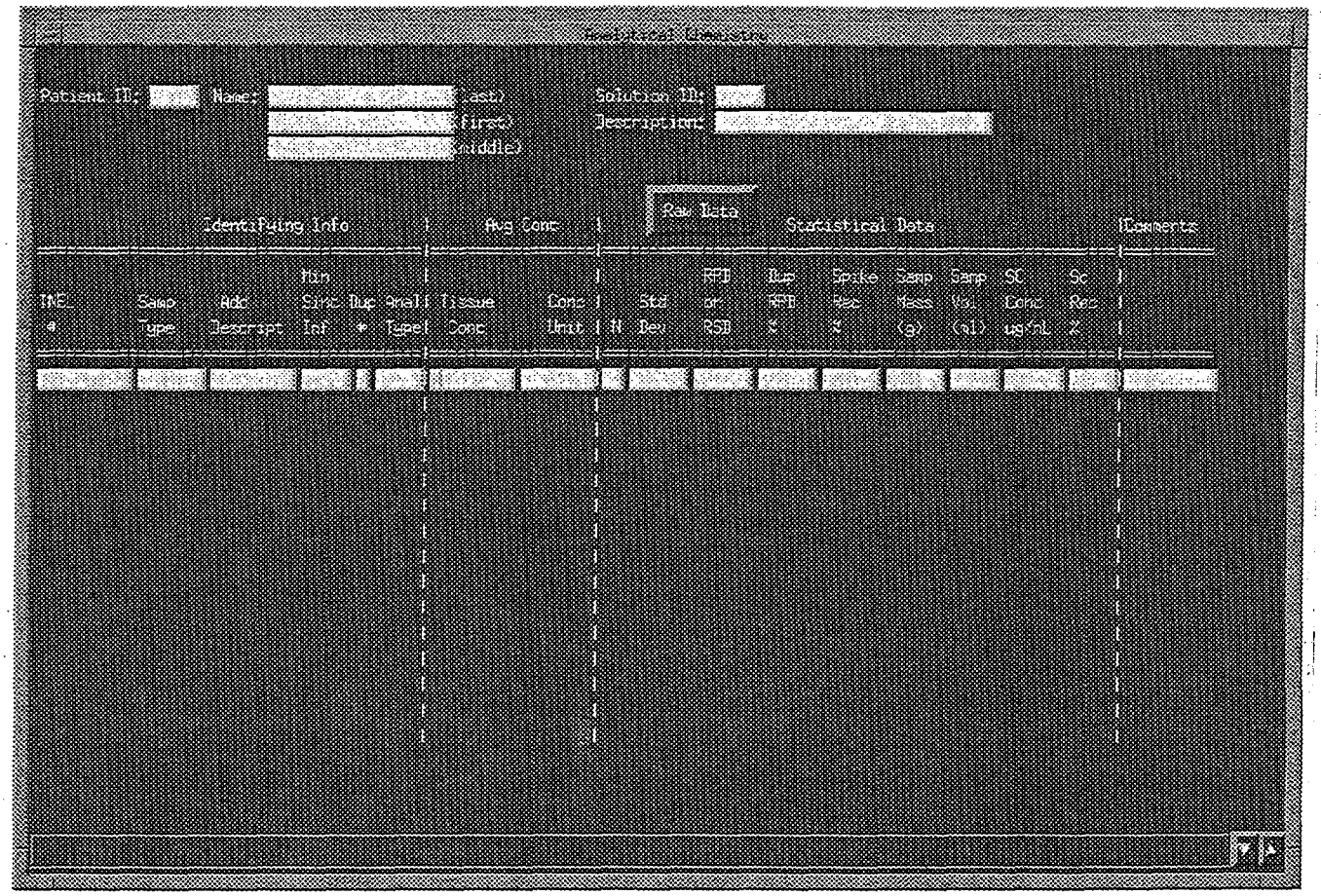

Figure 36. Analytic chemistry data screen.

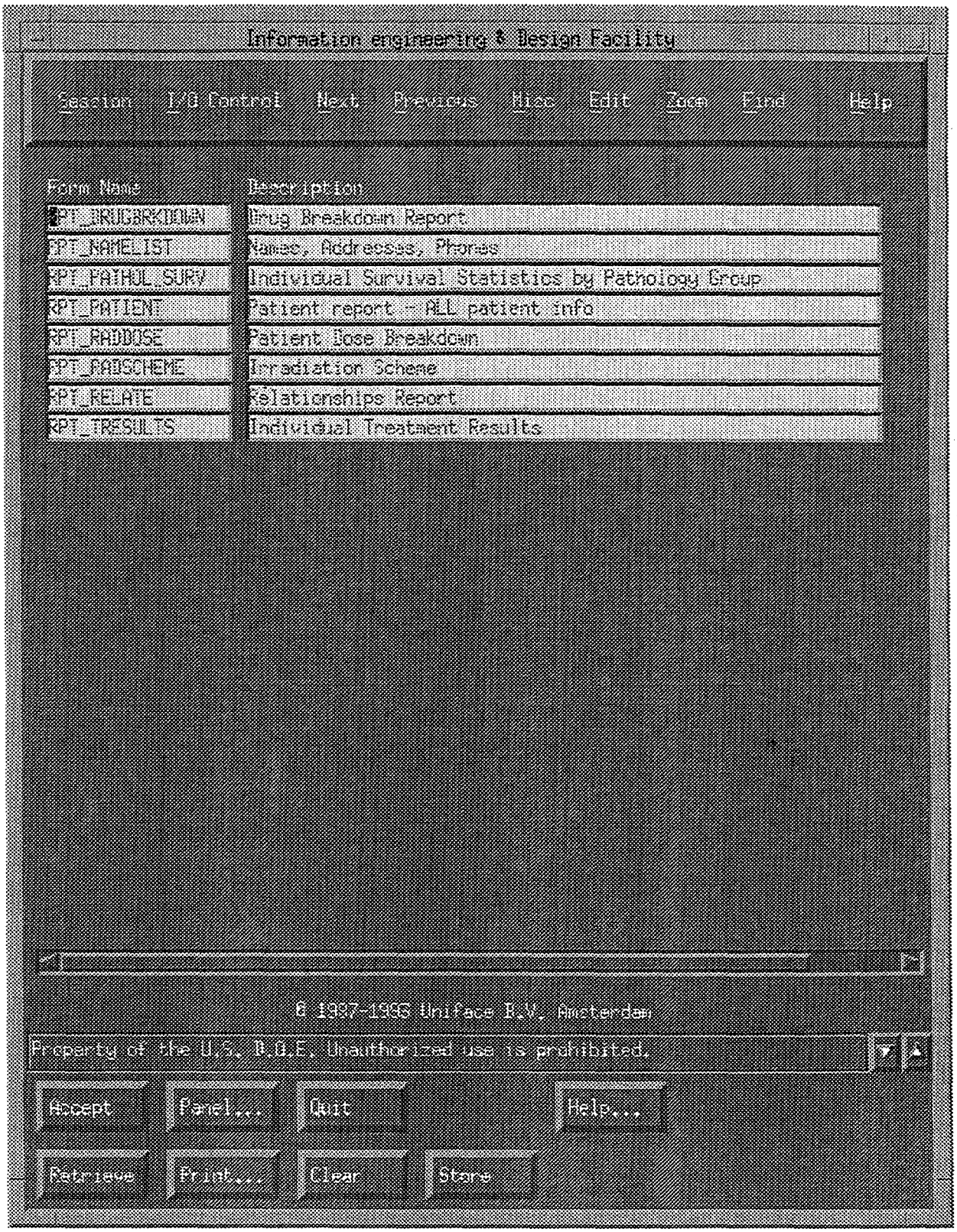

Figure 37. Reports selection screen.

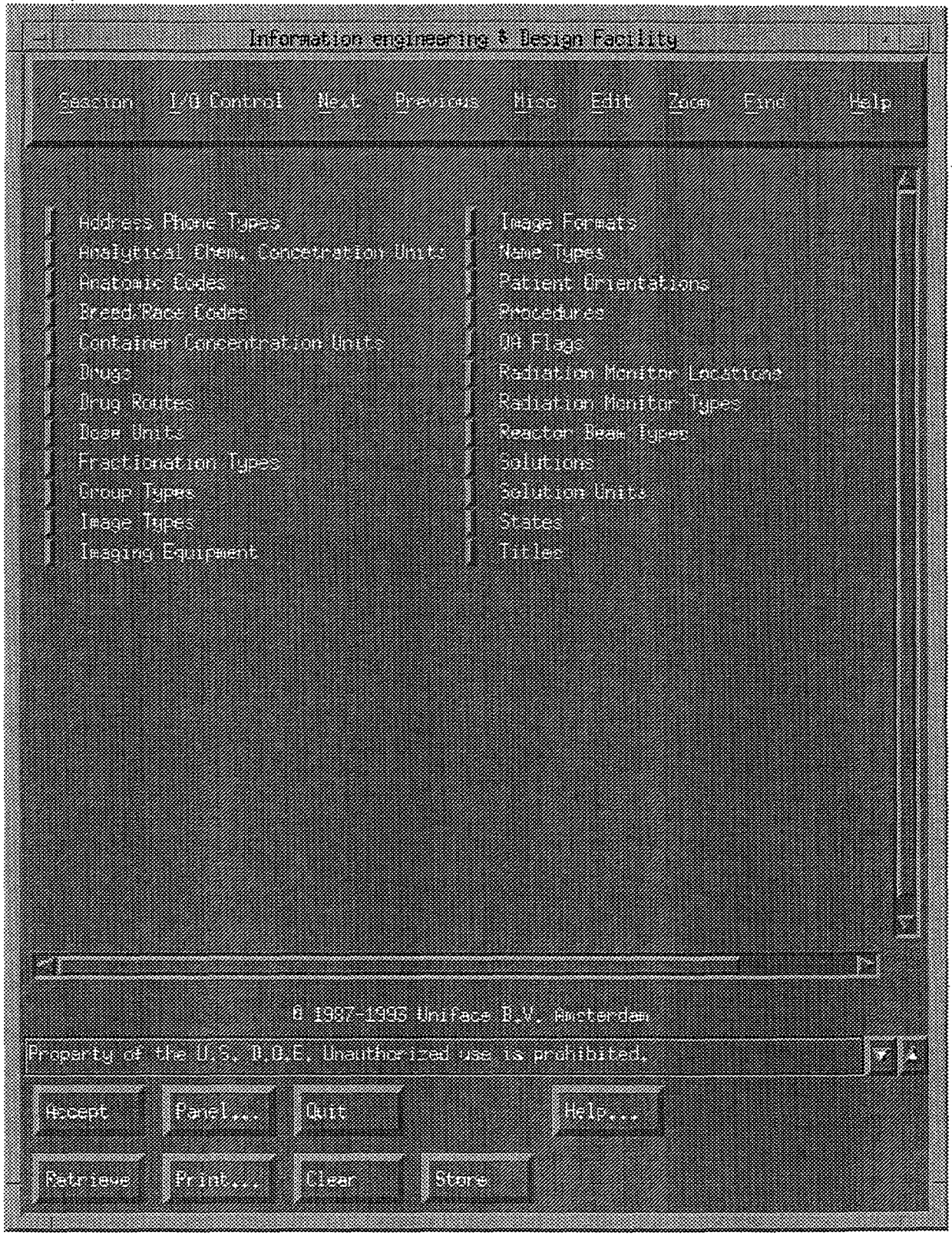

Figure 38. System administration selection screen.

During the September 1994 demonstration, several improvements were identified, and a new version of Uniface came out to support storing raw image data.

THE DATA STRUCTURES

When the new development team took over the project, the data model was simplified and enhanced to handle data from multiple fraction irradiation treatments and to better represent the drug solution information. Analytic chemistry data were also implemented for the first time. Although not presently implemented, the data structures have also been designed to handle protocols. Figures 39 and 40 show the current entity relationships.

Simplification of the data structures came mainly from eliminating cross-reference tables and serial keys. The overall philosophy now is to use serial keys only when they are absolutely required and to model the relationships with foreign keys. This is a more traditional approach to data design and will be easier to maintain because the relationships are more visible without the cross-reference tables.

Originally, the irradiations were performed using a single fraction. In the past year, however, studies have been done where the subject received multiple infusions of boron drug and multiple irradiations that constituted one treatment. The data structures that were in place when the new development team took over could only accommodate single fraction studies. The current structures can handle single infusion with multiple irradiations and multiple infusions with multiple irradiations. The tables also have space for the planned, working, and final irradiation data. These are presently manual entries; however, future plans include incorporating the calculations behind the working and final numbers.

The initial drug modeling did not include the concept of a solution wherein an infusion is composed of a mixture of drugs. The new model starts with a solution that has components that are made up of quantities from different containers. These containers are then associated with a drug lot that identifies the manufacture and the name of the drug, thus the researcher can identify, down to the specific container, each component of a solution that was given to a subject.

Analytic chemistry data had been included into the original design, but had never really been verified. The current structures relate the analysis to a particular solution and the data are loaded directly from the spreadsheets that the chemists produce as a result of their analysis. Loading the data currently requires operator intervention, but methods for automating that process have been examined and may be implemented. Both the raw data and the calculated values are stored in the database.

The other change to the structures is the concept of a procedure having subprocedures. This means that when a protocol is worked out, the protocol with all its subparts can be modeled in the database. Presently, only the basic procedures are included in the data. The decision to keep it simple was based on attempting to get a workable system in the hands of the researchers as soon as possible.

SYSTEM DOCUMENTATION

Before the start of the new development team, system documentation consisted of a single entity relationship diagram. Since then, the following documents have been prepared:

- Project plan
- Computer operating procedure
- Software requirements specification
- Revised entity relationship diagram
- Software quality assurance plan
- Configuration control procedures.

Documents to be prepared include:

- User manual
- Program maintenance manual
- Software verification and validation plan.

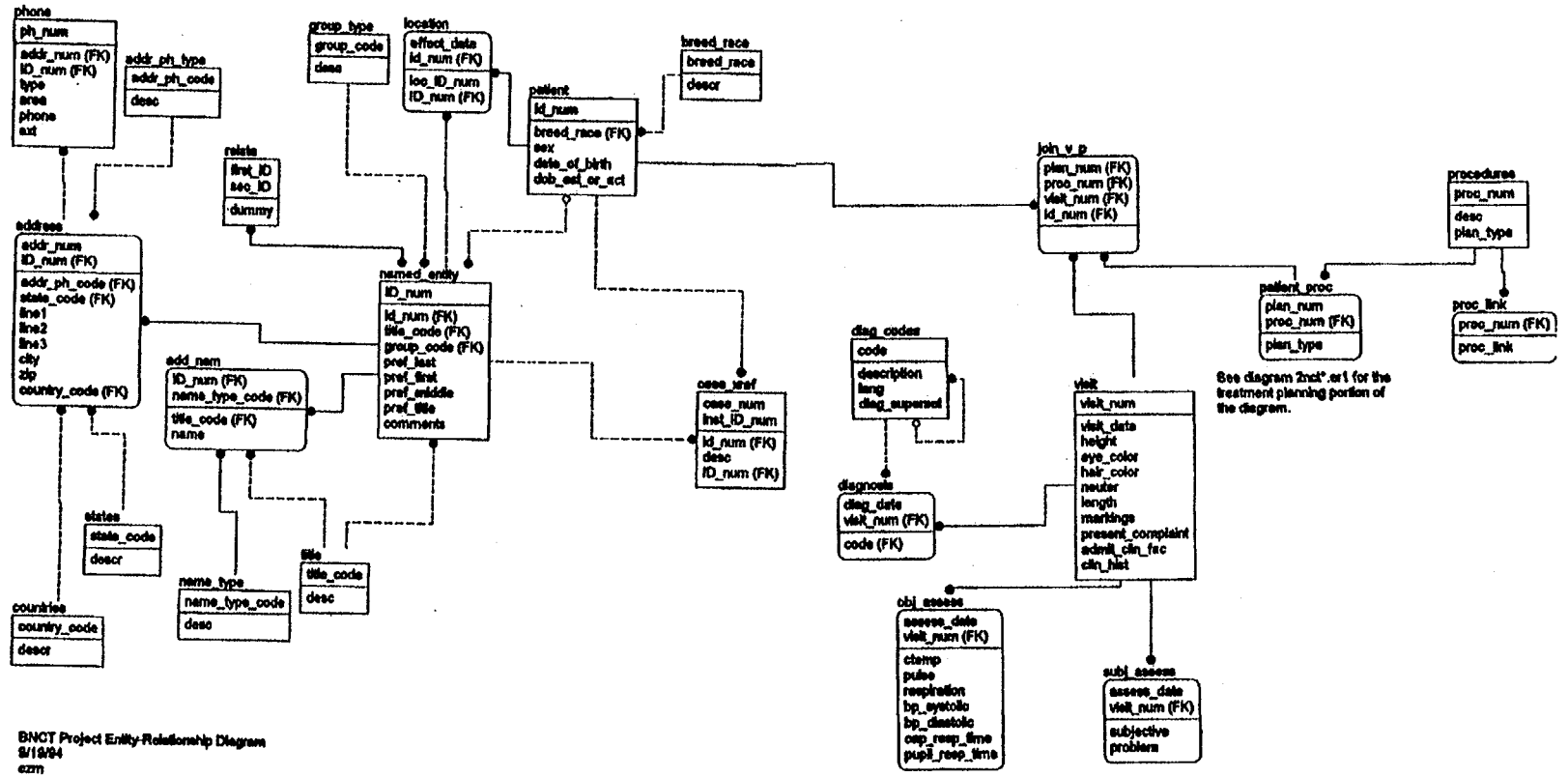

Figure 39. Part 1 of the Entity Relationship Diagram.

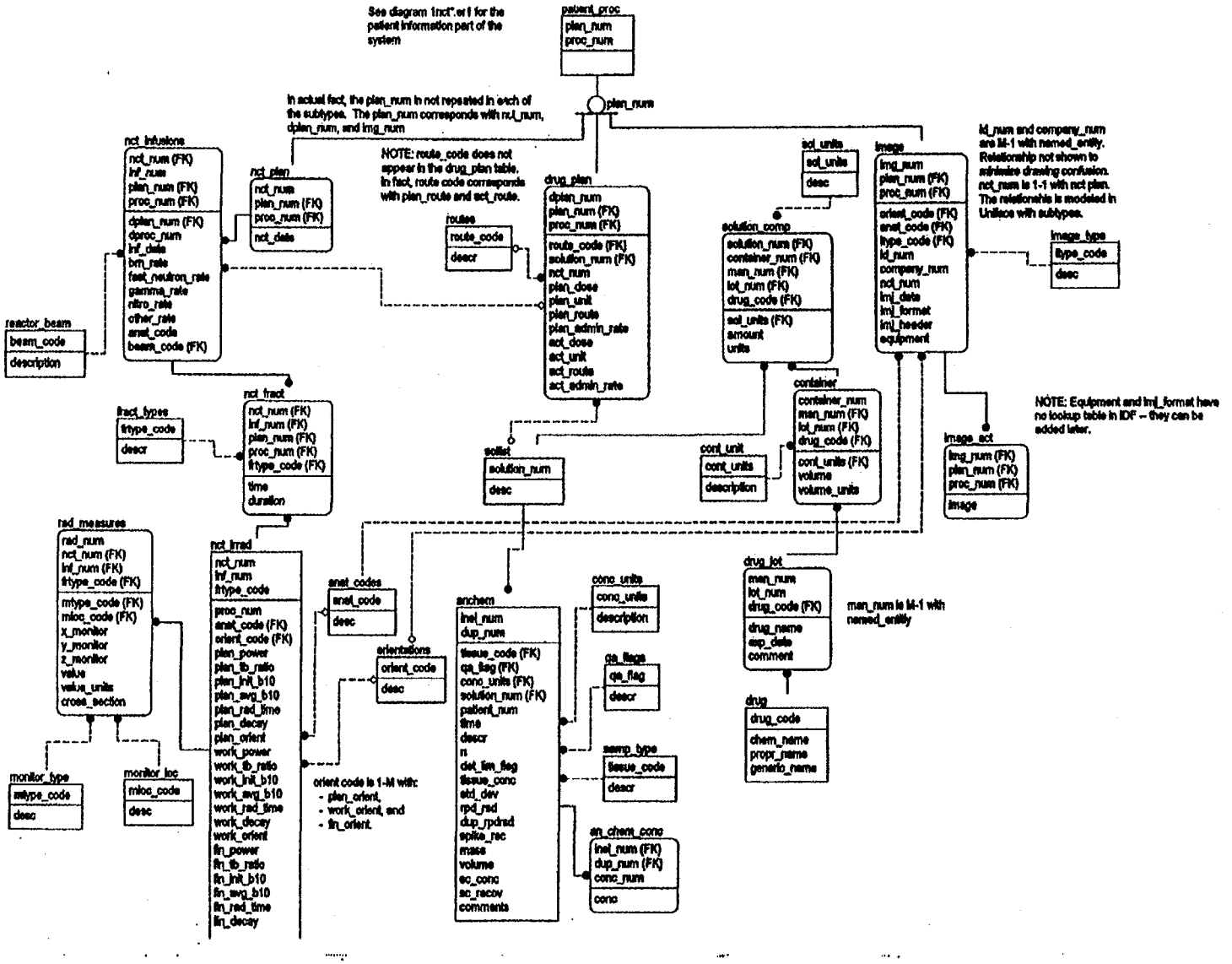

Figure 40. Part 2 of the Entity Relationship Diagram.

THE FUTURE

In calendar year 95, the development team will finish up some outstanding issues resulting from the software upgrade and September demonstration. When that activity is complete, the database will be distributed for field testing. While field testing is going on, the development team will be assisting with the data loading effort and updating project documentation. If funding allows, the development team will also look at hardware upgrades for the BNCT computer and investigate Uniface Version 6.0.

REAL-TIME MONITORING FOR HUMAN CLINICAL TRIALS

Y. D. Harker, Radiation Physics, INEL

INTRODUCTION

On August 3–4, 1994, an INEL team made measurements related to a real-time monitoring system for use on the epithermal beam facility at the BMRR. BNL has installed two fission chambers in front of the beam collimator, which are to monitor the beam coming from the reactor. These two monitors are located with one just above the 16-cm dia. front aperture and the other is just below. The fission chambers contain depleted uranium, but because of the small amount of U-235 present, they respond to thermal and near thermal neutrons rather than fast neutrons. This feature combined with their relatively small size (0.6 cm dia. x 4 cm long) makes them very good monitors in the BMRR epithermal neutron beam. The INEL team worked with H. B. Lui (BNL) in performing initial tests of these monitors and established the settings to achieve stable operation.

The main purpose of INEL's measurement studies was to establish a basis for a monitoring method that tracks the dose the patient is receiving rather than the neutron fluence being delivered down the beam line. In other words, INEL was seeking a patient dose monitor rather than a beam monitor. A patient monitor is needed because a beam monitor will not indicate if the patient is placed incorrectly or if the patient has moved. This is important for treatment at any neutron beam facility and it is particularly critical at BMRR. The angular flux in the BMRR beam is isotropic and this results in a beam intensity that drops off dramatically with respect to axial distance from the exit beam port. Floyd Wheeler (INEL) has calculated that the peak thermal flux in a subject drops off 1.4% per millimeter as the leading surface of the subject is moved axially from the plane of the exit aperture. This calculated gradient is based on the 8-cm exit dia. x 16-cm entrance dia. x 7.6-cm thick tapered collimator currently installed at BMRR.

REQUIREMENTS FOR A REAL-TIME MONITORING SYSTEM

The data for determining the sensitivity requirement of a monitoring system comes from the dog brain tolerance of BNCT studies performed by Dr. Pat Gavin (WSU) at BMRR and the High-Flux Reactor (HFR). From those studies an ED50 (MRI positive) = 12.7 Gy-eq with a 95% confidence interval of 12.5–12.8 Gy-eq was established. Current dose treatment planning calls for irradiating the first patient to 12 Gy-eq with a 98% confidence that the dose does not exceed 12.5 Gy-eq. Using these numbers as a basis, the dose must be controlled to 2% (1σ). Assuming that the major uncertainty in controlling the dose is the placement of the head in the neutron beam and using Wheeler's sensitivity factor from the previous section, the head must be positioned and controlled to 1.4 mm in the axial position. Similar control is also required for the lateral positioning as well. This requires that the real-time patient monitor system must be able to effectively measure position differences of 1 mm–2mm.

There are other requirements for the monitoring system, and all the requirements are summarized below.

- Provide a monitor of the irradiation history in real time.
- Signal must track the dose to the patient.
- Must be sensitive to 1 mm–2 mm changes in position of the patient's head.
- The system must not have a significant impact on the neutron beam.
- The system must not interfere with the placement of the subject's head at the exit port of the collimator.

- The system must not contribute significantly to the dose given the subject.

- The system must be adaptable to different physical sizes of heads and different orientations of the head to the beam.

- The system must be easily located or positioned so that changes in head orientation can be accomplished with minimal delay between dose fractions.

EXPERIMENT

To evaluate the sensitivity of the different real-time monitoring schemes, the INEL RANDO human phantom and three fission chambers were used at the BMRR epithermal beam. The first two chambers were those used in the BNL beam monitoring system; a third fission chamber, which is the same model as those in the BNL beam monitor, was used to monitor neutron flux at different locations on the phantom. For these tests the bottom fission chamber in the BNL beam monitor was disconnected from its electronics and those electronics were connected to the third chamber. The electronics used for each chamber were: high voltage bias supply, signal preamplifier, amplifier/discriminator, and scaler/timer, all of which are standard counting electronics.

To test the sensitivity of the beam monitor chamber and the third chamber, count rates were measured as the phantom orientation was changed with respect to the beam axis while the beam monitor chamber remained fixed relative to the beam and the third chamber remained fixed at a set location relative to the phantom. The third fission chamber locations were limited to locations on the head and neck. The phantom orientation was varied by 5-cm changes in the top of the head location with respect to the beam. The phantom was basically laying flat on its back situated for a straight on irradiation with the beam entering the top of the head.

The first location for third fission chamber was on the top of the head, 3.5 cm to the left of the established central point of the top of the head. (On the RANDO phantom the central point of the head was the center of the circular ring groove located on the crown slice of the head.) In medical coordinates the center of the fission chamber was at (+3.5 cm, 0,+0.3 cm) when the central point of the top of the head was located at origin (0,0,0). At this location the chamber was oriented such that its cylindrical axis was vertical.

With the phantom lying on its back, the second location of the third fission chamber was above the left ear and oriented such that its cylindrical axis was horizontal. The medical coordinates for the center of the chamber was (≈4cm–0.5 cm,7 cm) when the central point of the top of the head was located at the origin (0,0,0).

RESULTS

Tables 12 and 13 contain the tabulated results of the response of fission chamber #3 at two locations on the phantom head as the head position was varied with respect to the beam. In these tables the coordinates of the head position are for the center of the top of the head relative to the beam center. For example under this convention, coordinates (0,0,0) indicate that the center of the top of the head is aligned with the beam axis and that the crown of the head is flush with the plane of the exit aperture.

In these measurements the count rate of the one functioning beam monitor fission chamber was monitored. As expected, its response was insensitive to changes in the head position and the average count rate over all experimental configurations studied was 7,358 counts per minute (cpm) at a reactor power of 1 MW. The standard deviation over this ensemble was 52 cpm, which is consistent with Poisson counting statistics.

Discussion of Results

In analyzing these data it is important to realize that the uncertainties quoted are for beam intensities with the reactor at 1 MW. In an actual treatment procedure, the reactor power will be at 3 MW. Therefore, the relative uncertainties for monitoring during treatment will about 0.6 times the relative uncertainties given here.

Table 12. Fission Chamber #3 at the top of head (Position #1).

Head position (x,y,z) cm	Fission Chamber #3 response (cpm)		Relative change[a] (percent)		Detectable change in position (mm)
(0,0,0)	12,360	(2.1%)[b]	0.0		—
(+0.5,0,0)	10,300	(2.3%)	-16.7	(2.6)[c]	0.78
(-0.5,0,0)	13,610	(0.86%)	+10.1	(2.5)	1.2
(0,+0.5,0)	9,760	(1.0%)	-21.0	(1.8)	0.43
(0,-0.5,0)	11,210	(1.5%)	- 9.3	(2.4)	1.3
(0,0,+0.5)	9,950	(1.6%)	-19.5	(2.1)	0.54

a. Relative change is based on response with head position at (0,0,0).

b. Numbers in parentheses are standard deviations (in percent) based on a sample of five 1-min counts.

c. Numbers in parentheses are the standard deviations in the relative change.

Table 13. Fission Chamber #3 at left ear (Position #2).

Head position (x,y,z) cm	Fission Chamber #3 response (cpm)		Relative change[a] (percent)		Detectable change in position (mm)
(0,0,0)	933	(2.9%)[b]	0.0		—
(+0.5,0,0)	831	(3.6%)	-10.9	(4.1)[c]	1.9
(0,0,+0.5)	882	(4.2%)	-5.5	(4.8)	4.4

a. Relative change is based on response with head position at (0,0,0).

b. Numbers in parentheses are standard deviations (in percent) based on a sample of five 1-min counts.

c. Numbers in parentheses are the standard deviations in the relative change.

Based on the data in Table 12, a fission chamber located 3.5 cm off the head center would be able to detect a change in head position of ≈1 mm. Based on Wheeler's calculated sensitivity value of 1.4% change in peak thermal neutron flux per mm axial change in the head position, this type of monitor configuration would be able to detect a change in the peak thermal neutron flux of 1.4%. If one adjusts these numbers to a 3 MW treatment scenario, the fission chamber would be able detect changes in position of ≈0.6 mm and the corresponding change in peak thermal neutron flux for an axial change of this order would be ≈0.8%. These performance values are very consistent with a monitoring system requirement to detect a head position change of 1 mm – 2 mm.

Because of the lower count rate, the data in Table 13 are less impressive. With the detector located on the side of the head, one can expect to detect a change in head position of ≈3 mm, which means that the peak thermal neutron flux in the

subject could vary by as much as 4% without detection. Adjusting for 3 MW treatment scenario would lower these estimates to ≈2 mm and 3%, respectively. Depending on the treatment plan these values may be acceptable. Also the count rate could be increased by using a more sensitive neutron detector. Because of the shortness of time, however, this option is not available for this first patient.

Conclusions and Recommendations

Ideally the real-time monitoring system that satisfies all the requirements with redundancy included would have at least five neutron detectors that monitor the neutron flux in the beam and neutron field on or near the subject's head. In a five detector array, two detectors would be used to monitor the beam and three detectors would be used to monitor the subject.

The detector array for monitoring the beam would be the same as currently installed on the BNL tapered collimator.

The detector array for monitoring the patient would consist of three detectors mounted symmetrically on a circular ring fixture. The ring fixture would be constructed of low mass, low neutron absorption/activation material. The radius of the detector circle would be between 3 cm and 4 cm so that the detectors are located on or near the periphery of the beam. This would result in a positional sensitivity similar to that shown in Table 12. The ring fixture would be attached to the head such that it is fixed relative to patient. It would be positioned on the head such that the center of the fixture coincides with the target point of the beam on the head. (The target point is defined as the point on the head where the centerline of the neutron beam intersects the surface of the head.) The fixture would be oriented such that the plane of the fixture is parallel to the plane of the beam aperture. The inner hole in the fixture is there to reduce interference with the incident beam and to allow the surface of the head in and around the target point to protrude through the hole so that the surface of the head can be positioned flush with the plane of the aperture.

The initial fixture would be designed to accommodate three fission chamber neutron monitors mounted on it. If forthcoming evaluation measurements involving lithium loaded fiber optic neutron detectors yield positive results, the fission chambers will be replaced by the smaller and less perturbing fiber neutron detectors. The fiber optic neutron detectors could also be used inside catheters to measure the neutron flux at points inside the brain.

To monitor the gamma field in real time, an ion chamber array is recommended. The purpose of gamma chambers would be to monitor the general gamma field on or near the patient. Because neutron capture is the major source of gamma radiation associated with epithermal neutron irradiation at BMRR, the gamma chambers should be placed such that they measure the gamma radiation coming from the patient's head. The ion chamber with the appropriate buildup cap is physically about a factor of three larger than a fission chamber. Because of its physical size it would not be practical to place the gamma chambers in the proximity of the beam aperture in a similar fashion as the fission chambers. Their positions must be symmetrically located around the sides of the head.

The system described above calls for five neutron detectors and a gamma chamber array for the real-time monitoring system. At this time there are only three functioning fission chambers and one gamma ion chamber available for monitoring on the first human patient. With the available resources there are basically four options for a monitoring system:

1. Use the three existing fission chambers as the patient monitor array and rely on the reactor instrumentation and beam shutter control to monitor and control the neutron beam.

2. Use one fission chamber as a beam monitor and the other two fission chambers to monitor the patient.

3. Use two fission chambers to monitor the beam and the third chamber to monitor the patient.

4. Use only two fission chambers to monitor the beam and not have a patient monitor system at all.

In all options the gamma chamber would be used to monitor the gamma field near the head at a preselected point.

With respect to the first option, one can argue that beam intensity monitoring is not required. This is because the reactor, shutter, and filter are all well controlled by existing instrumentation and by the physical characteristics of the reactor and filter design. Neutron activation measurements performed by BNL and INEL show that beam intensity is well controlled and support this hypothesis. Therefore, the three fission chambers would be better used in monitoring the radiation delivered to and/or coming from the patient in the fashion described above for the patient monitor array.

The fourth option would have no monitoring of the patient and would rely on the patient and/or the head positioning system to maintain the head in proper alignment. There would be no verification that alignment is maintained during the irradiation and that dose to the patient has been delivered as prescribed. This is considered to be totally unsatisfactory because it is the patient dose that must be controlled and verified.

It is our firm opinion that all fission chambers should be used in the monitoring system for the first patient. It is better to error on the side of over monitoring than to end up with insufficient data. The order of the options listed above is according to their priority concerning monitoring patient dose delivery.

If for some reason a fission chamber cannot be used and replacement is not available, the use of the remaining fission chambers should provide some degree of patient monitoring as a first priority.

NEUTRON BEAM MEASUREMENT DOSIMETRY

C. R. Amaro, Reactor Physics, INEL

Animal Dosimetry

During 1994, 12 dogs, labrador-cross and beagles, were irradiated at BMRR as part of a 4 fraction dose tolerance study conducted by WSU. The animals were infused with BSH and irradiated daily, for 4 consecutive days. BNL irradiated two beagles as part of their dose tolerance study using BPA fructose. Dose tolerance irradiations were performed on the right hemisphere at 3 MW using a 5 x 10-cm aperture contained in a 5-cm thick LiOH-polyethylene mask in the beam port.

In addition to the dose tolerance dogs, a client dog of WSU was irradiated at BMRR after an infusion of BPA fructose. The client dog was irradiated with a conical aperture that was tapered from 16 cm, which faced the beam port, to 8 cm, and was 12.7 cm thick. The animal was irradiated at 2 MW for 60 min for a desired dose of 10.5 Gy with an average boron concentration of 7.6 ppm. The client dog irradiation was performed to simulate the dose received by a human patient of BNL.

A dosimeter package consists of a 1.3 x 2.5-cm black polyethylene envelope containing 3 TLD-400 rods (6 x 1 x 1 mm) for gamma dose, and a coiled or a straight piece of 1.5% Au-Cu wire, approximately 1 mm diameter and 1 cm in length, used to measure thermal and epithermal neutron flux induced by neutron activation. The dosimeter locations for dose tolerance dogs were the beam center at the top of the skull and the rear of the skull. An additional dosimeter packet was placed inside the throat at the trachea. For each irradiation a neutron flux monitor of the same Au-Cu wire was placed in front of the beam aperture next to the bismuth face of the beam port and approximately 3 cm to the side of the aperture opening. To reduce neutron albedo effects from the lithiated polyethylene, the beam monitor packet had a 2.5-cm diameter x 0.05-cm thick cadmium piece placed between the dosimeter packet and the lithiated polyethylene.

Dosimetry used for the client dog was expanded to include the following positions: over the left and right eye, the center of the spine at the shoulder, on the throat at the thyroid, on the chest above the heart, and the genital position.

Table 14 gives a summary of the desired doses, and the range of irradiation times and boron concentrations used for the fractionated study. Each animal was infused with BSH then irradiated to one quarter of the total desired dose. The process of infusion-irradiation was repeated each day for each dog for a total of 4 days.

Phantom Measurements

During August 1994, the INEL BNCT dosimetry team measured neutron flux and gamma dose profiles in two phantoms exposed to the epithermal neutron beam at the BMRR. These measurements were performed as a preparatory step to the commencement of human clinical trials now in progress at the BMRR. The measurements were needed to benchmark the INEL Patient Treatment Planning software for the case where the new conical beam aperture developed by BNL is used. The measurement plan called for:

Table 14. Summary of fractionated dose tolerance dog irradiations for 1994.

Number of dogs	Total desired dose cGy	Irradiation time (hr)	Desired boron conc. (ppm)
4	2,800	0.4–0.6	25
4	3,200	0.4–0.6	25
4	2,400	0.3–0.6	25

- Remeasurement of the neutron flux and gamma profiles inside the cylindrical phantom with a 7.6-cm diameter cylindrical aperture. The cylindrical phantom and aperture were used earlier in the BMRR epithermal neutron beam to benchmark the planning software, and this test was a repeat to ensure that nothing had changed.

- Measurement of the new neutron flux and gamma profiles in the same cylinder when the new conical aperture is used.

- Measurement the neutron flux and gamma profiles in a full head plus torso humanoid phantom using the BNL conical beam aperture.

Thermal and epithermal neutron flux profiles were measured using Au-Cu alloy wires (1.5% gold). The gamma dose profiles were measured using CaF_2:Mn thermoluminescent dosimeters (TLDs) (TLD-400). These measurements initiated the use of the Lockheed Idaho Technologies Company (LITCO) dosimetry group's new handling and analysis procedures for TLD-400, which were designed to eliminate the large variations experienced earlier when the original DOE handling and analysis procedures were used.

The cylindrical phantom is made of acrylic plastic and is 17.8 cm long and 12.7 cm in diameter. For profiles as function of depth along the phantom axis, flux wires and TLDs are positioned in holes drilled at 1-cm intervals in a removable central rod made of the same plastic as the phantom body. For profiles across the beam diameter, flux wires and TLDs were placed in holes drilled at 1-cm intervals across four removable cross blocks made of the same plastic.

The humanoid phantom (referred to as the RANDO phantom) is a standard man phantom without appendages. It is constructed of human skeleton with isocyanate rubber to represent organs and tissue. The density of the rubber was gaged to give radio-equivalent representation of the organs and tissue in a standard man. The phantom is sectioned into 2.5-cm thick transverse sections from the top of the head to the upper thigh. Inside each section there is a square lattice with 2.5- cm spacing of 3-mm diameter instrumentation holes. These holes were used to place the flux wires and TLDs.

The 7.6-cm hole diameter x 5.1-cm thick aperture structure used in the first irradiation of the cylindrical phantom is constructed of polyethylene doped with 30 wt.% Li_2CO_3 enriched to 96% ^6Li. The conical aperture used in the second irradiation of the cylindrical phantom and in the humanoid phantom irradiations is constructed of the same polyethylene. This aperture structure is 12.7 cm thick and the aperture hole is tapered with 16 cm diameter on the side facing the reactor and 8 cm diameter on the output side.

Listed in Tables 15 and 16 are the neutron flux and gamma dose data for the cylindrical phantom irradiations, respectively. For these irradiations the cylinder axis coincides with the beam axis and the front end of the cylinder is flush with the output plane of the aperture. The coordinates indicated in the tables are based on the right-handed medical convention where the origin is the point where the center of the beam intersects the front surface of the cylinder, the z-axis is along the beam axis, the x-axis is horizontal, and the y-axis is vertical. The data in these tables indicate that neutron flux and gamma dose are greater for the conical aperture than for the circular aperture with relative numbers ranging from 1.04 for the front face gamma dose on beam axis to 1.48 for the epithermal neutron flux at a depth of 6.5 cm near the beam axis. The peak thermal neutron flux for the conical aperture is 1.32 times that for the circular aperture; whereas, the gamma dose is 1.19 times that for the circular aperture. However, at depths of ≈8 cm there is little difference between the thermal neutron fluxes for the two apertures. The same is true for the gamma doses at that depth. These results indicate that the aperture shape (conical versus cylindrical) appears to have little effect once the depth is greater than one or two mean free paths.

Comparisons of the neutron and gamma data for the humanoid phantom irradiations with calculations indicated that there must be unaccounted neutron absorbers in the radio-equivalent rubber compound. This prompted the need for a complete chemical analysis. Samples have been taken of the rubber compound but at this time analyses results are not available. Therefore, a presentation of the humanoid phantom data will be delayed until the chemical analyses are complete and a comparison with calculations are possible.

New TLD handling and analysis procedures were implemented in these tests to account for loss of sensitivity due to exposure to high doses of radiation and for light stimulated fade. TLDs are known to lose sensitivity as they are repeatedly exposed to high doses of gamma radiation; therefore, in the new procedures the sensitivity of each TLD is tracked over its lifetime. The fade characteristics of TLD-400s are very sensitive to the amount of visible and ultraviolet light that they are exposed to during and following irradiation; therefore, the TLDs exposure to light is minimized in the new handling procedures. In the review of the gamma data from these tests there is strong evidence that a considerable improvement has been made in the reliability of the gamma dose data taken with TLD-400 dosimeters. These improvements are very important to BNCT dosimetry because the TLD-400 does not require a large neutron correction to its response and can be used reliably in high gamma fields.

Table 15. Neutron flux as measured in the cylindrical phantom.

Dosimeter position			Irradiations were performed on 08/02/94			
X (cm)	Y (cm)	Z (cm)	Circular Phi-thermal flux (n/cm^2-sec)	Conical Phi-thermal flux (n/cm^2-sec)	Circular Phi-epithermal flux (n/cm^2-sec)	Conical Phi-epithermal flux (n/cm^2-sec)
0	-0.5	0.5	7.13E+08	8.84E+08	1.02E+09	1.17E+09
0	-0.5	1.5	1.15E+09	1.49E+09	6.93E+08	8.57E+08
0	-0.5	2.5	1.36E+09	1.80E+09	4.57E+08	6.12E+08
0	-0.5	4.5	1.17E+09	1.42E+09	1.57E+08	1.94E+08
0	-0.5	6.5	6.86E+08	7.89E+08	3.72E+07	5.52E+07
0	-0.5	8.5	3.74E+08	3.93E+08	1.32E+07	1.28E+07
-1.5	-0.5	1.5	1.24E+09	1.61E+09	6.74E+08	8.14E+08
-2.5	-0.5	1.5	1.20E+09	1.58E+09	5.77E+08	7.73E+08
-3.5	-0.5	1.5	9.79E+08	1.36E+09	4.40E+08	6.77E+08
-4.5	-0.5	1.5	6.79E+08	9.65E+08	2.79E+08	4.63E+08
1.5	-0.5	1.5	1.3OE+09	1.61E+09	7.31E+08	8.22E+08
2.5	-0.5	1.5	1.27E+09	1.59E+09	6.64E+08	8.06E+08
3.5	-0.5	1.5	1.11E+09	1.37E+09	5.66E+08	6.67E+08
4.5	-0.5	1.5	7.89E+08	9.96E+08	3.84E+08	4.73E+08

Table 16. Gamma dose as measured in the cylindrical phantom.

Dosimeter position			Irradiations were performed on 08/02/94	
X (cm)	Y (cm)	Z (cm)	Circular dose (rem)	Conical dose (rem)
0	0.5	0.5	158.49	165.58
0	0.5	1.5	171.49	191.35
0	0.5	2.5	187.18	221.29
0	0.5	4.5	176.06	196.29
0	0.5	6.5	132.53	134.64
0	0.5	8.5	93.55	88.32
-1.5	0.5	1.5	195.26	209.32
-2.5	0.5	1.5	175.94	209.32
-3.5	0.5	1.5	158.19	183.16
-4.5	0.5	1.5	130.52	144.36
1.5	0.5	1.5	183.76	214.13
2.5	0.5	1.5	183.16	207.22
3.5	0.5	1.5	170.83	153.68[a]
4.5	0.5	1.5	131.13	149.17

a. TLD rod tip was broken when it arrived for analysis.

PITUITARY TUMOR EVALUATION

Dr. B. Albertson, PI, Oregon Health Science University (OHSU), Division of Endocrinology Diabetes, and Clinical Nutrition, Department of Medicine; Dr. S. Binney, PI, Oregon State University (OSU), Department of Nuclear Engineering

Experiments conducted through calendar year 1994 continue to support the hypothesis that:

- Releasing hormone ligands can be synthesized and conjugated to a $^{10}B_{10}$–cage in a manner that preserves the biological activity (receptor binding and signal transduction) of the polypeptide hormone used for targeted pituitary tumor cells *in vitro*.

- The incubation of receptor positive cells with the appropriate $^{10}B_{10}$ conjugated ligand makes them susceptible to BNCT. Moreover, it appears that this effect is mediated through the receptor, providing evidence that other cells can be targeted via specific membrane receptors and killed with hormone $^{10}B_{10}$ conjugates.

Data to support these hypotheses are described below.

The Structure of $^{10}B_{10}$–ovine Corticotropin Releasing Hormone ($^{10}B_{10}$–oCRH) and $^{10}B_{10}$–Growth Hormone Releasing Hormone ($^{10}B_{10}$–GHRH)

A $^{10}B_{10}$ cage has been synthesized and supplied by Professor M. Frederick Hawthorne and colleagues, Department of Chemistry and Biochemistry, UCLA. The cage contains ten ^{10}B atoms covalently linked to four carbon atoms; two in the cage structure itself and two outside the cage in a two carbon tail. The most distal carbon of the tail has a reactive acetate group attached. The isotopic ratio of ^{10}B to ^{11}B in this cage is approximately 96:4. Conjugation of the cage to the "inactive" end of oCRH is carried out using a modified carbodiimide reaction. The structure of final conjugate is shown in Figure 41.

A similar construct has been synthesized with human Growth Hormone Releasing Hormone (GHRH) shown in Figure 42. Here the $^{10}B_{10}$–cage has been conjugated to the carboxyl terminal amino acid since the biological activity of GHRH resides in the amino terminal end of the molecule.

Biological activity of both of these releasing hormone $^{10}B_{10}$ conjugates is preserved.

The BNCT Effect on AtT–20 cell $^{10}B_{10}$–oCRH Incubations *in vitro*

AtT–20 cells were incubated with o–CRH (10^{-6} M) or $^{10}B_{10}$–oCRH conjugate (10_{-6} M) for 5 and 10 min at 37°C, washed with sterile phosphate buffered saline (PBS), and irradiated for 3 min at 1 MW. Incubation times were based on published data suggesting that the time interval needed for binding and activation of the CRH receptor by oCRH and the time of internalization

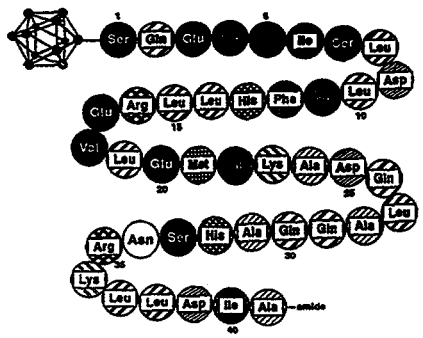

Figure 41. The amino acid sequence of oCRH is shown with the conjugated carborane cage ($^{10}B_{10}$) attached. Carbonyl cage $^{10}B_{10}$ atoms are shown as black circles; carbon atoms are shown as open circles. A reactive acetate group located on the distal most carbon atom of the carbonyl cage is conjugated to the first serine of oCRH. The carborane cage–oCRH conjugate is purified by high pressure liquid chromatography.

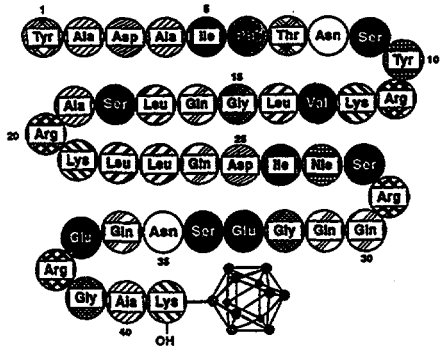

Figure 42. GHRH is shown conjugated to a carbonyl cage ($^{10}B_{10}$). Human GHRH is synthesized with a lysine residue at position number 41, to which the $^{10}B_{10}$ cage is conjugated.

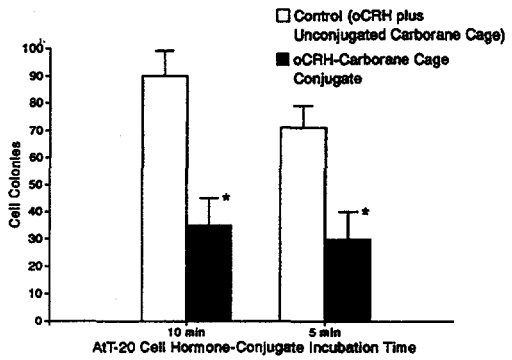

Figure 43. AtT–20 cells incubated for 5 and 10 min with $^{10}B_{10}$–oCRH carbonyl cage conjugate had significantly fewer cell colonies surviving 14 days after irradiation than cells incubated with oCRH plus unconjugated $^{10}B_{10}$–cage. Bars are the mean ± 1 SD of triplicate culture dishes. Means are statistically different (p = 0.001).

of ^{125}I–CRH into corticotrophs is short, on the order of 2–5 min. The cells were removed from the reactor thermal column, diluted, and pipetted into 100 mm culture dishes. The cells were allowed to grow at 37°C (CO_2 incubator) for 14 days. Cell survival immediately after reactor irradiation was assessed with trypan blue exclusion and was greater than 90%. After 14 days, the culture dishes were washed, fixed with 20% formaldehyde, stained with Geimsa, and the colonies counted. The results are shown in Figure 43.

AtT–20 cell colony numbers are significantly reduced when the cells are incubated with $^{10}B_{10}$–oCRH and subjected to neutron radiation compared to cells irradiated after incubation with unconjugated oCRH at a similar concentration. Similar effects were observed for both the 5 and 10 min AtT–20 cell $^{10}B_{10}$–oCRH incubations.

BNCT Effect on GH_4C_1 Cell $^{10}B_{10}$–Growth Hormone Releasing Hormone (GHRH) incubation *in vitro*.

A similar experiment has examined the effects of BNCT using $^{10}B_{10}$–GHRH and GH_4C_1 rodent pituitary somatotroph tumor cells. GH_4C_1 cells were incubated for 5 min with either GHRH (10^{-6} M) alone or $^{10}B_{10}$–GHRH (10^{-6}). Cells were washed in cold PBS and irradiated in the reactor thermal column (3 min at 1 MW). After irradiation, the cells were washed and subcultured in T–75 culture flasks. The cells were kept in a CO_2 incubator for 20 days and were then washed, fixed, and stained with Geisma. The results are shown in Figure 44.

Competitive Inhibition of AtT–20 Cell BNCT Effect

To provide evidence that observed AtT–20 cell killing by BNCT is CRH receptor mediated, cells were incubated for 10 min in the presence of 10^{-6} M oCRH, 10^{-6} M $^{10}B_{10}$–carborane oCRH, or 10^{-6} M $^{10}B_{10}$–oCRH plus excess oCRH (2 x 10^{-5} M), washed, irradiated for 1 min at 3 MW, and cultured for colony counting. The results are shown in Figure 45.

AtT–20 cell colonies were significantly lower in number (i.e., indicating greater cell killing) when cells were incubated with $^{10}B_{10}$–oCRH compared to unconjugated oCRH. However, this difference was eliminated (i.e., AtT–20 cell death was significantly reduced) when cells were incubated with $^{10}B_{10}$–oCRH plus excess oCRH. These results are consistent with a BNCT effect mediated through the AtT–20 cell CRH receptor.

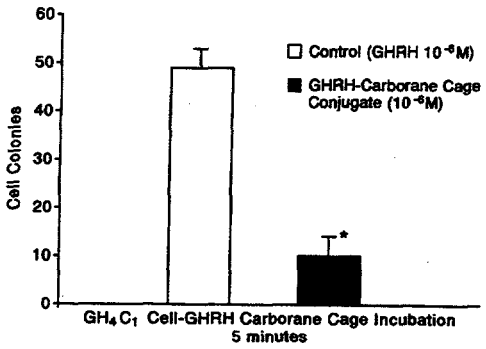

Figure 44. BNCT effect on GH_4C_1 cell $^{10}B_{10}$–Growth Hormone Releasing Hormone (GHRH) incubation in vitro. Note: GH_4C_1 cell colonies are shown on the Y axis; Cell incubation conditions on the X axis. Flasks inoculated with a similar number of nonirradiated cells grew approximately 200 colonies at the end of the 20 days. Cells incubated with Human Growth Hormone Releasing Hormone (hGHRH) alone had approximately 50 colonies per dish (triplicate flasks) versus approximately 10 colonies ($p = 0.001$) in the flasks in which cells were incubated with $^{10}B_{10}$–hGHRH.

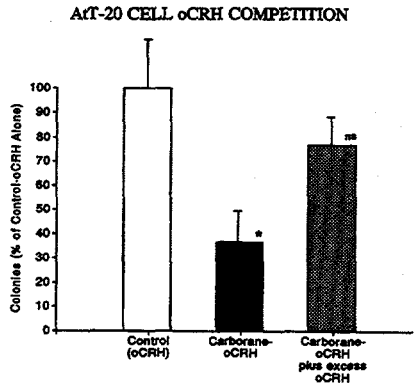

Figure 45. Competitive inhibition of AtT–20 cell BNCT effect. Note: AtT–20 cell colonies are shown on the Y axis as percent of control, that is, 10^{-6} M oCRH alone. Cells incubated with 10^{-6} $^{10}B_{10}$–oCRH for 10 min had significantly fewer colonies 14 days after radiation than control dishes. This difference was reversible by the addition of excess (2×10^{-5} M) oCRH to the incubation media. Bars are means of colony counts of three culture flasks ± 1 SD. ns = not statistically significant. *p, 0.001.

Evaluation of Carborane Cage Toxicity In Vitro

To test for potential ^{10}B toxicity in AtT–20 and GH_4C_1 cells, 10^{-6} M $^{10}B_{10}$–oCRH or native CRH was incubated for 10 min with AtT–20 cells, and 10^{-6} M $^{10}B_{10}$–GHRH or native GHRH with GH_4C_1 cells. Cells were incubated and colonies counted 14 days (AtT–20 cells) or 20 days (GH_4C_1 cells) later. The number of colonies formed in the presence or absence of ^{10}B was the same for both cell types and is shown in Figure 46.

In Vivo Tissue Distribution of a Single Acute I.V. Bolus Injection of 100 μg $^{10}B_{10}$–oCRH Using a Rat Animal Model

200 gram Sprague–Dawley rats were injected with 100 μg $^{10}B_{10}$–oCRH i.v. into the femoral artery, and sacrificed at specified times (0, 7 min, 15 min, 30 min, 1 hr, 3 hr, 6 hr, and 24 hr) after the injection. Blood, liver, spleen, brain (cortex), kidney, gonads (testes), skin, eyes, and muscle were collected after sacrifice and subjected to inductively coupled plasma–mass spectroscopy (ICP–MS) by Bill Bauer (INEL). Baseline (vehicle injected control) ^{10}B levels varied widely from tissue to tissue, ranging from 35 parts per billion (ppb) (blood) to 140 ppb (kidney). Blood levels of ^{10}B increased from 35 ppb to 131 ppb within 7 min, then declined to basal levels by 6 hr. Liver ^{10}B levels paralleled those ^{10}B levels observed in the blood, but were consistently below by approximately 20%. Muscle, skin, spleen, cortex, and gonadal ^{10}B levels remained unchanged over the entire time of the experiment. ^{10}B levels in the kidney were highest at virtually all time points, including basally, and rose after injection to approximately 250 ppb at 7 min and fell to basal levels by 6 hr. ^{10}B levels in the eyes were 363 ppb basally and fell progressively throughout the experiment to approximately 150 ppb at the 15–min time period and remained at this level for the duration of the study. ^{10}B pituitary levels are not yet available.

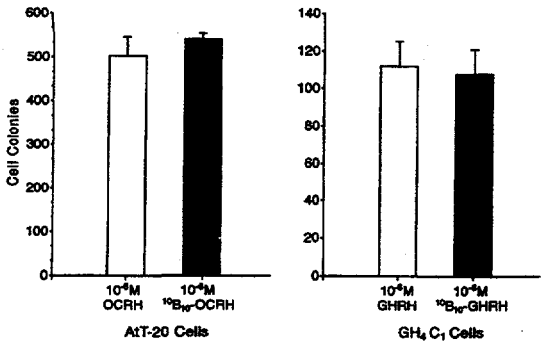

Figure 46. Evaluation of carborane cage toxicity in vitro. Note: AtT–20 and GH_4C_1 cells were incubated with their respective $^{10}B_{10}$–ligands for 10 min, washed, and plated in culture flasks. Cell colonies were counted after fixation and staining. Cells incubated in the presence of $^{10}B_{10}$–ligands formed colonies identical in number to cells incubated with hormone ligand alone, suggesting that the carborane cage conjugate has no toxic effect on cell viability under these experimental conditions.

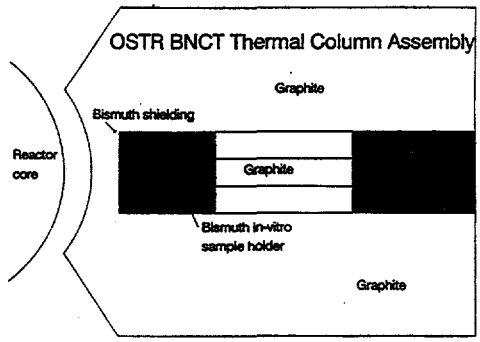

Figure 47. Aerial cutaway diagram of the reactor core, thermal column, and in vitro sample holder placement during cell irradiations.

Oregon State University Research Reactor

Radiation experiments were conducted in the thermal column of a 1 MW TRIGA Mark II Oregon State TRIGA Reactor (OSTR) located at OSU. Three graphite stringers of the thermal column are removed to produce a 10 x 30–cm cross–sectional beam. The innermost end of this region is filled with a bismuth shield assembly that holds the cell samples. This is followed by a 50 cm graphite moderator/reflector. The bismuth cell holder includes a tongue and groove fitted lid that sits on a milled base holding six 5–mL sterile vials. Slots are located between each of the sample wells for TLDs that measure gamma dose, and gold foils that measure neutron fluence (Figure 47).

The thermal neutron flux at the sample location is 5.2×10^{10} n–cm^{-2}–s^{-1} at 1 MW power. A reasonably pure thermal neutron beam has been achieved: $\phi_{th}/\phi_{epi} = 56$; $\phi_{th}/\phi_{fast} = 350$.

Gamma ray dose is measured with TLD–400 (CaF_2:Mn) thermoluminescent dosimeters. The gamma dose rate at 1 MW at the sample location is 1.1 cGy/s.

After thermal column modifications, the contaminating dose components were minimized and the thermal neutron flux maximized, resulting in a gamma ray dose to thermal neutron fluence of about 2×10^{-11} cGy–cm^2. This is a target ratio known to be effective for BNCT at thermal neutron fluences of about 10^{13} n/cm^2 (1.0 MW for 3 min). This suggests that there will be minimal cell mortality from contaminating components in one irradiation beam (Figure 48).

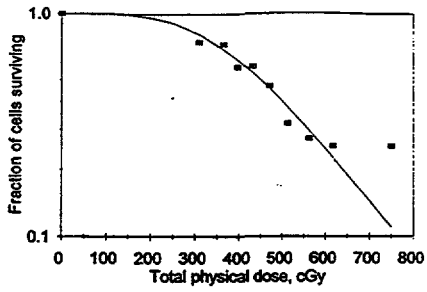

Figure 48. AtT–20 cell survival, assessed by cell counting, 5 days after exposure to varying gamma/neutron irradiation doses in the reactor thermal column.

Cell Survival: Reactor Dosimetry

The OSTR produces the dose components at the *in vitro* sample holder position at the thermal neutron fluence of 10^{13} n/cm^2 as shown in Table 17.

Table 17. Sample holder dose components.

Dose component	Dose cGy
$^{14}N(n,p)$	110
$^{1}H(n,\gamma)$	negligible
fast neutron	$23
gamma ray (typical value)	$150
$^{10}B(n,\alpha)$	76 (per each ppm ^{10}B)
Total:	$283 + 76 (per each ppm ^{10}B)

REFERENCES

1. Douglas E. Moore, Yohanes Setiawan, and Ned Blagojevic, "FTIR Spectrometry for the Assay of Polyhadral Boron Compounds in Plasma," *Advances in Neutron Capture Therapy*, Plenum Press, New York, 1993, pp. 413–417.

2. Kenneth Shelly, Debra A. Feakes, M. Frederick Hawthorne, Paul G. Schmidt, Teresa A. Krisch, and William F. Bauer, "Model Studies Directed Toward the Boron Neutron Capture Therapy of Cancer: Boron Delivery to Murine Tumors with Liposomes," *Proc. Natl. Acad. Sci. U.S.A.*, 89, 1992, pp. 9039–9043.

3. M. Frederick Hawthorne, Richard L. Pilling, and Phillip M. Garrett, "A Study of the Reaction of Hydroxide Ion with $B_{20}H_{18}^{2-}$," *J. Am. Chem. Soc.*, 87, 1965, p. 4740.

4. Kenneth Shelly, Carolyn B. Knobler, and M. Frederick Hawthorne, "Synthesis of Monosubstituted Derivatives of *closo*-Decahydro- decaborate(2-): X-ray Crystal Structures of [*closo*-2-$B_{10}H_9CO]^-$ and [*closo*-2-$B_{10}H_9NCO]^{2-}$," *Inorg. Chem.*, 31, 1992, pp. 2889–2892.

5. Lai-Ling Ng, Bradford Ng, Carolyn B. Knobler, and M. Frederick Hawthorne, "Structural Analysis of the e^2 and a^2 Isomers of $B_{20}H_{18}^{2-}$," *Inorg. Chem.*, 31, 1992, pp. 3669–3671.

6. Hisao Nemoto, J. Gerald Wilson, Hiroyuki Nakamura, and Yoshinori Yamamoto, "Polyols of a Cascade Type as a Water-Solubilizing Element of Carborane Derivatives for Boron Neutron Capture Therapy," *J. Org. Chem.*, 57, 1992, p. 435.

7. N. J. Holtz and W. F. Bauer, "Determination of Strongly Protein-Bound Borocaptate Species by HPLC with On-line ICP-AES Detection of Boron," *Advances in Neutron Capture Therapy*, Plenum Press, New York, 1993, pp. 439–443.

8. Darrel D. Joel, Daniel N. Slatkin, and Jeffery A. Coderre, "Uptake of 10B in Gliosarcomas Following the Injection of Glutathione Monoethyl Ester and Sulfyhdryl Borane," *Advances in Neutron Capture Therapy*, Plenum Press, New York, 1993, pp. 501–504.

9. J. Carlsson, S. Sjoberg, and B. S. Larsson, "Present Status of Boron Neutron Capture Therapy," *Acta Oncol, 31*, 8, 1992, pp. 803–813.

10. H. D. Thames and J. H. Hendry, *Fractionation in Radiotherapy*, New York, Taylor and Francis, 1987, pp. 189–193.

11. J. W. Hopewell, D. W. H. Barnes, M. E. C. Robbins, J. M. Sansom, J. F. Knowles, and G. J. M. J. Van den Aardweg, "The Relative Biological Effectiveness of Fractionated Doses of Fast Neutrons for Normal Tissues in the Pig," *Brit J Radiol, 61*, 730, October 1988, pp. 928–938.

12. A. Wambersie A and L. E. Feinendegen, moderators, *Working Group on Optimization of Radiation Dose Delivery, Clinical Aspects of Neutron Capture Therapy*, R. G. Fairchild, V. P. Bond, and A. D. Woodhead (eds.), New York, Plenum Press, 1989, pp. 53–61.

13. H. Hatanaka, M. Moritani, and M. Canillo, "Possible Alteration of the Blood-Brain Barrier by Boron Neutron Capture Therapy," *Acta Oncol., 30*, 3, 1991, pp. 375–378.

14. D. W. Nigg, "Methods for Radiation Dose Distribution Analysis and Treatment Planning in Boron Neutron Capture Therapy," *Int. Jour. of Radiation Oncology Biology-Physics*, Vol. 28, No. 5, 1994.

15. J. F. Breimeister, ed., *MCNP—A General Monte Carlo Code for Neutron and Photon Transport, Version 3A*, Los Alamos National Laboratory, LA-7396-M, Rev. 2, 1986.

16. W. A. Rhodes and R. L. Childs, *The TORT Three-Dimensional Discrete Ordinates Neutron/Photon Transport Code*, ORNL-6268, 1987.

17. F. J. Wheeler, *Radiation Transport in Tissue by Monte Carlo—Version X02*, EGG-BNCT-11178, 1994.

18. C. P. J. Raaijmakers, M. W. Konijnenberg, H. Verhaben, B. J. Mijnheer, "Determination of Dose Components in Phantoms Irradiated With an Epithermal Neutron Beam for Boron Neutron Capture Therapy", *Medical Physics*, 23, 1995, pp. 321–329.

19. D. E. Wessol and R. S. Babcock, "BNCT_Rtpe: BNCT Radiation Planning Environment Users' Manual," to be published.

20. D. E. Wessol and F. J. Wheeler, "Creating and Using a Type of Free-Form Geometry in Monte Carlo Particle Transport," *Nucl. Sci. Eng.*, 113, 1993, pp. 314–323.

21. C. K. Wang et al., "A Neutronic Study of an Accelerator-Based Neutron Irradiation Facility for Boron Neutron Capture Therapy," *Nuclear Technology, 84*, 93, 1989.

22. J. C. Yanch et al., *Accelerator-Based Epithermal Neutron Beams for Neutron Capture Therapy, Advances in Neutron Capture Therapy,* R. Barth and A. Soloway, (eds.), New York: Plenum Press, 1993, pp. 95–98.

23. J. E. Crawford et al., *Neutrons for Capture Therapy Produced by 72 MeV Protons, Progress in Neutron Capture Therapy for Cancer*, B.J. Allen et al., (eds.), New York: Plenum Press, 1992.

24. J. A. Hablieb and T. A. Mehlhorn, ITS - *The Integrated TIGER Series of Coupled Electron/Photon Monte Carlo Transport Codes*, SAND84-05873, Sandia National Laboratory, November 1984.

25. W. A. Rhoades and R. L. Childs, *An Updated Version of the DOT-4 One- and Two-Dimensional Neutron/Photon Transport Code*, ORNL-5851, Oak Ridge National Laboratory, 1982.

26. R. W. Roussin, *BUGLE-80 Coupled 47-Neutron, 20 Gamma-Ray P_3 Cross Section for LWR Shielding Calculations*, DLC-75, Radiation Shielding Information Center, Oak Ridge National Laboratory, 1980.

27. J.F. Briesmeister (ed.), MCNP - *A General Monte Carlo Code for Neutron and Photon Transport*, LA-7396, Rev. 2, Los Alamos National Laboratory, September 1986.

28. W. J. Curran, C. B. Scott, J. Horton, J. S. Nelson, A. S. Weinstein, J. Fischbach, C. H. Chang, M. Rotman, S. O. Asbell, R. E. Krisch, and D. F. Nelson, "Recursive Partitioning Analysis of Prognostic Factors in Three Radiation Therapy Oncology Group Malignant Glioma Trials," *J Nat Cancer Inst, 85*, 1993, pp. 704–710.

29. J. S. Nelson, D. Schoenfield, Y. Tsukada, K. Fulling, J. Lamarche, and N. Peress, "Necrosis as a Prognostic Criterion in Malignant, Supratentorial Astrocytic Gliomas," *Cancer, 52*, 1983, pp. 550–554.